Available online at www.sciencedirect.com

ScienceDirect

Geochimica et Cosmochimica Acta 321 (2022) 206–243

Geochimica et Cosmochimica Acta

www.elsevier.com/locate/gca

U-Pb isotope systematics and impact ages recorded by a chemically diverse population of glasses from an Apollo 14 lunar soil

A.A. Nemchin [a,*], M.D. Norman [b], M.L. Grange [c], R.A. Zeigler [d], M.J. Whitehouse [c], J.R. Muhling [e], R. Merle [f]

[a] School of Earth and Planetary Sciences, Curtin University, Australia
[b] Research School of Earth Sciences, The Australian National University, Canberra, ACT 2601, Australia
[c] Swedish Museum of Natural History, S-104 05 Stockholm, Sweden
[d] Astromaterials Acquisition and Curation Office, NASA Johnson Space Center, Houston, TX, USA
[e] School of Earth Sciences, The University of Western Australia, 6009 Perth, Australia
[f] Department of Earth Sciences, Natural Resources and Sustainable Development, Uppsala University, Sweden

Received 23 June 2021; accepted in revised form 13 December 2021; Available online 20 December 2021

Abstract

Glass beads formed by ejection of impact-melted lunar rocks and soils are an important component of lunar soils. These glasses range from 10′s of microns to up to a few cm in diameter and contain variable, but usually relatively low (several hundred ppb to a few ppm), quantities of U. Because Pb is a volatile element, it tends to be lost from the melts, so individual impact glasses can be dated by the U-Th-Pb isotopic systems. The presence of two additional Pb components in lunar glasses, likely linked to addition of lunar Pb to the beads during their residence on the lunar surface and from terrestrial laboratory contamination, require corrections to the data before accurate formation ages of the glasses can be determined. Here we report a U-Th-Pb isotopic and geochemical study of impact glasses from the Apollo 14 soil 14163, which documents multiple impacts into chemically diverse targets that can be linked to the main groups of rocks found on the Moon, i.e., mare basalts, highlands plagioclase-rich rocks, and KREEP (from high contents of K, REE and P) enriched rocks. The impact ages show a bimodal distribution with peaks at ~3500–3700 Ma and <1000 Ma, similar to that obtained previously by ^{40}Ar-^{39}Ar dating of other suites of lunar regolith glasses. Our data suggest two predominant age peaks at ~100 Ma and ~500 Ma, with other statistically definable clusters of ages also possible. As Pb is relatively resistant to subsolidus diffusive loss in these glasses, the age clusters probably represent primary formation ages during impact events, although processes such as preferential preservation of young glasses and impact conditions necessary for production of regolith glasses need further quantification.
© 2021 The Authors. Published by Elsevier Ltd. This is an open access article under the CC BY-NC-ND license (http://creativecommons.org/licenses/by-nc-nd/4.0/).

Keywords: Moon; Impact glasses; U-Pb ages; Apollo 14

1. INTRODUCTION

Spherules and fragments of glass ranging in size from a few micrometres to a few centimeters are common in the lunar regolith. Initial studies of Apollo samples established the ubiquity of regolith glass across the lunar surface and their diverse petrographic and geochemical characteristics

* Corresponding author.
E-mail address: nemchina@kalg.curtin.edu.au (A.A. Nemchin).

https://doi.org/10.1016/j.gca.2021.12.013
0016-7037/© 2021 The Authors. Published by Elsevier Ltd.
This is an open access article under the CC BY-NC-ND license (http://creativecommons.org/licenses/by-nc-nd/4.0/).

(e.g., McKay et al., 1970; Fulchignoni et al., 1971). Subsequent work considered the petrogenetic implications of their chemical compositions in greater detail (e.g., Reid et al., 1972; Chao et al., 1972; Ridley et al., 1973; Glass 1976; Delano et al., 1981; Delano and Livi 1981; Simon et al., 1989; Wentworth and McKay, 1991; Shearer and Papike, 1993; Delano et al., 2007; Korotev et al., 2010; Norman et al., 2012; Brown and Grove 2015; Zellner 2019, and many others). Two main types of lunar regolith glasses have been distinguished based on their origins as products of pyroclastic fire fountains and impact ejecta. Several chemical and petrographic criteria have been proposed for distinguishing volcanic from impact lunar glasses (Delano 1986).

Major- and trace-element compositions of picritic volcanic glass spherules tend to form tight clusters with distinctive characteristics such as high Mg/Al (Fig. 1). The limited compositional variations within these groups are consistent with magmatic trends that provide unique information about the origin and evolution of basaltic magmas on the Moon and the nature of the lunar mantle (Delano, 1986; Shearer et al., 1990, 1991; Shearer and Papike 1993; Hughes et al., 1990). In contrast, impact glasses have a broad and continuous range of chemical compositions that are more consistent with mixing of diverse components either within the lunar regolith prior to the bead-forming impact or during the impact process itself. Analogous to the variations observed in lunar breccias and the regolith, the range of compositions in lunar impact glasses can be broadly described in terms of their correlated variations in Al_2O_3 and FeO_t (=total Fe expressed as FeO), reflecting feldspathic and mafic components in the lunar crust, plus a variable contribution of a incompatible element-enriched KREEP-like component (Korotev et al., 2010). TiO_2 also provides important information on the type (i.e., low-Ti vs. high-Ti basalts) and abundance of mare materials that were incorporated into the melt (Delano et al., 2007; Zeigler et al., 2006; Norman et al., 2012). However, while the compositions of lunar impact glasses have the potential to provide important information about crustal compositions, the pervasive nature of impact mixing on the lunar surface and during the spherule-producing events tend to produce diffuse clusters of predominantly intermediate compositions that are difficult to relate to specific targets or impact events.

Early studies of lunar impact glasses sought to relate their compositions to lithologies thought to be common on the lunar surface (Reid et al., 1972). More recently, lunar spherule compositions have been compared with those of the regolith at each landing site to distinguish locally-derived from exotic particles that might have been transported for long distances (Zellner et al., 2002; Delano et al., 2007; Korotev et al., 2010; Norman et al., 2012, 2019; Zellner, 2019). The significance of this distinction relates to understanding the size of the impact event that produced the spherule, the compositional diversity of the lunar crust, and attempts to constrain the size, number and dynamics of impact events recorded by the spherule populations. Major and trace element compositions of lunar impact glasses have revealed a strong regionality to their distribution (Zellner et al., 2002; Delano et al., 2007; Korotev et al., 2010; Norman et al., 2012; Zellner, 2019), implying that most of spherical glasses were formed by 'local' events although the size and scale of these impacts and the transport distances involved are not well-constrained (Zellner et al., 2002; Norman et al., 2012, 2019; Zellner, 2019).

Additional information about the timing of volcanic and impact events on the Moon can be gained from the ages of individual glass particles (Zellner, 2017, 2019). Most of the previously published data were obtained from the $^{40}Ar/^{39}Ar$ system. For example, Huneke (1978) measured ^{40}Ar-^{39}Ar compositions of five individual spherules of Apollo 17 orange volcanic glass and obtained a solidification age of 3.60 ± 0.04 Ga. Spangler and Delano (1984) measured multi-step $^{40}Ar/^{39}Ar$ ages of individual particles

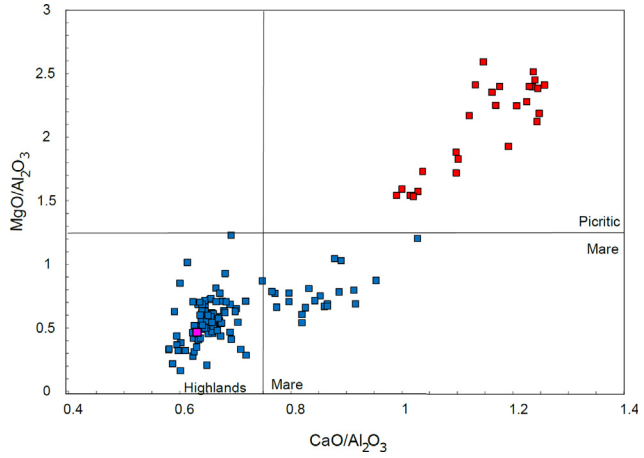

Fig. 1. MgO/Al_2O_3 versus CaO/Al_2O_3 plot for glass spherules investigated in the soil sample 14163, with the fields for glasses of different origin defined following Zeigler et al., (2006). Red squares represent beads of volcanic origin described in detail by Nemchin et al. (2011), blue squares correspond to the impact glasses discussed here, and the pink square represents the mean composition of soil 14163. (For interpretation of the references to colour in this figure legend, the reader is referred to the web version of this article.)

of three types of Apollo 15 volcanic glasses using a laser microprobe, and found resolvable differences in ages that were correlated with compositional groups. They interpreted those data as eruption ages ranging from 3.35 ± 0.18 to 3.62 ± 0.07 Ga. Five pieces of Apollo 15 yellow impact glass measured by Spangler and Delano (1984) using the same technique yielded an apparent age of 3.35 ± 0.05 Ga after correction for large amounts of trapped, surface-correlated ^{40}Ar. The ^{40}Ar/^{39}Ar compositions of larger populations of individual spherules separated from Apollo 12 and 14 regolith were measured by Levine et al. (2005, n = 81) and Culler et al. (2000, n = 155), respectively. Levine et al. (2005) obtained reconnaissance major element data on each spherule prior to the isotopic analyses in order to distinguish volcanic from impact spherules, whereas no additional geochemical information aside from the Ca/K implied by the Ar isotopic data was obtained on the spherules studied by Culler et al. (2000).

More recent studies have begun to examine possible complexities in the interpretation of lunar impact glass ages, including potential biases related to transport, preservation, and resetting during residence in the regolith, as well as the significance of the age distributions for lunar impact history. For example, Delano et al. (2007) reported ^{40}Ar/^{39}Ar ages and major element data for four high-K glass particles considered to be exotic to the Apollo 16 landing site. Plateau ages of these individual particles ranged from 3721 ± 60 Ma to 3785 ± 10 Ma, and were interpreted to represent delivery of the glasses from the Procellarum-KREEP terrane by an impact event at ~3730 Ma. Zellner et al. (2009) reported major element compositions and ^{40}Ar/^{39}Ar ages of nine impact glasses from the Apollo 14, 16, and 17 landing sites, and proposed at least seven distinct impact events with ages ~800 Ma based on the range of major element compositions observed in this group of glasses. Norman et al. (2019) reported major-element, trace-element, and ^{40}Ar/^{39}Ar data on glass particles from Apollo 16 regolith 66031. The major and trace element data were used to evaluate source characeristics of the dated glasses and the possibility that single impact events may have contributed multiple spherules to the population, which could bias the apparent age distribution. Zellner and Delano (2015) presented ^{40}Ar/^{39}Ar analyses of more than 70 glasses from the Apollo 14, 16, and 17 landing sites and argued that ^{40}Ar/^{39}Ar data obtained for these and other impact glasses can be biased towards younger ages as a result of combined effects of shattering and Ar diffusion. Most recently, Nguyen and Zellner (2019) reported major element and ^{40}Ar/^{39}Ar data for 43 glasses from the Apollo 14, 16, and 17 sites and proposed additional physical and compositional characteristics that may increase the likelihood of obtaining reliable ages.

Microbeam analyses of U-Th-Pb abundances and isotopic compositions in volcanic and impact spherules from the lunar regolith have been also used to determine ages of individual glass beads. Nemchin et al. (2011) obtained ion microprobe U-Pb isotopic data for 20 Apollo 14 volcanic glasses, identified by their characteristic major element compositions. Although their study was focused on the investigation of μ-values in the lunar mantle, ages of 3.25–3.36 Ga were also calculated from the data arrays. Norman et al. (2012) measured trace element and Pb isotopic compositions of Apollo 17 volcanic and impact glasses using laser ablation ICP-MS, and developed a U-Th-Pb 'chemical age model' for individual spherules. This model is based on the assumptions that all Pb was lost from the melt during the event that produced the glass (volcanic eruption or impact), and that all Pb now present in the spherule accumulated from in-situ U-Th decay and is therefore linked directly to the age of the glass.

This paper presents new U-Th-Pb isotopic compositions together with major- and trace-element data obtained on impact glasses from Apollo 14 soil 14163. The aim of this paper is to investigate the geochemical behaviour of Pb isotopes in these glasses spherules and to discuss implications of the compositional and isotopic data for the impact history of the Moon.

2. SAMPLES AND ANALYTICAL TECHNIQUES

A total of 250 glass beads with diameters between about 100 and 200 μm were handpicked from the Apollo 14 soil sample 14163,914, mounted in a 25 mm diameter epoxy disc and polished. Initial screening to identify beads containing at least some homogenous areas large enough to attempt U-Th-Pb dating was based on backscattered electron (BSE) images obtained at Curtin University of Technology, using a Phillips XL 30 (20 kV accelerating voltage and 15 mm working distance). Images of 58 glasses showing heterogeneous internal features are presented in the supplementary file; 37 of these inhomogenous glasses were not analyzed further (Fig. 2). Texturally homogenous spherules were identified visually but images were not collected to avoid unnecessary surfase damage. The homogenous glasses and 21 beads containing some inclusions and fragments, but also showing areas that appear to be homogenous (Fig. 2) were analysed for the chemical compositions. Major element compositions of homogenous beads were determined by wavelength-dispersive electron microprobe analyses at the Centre for Microscopy, Characterization and Analysis (CMCA) at the University of Western Australia. Operating conditions were 15 kV accelerating voltage and 20 nA beam current using three crystal spectrometers mounted on a JEOL JSM6400 electron microscope. Well-characterised natural minerals were used as standards, and an optical microscope was used to ensure correct focus of all analytical points. At least three point analyses were made within each spherule to evaluate their chemical homogeneity.

2.1. U-Th-Pb Ion probe analysis

Uranium-Th-Pb isotope data were obtained using the Cameca IMS1280 ion probe at the Swedish Museum of Natural History in Stockholm (NordSIMS facility). Analyses of 143 chemically homogenous glasses that were identified as being of impact origin are reported here. See Nemchin et al. (2011) for compositions of volcanic glasses from this sample. All analyses were performed in fully automated chain sequences.

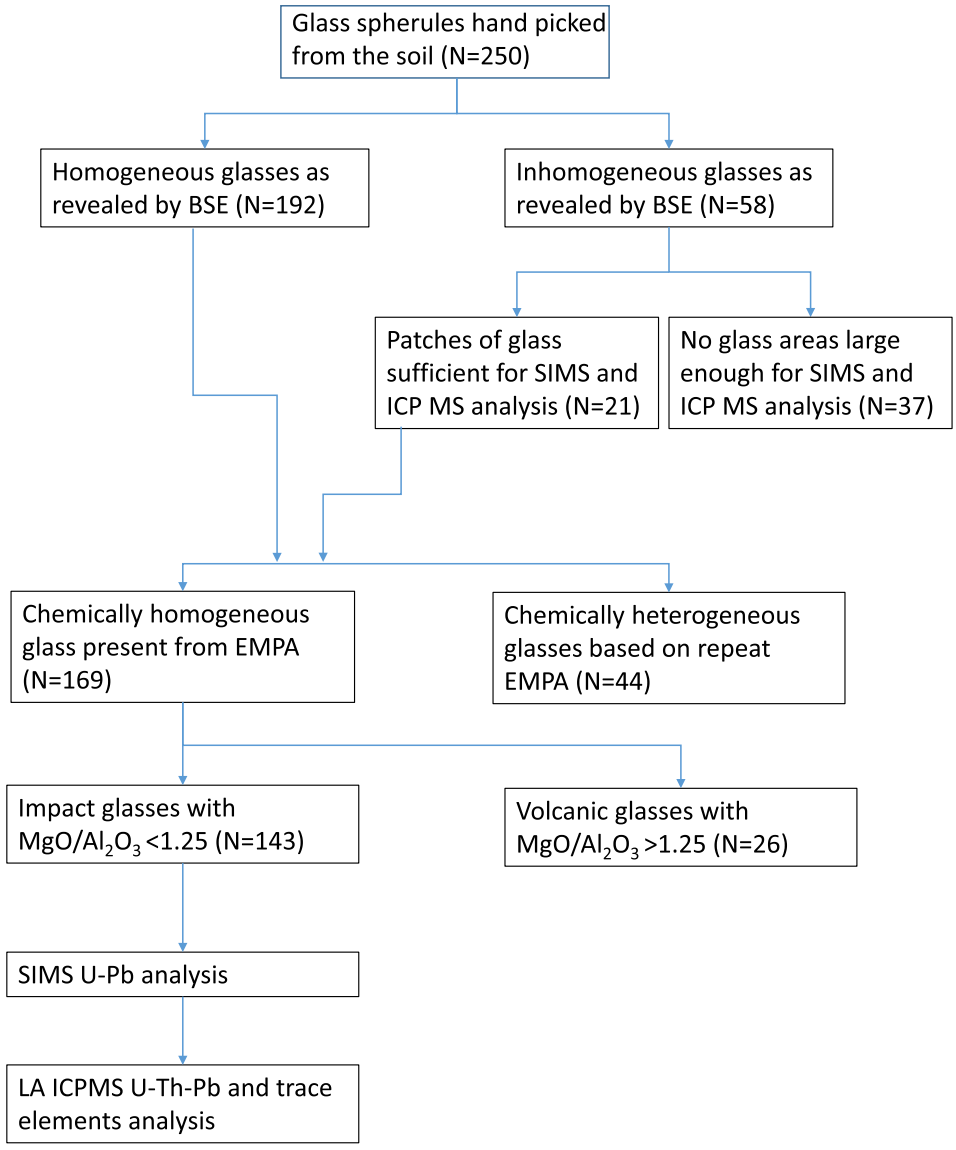

Fig. 2. Flowchart showing filtering and selection of glass beads from the sample 14163 for U-Th-Pb and chemical study, using chriteria based on textural characteristics and major elements analysis of glasses.

A ~10 nA O_2^- primary beam with 23 kV energy (-13 kV primary, 10 kV secondary) was used in aperture illumination (Köhler) mode to produce a ~25 μm, flat-bottomed analytical pit. To minimize possible surface contamination each analytical spot was pre-sputtered for 100 seconds using a 25 × 25 μm raster to remove the gold coating over an area similar to the sample field of view admitted to the mass spectrometer using the highest magnification (equivalent to the highest transmission) transfer lens setting in combination with a 6000 μm field aperture. The mass spectrometer was operated at a mass resolution of 4860 (M/ΔM), sufficient to resolve Pb from molecular interferences in basaltic glass using a 75 μm entrance slit and 250 μm exit slit. Secondary ions with 10 kV energy were centred in the field aperture and detected using four ion counting electron multipliers (EMs), with $^{204}Pb^+$, $^{206}Pb^+$, $^{207}Pb^+$ and $^{208}Pb^+$ isotopes detected simultaneously, followed by stepping of the magnet field through a background (also measured simultaneously, at a mass station 0.3 a.m.u. higher than the Pb peaks), $^{238}U^+$, $^{232}Th^{16}O^+$ and $^{238}U^{16}O^+$ which were measured sequentially in the multicollector EM positioned on the axis. The EMs were tuned for optimum yield and lowest noise using the pulse height analysis routine of the Cameca CIPS software which gave relative yields within ± 5% of unity. Actual relative detector yields were determined using replicate analyses of the BCR-2G basaltic glass reference material assuming the Pb isotope composition reported by Woodhead and Hergt (2000).

Background counts for each channel measured at a mass station 0.3 Da above the nominal species mass were integrated over each of the two analytical sessions to provide average count rates and uncertainties on each Pb isotope. For each session respectively, these backgrounds and 1SD errors were: $^{204}Pb = 0.014 \pm 0.019$ cps and 0.004 ± 0.005

cps; $^{206}Pb = 0.0018 \pm 0.0038$ cps and 0.0040 ± 0.0030 cps; $^{207}Pb = 0.0008 \pm 0.0025$ cps and 0.0005 ± 0.0030 cps; $^{208}Pb = 0.0059 \pm 0.0066$ cps and 0.0026 ± 0.0061 cps, the very large errors reflecting essentially random and infrequent non ion-arrival induced pulses. Peak-to-background ratios for ^{206}Pb, ^{207}Pb and ^{208}Pb in all cases have a negligible effect on measured $^{207}Pb/^{206}Pb$ and $^{208}Pb/^{206}Pb$ ratios and uncertainties. For ^{204}Pb however, peak-to-background ratios are much lower, requiring both a correction and propagation of errors to calculate accurate $^{204}Pb/^{206}Pb$ ratios and realistic uncertainty.

U/Pb concentration ratios in the glass beads were calibrated using the BCR-2G basalt glass reference material. BCR-2G and lunar glass analyses fall on parallel trends with similar slopes of 1.63 in Ln($^{206}Pb/^{238}U$) versus Ln ($^{238}U^{16}O/^{238}U$) coordinates. This slope was used for the correction of U-Pb data in the glass beads that followed the protocol utilised for the correction of ion probe zircon analyses (Williams, 1998). Because the Th/U ratio in the reference material did not change during a single session, an average Th/U concentration ratio was calculated on the basis of all BCR-2G analyses obtained for a session and used to define a correction factor for the analyses of lunar glasses. True Pb/U and Th/U ratios in BCR-2G were determined by averaging published Pb, U and Th concentrations (Gao et al., 2002; Norman et al., 1998; Dulski, 2001; Jochum and Nohl, 2008), presented in table 3.

2.2. LA-ICP-MS trace elements

Trace-element compositions of individual particles were measured at RSES-ANU by laser ablation ICPMS using a Lambda Physik Compex excimer laser coupled to an Agilent 7500 quadrupole ICPMS following procedures described by Norman et al. (2004, 2012, 2019). The glasses were ablated under a mixed He-H_2 gas in a custom designed cell using a 47 μm-diameter laser spot and a 5 Hz laser pulse rate. Each analysis consisted of 25 s of instrument background measured on the carrier gas and 50 s of ablation. The NIST612 glass was used for calibration of isotopic sensitivities and each analysis was normalized to the CaO concentration of the sample to correct for variations in ablation yield. Dwell times were 20 ms per mass per sweep of the mass range except for the three Pb isotopes where dwell times were 0.1 sec per mass. The USGS basaltic glasses BHVO-2G, BCR-2G and BIR-1G were analyzed as unknowns for quality control (Table 1).

The U, Th and Pb concentration data obtained from the ICP-MS analyses allow calculation of 'chemical ages' of individual spherules based on the assumption that all of the Pb present in a bead was accumulated from decay of U and Th since the bead formed. Total Pb was calculated by summing the intensities measured on each of the Pb isotopes (masses 206, 207, 208) and normalising these sums in the unknowns to those obtained in NIST612 which has a known concentration of total Pb. Chemical ages were obtained using Newton's approximation method with analytical uncertainties, including average uncertainties obtained for the standard fully propagated. Isotope ratio information is also available from these data although at

Table 1
ICP MS trace elements data for standards analysd together with the glasses from Apollo 14 sample. IS = internal standard.

Element		CaO (IS)	Sc	Ti	TiO2	V	Cr	Mn	Co	Ni	Rb	Sr	Y	Zr	Nb	Ba	La	Ce	Pr	Nd	Sm	Eu	Eu	Gd	Tb	Dy	Ho	Er	Yb	Lu	Hf	Ta	Pb	Th	U
Mass		43	45	49		51	53	55	59	60	85	88	89	90	93	138	139	140	141	146	147	151	153	160	159	163	165	166	174	175.00	178	181.00	sum	232	238
Units		wt%	ppm	ppm	wt%.	ppm	ppm	ppm	ppm	ppm	ppm	ppm	ppm	ppm	ppm	ppm	ppm	ppm	ppm	ppm	ppm	ppm	ppm	ppm	ppm	ppm	ppm	ppm	ppm	ppm	ppm	ppm	ppm	ppm	ppm	ppm
NIST612	calibration values	11.9	40.8	41.5		33.2	36.9	36.6	34.7	36.8	26.7	77.7	40.9	41.9	40.8	38.9	36.5	38.4	37.9	36.2	38.0	36.2	36.2	39.1	38.0	37.1	40.2	40.1	40.2	39.6	37.3	41.4	36.9	39.7	33.2
	1SD (n=18)		0.2	0.7		0.2	0.5	0.2	0.2	0.4	0.2	0.5	0.2	0.3	0.2	0.2	0.1	0.3	0.2	0.3	0.3	0.2	0.2	0.2	0.2	0.2	0.3	0.2	0.3	0.2	0.2	0.2	0.2	0.2	0.2
BCR-2G	average	7.1	34.3	14102	2.35	373	15.8	1501	38.0	11.6	42.1	331	34.0	189	12.7	661	24.4	50.9	6.38	27.8	6.36	1.93	1.92	6.47	0.97	6.22	1.29	3.61	3.33	0.51	4.69	0.80	11.0	6.01	1.50
	1SD (n=12)		0.4	183	0.03	5	0.8	31	0.9	0.3	0.7	3	0.5	2	0.2	7	0.3	0.5	0.10	0.4	0.08	0.05	0.05	0.17	0.02	0.08	0.04	0.05	0.06	0.02	0.10	0.02	0.2	0.10	0.02
	%1RSD		1.2	1.3	1.3	1.3	4.8	2.0	2.3	2.6	1.6	0.9	1.4	1.0	1.4	1.0	1.1	1.1	1.6	1.5	1.3	2.4	2.6	2.6	2.0	1.2	2.9	1.5	1.7	3.2	2.1	2.8	1.9	1.7	1.4
BHVO-2G	average	11.4	32.5	16873	2.82	281	297	1293	46.1	120	8.23	383	24.3	170	18.3	126	14.7	35.8	4.96	23.55	5.85	2.02	2.02	5.93	0.85	5.09	0.96	2.49	1.96	0.27	4.16	1.16	2.04	1.23	0.39
	1SD (n=10)		0.5	248	0.04	3	5	14	0.7	2	0.11	4	0.3	2	0.2	1	0.1	0.3	0.05	0.18	0.11	0.04	0.05	0.14	0.01	0.10	0.02	0.05	0.04	0.01	0.12	0.02	0.12	0.03	0.01
	%1RSD		1.4	1.5	1.5	1.2	1.8	1.1	1.5	2.0	1.3	0.9	1.0	1.2	0.9	1.0	0.8	0.8	1.0	0.8	1.8	1.9	2.3	2.4	1.3	1.9	1.6	2.0	1.8	4.1	2.9	1.7	5.8	2.1	3.5
BIR-1G	average	13.3	45.0	5932	0.99	292	413	1366	56.9	183	0.18	107	14.7	14.6	0.54	6.33	0.59	1.82	0.35	2.31	1.06	0.50	0.50	1.77	0.33	2.53	0.57	1.70	1.63	0.25	0.567	0.036	3.69	0.029	0.016
	1SD (n=10)		0.6	104	0.02	5	8	16	1.0	3	0.02	1	0.2	0.3	0.02	0.08	0.02	0.02	0.01	0.09	0.05	0.02	0.02	0.07	0.02	0.09	0.02	0.07	0.03	0.01	0.030	0.005	0.06	0.003	0.003
	%1RSD		1.4	1.7	1.7	1.6	1.8	1.2	1.7	1.6	8.5	1.1	1.7	1.9	4.1	1.3	3.3	1.3	3.6	3.7	5.0	3.5	4.0	4.2	5.6	3.6	3.6	3.9	1.7	4.0	5.4	13.6	1.8	10.1	17.4

a lower precision than obtained by SIMS. Instrumental mass bias on the Pb isotopes was corrected by normalizing measured isotope ratios to the BCR-2G glass using the values of Woodhead and Hergt (2000). $^{207}Pb/^{206}Pb$ ages were calculated for individual spherules using ISOPLOT (Ludwig, 2008).

3. RESULTS

3.1. Petrography

Glass beads extracted from lunar soils consist of pristine glasses of volcanic origin and impact-generated glasses. Several textural and chemical criteria have been proposed to distinguish between impact and volcanic glasses (e.g., Delano, 1986) and some of these criteria were used to identify volcanic and impact glasses in the population extracted from sample 14163. Initial screening of an original group of 250 beads was done using BSE images, based on the assumption that inclusions, clasts, and schlieren are diagnostic for impact glasses (Delano, 1986). Glass beads containing skeletal and dendritic crystals and having regular shapes and absence of vesicles were interpreted as volcanic in origin while spherules containing irregular or rounded mineral inclusions or clasts, large vesicles, and irregular shapes were classified as impact melts. About 25% (n = 58) of the investigated glasses had petrographic features (such as some listed above) that allowed for a clear classification as either volcanic or impact origin based on these criteria. A subset of these beads (n = 37) shows a large number of inclusions preventing chemical and isotopic analysis of pure glass. These beads were excluded from further study in order to focus the analyses on homogeneous glasses of likely impact origin. The other 21 particles with inclusions show areas of homogenous glass large enough for U-Th-Pb analysis and where included in the chemical characterisation (Fig. 2).

3.2. Major and trace element compositions

Chemical inhomogeneity was suggested by Delano (1986) as diagnostic of impact glasses. In this study we focussed on chemically homogenous glass beads or glass patches in some texturally heterogenous spherules to avoid possible complications with interpretation of the U-Pb isotopic systems. Consequently, the final stage of sample selection excluded beads that were chemically heterogeneous. About 20% of the beads remaining after the initial BSE-based screening (n = 44) showed differences between repeat analyses of major elements compositions that exceeded the analytical uncertainties. We classified these compositionally heterogeneous particles as impact glasses, but they were excluded from further analyses.

Lunar impact and volcanic glasses can be distinguished by their MgO/Al_2O_3 and CaO/Al_2O_3 compositions (Delano 1986; Zeigler et al., 2006). Following this scheme, 169 texturally and compositionally homogeneous glasses were classified as 'volcanic' ($MgO/Al_2O_3 > 1.25$) or 'impact' ($MgO/Al_2O_3 < 1.25$) (Fig. 1). The full selection process for the glasses analyzed here is shown schematically in Fig. 2.

Glasses classified as 'impact' have compositions that cluster around the bulk composition of soil 14163 and were further subdivided into mare and highlands groups based on their CaO/Al_2O_3 (Table 1). About 16% of the homogeneous glasses (n = 22) were classified as 'mare' based on their major element compositions ($CaO/Al_2O_3 > 0.75$). These mare glasses (Fig. 3) have high FeO_t (>13 wt%), low to very low TiO_2 (0.68–5.78 wt%), and relatively low contents of incompatible elements (e.g., <60 ppm of La, Fig. 4a). All but one of these glass compositions would be classified as 'aluminous mare' with 10.5–14.8 wt% Al_2O_3 (see Norman et al., 2012 for further discussion)

Eleven (8%) of the impact glasses are highly aluminous Al_2O_3 (>19 wt. %) with corresponding depletions in FeO_t (<8%), and low concentrations of incompatible elements, mostly <10 ppm La although two samples have somewhat higher concentrations of incompatible elements (Fig. 4a, Table 1). There is a general anti-correlation between Al_2O_3 and Mg# (molar Mg/Mg + Fe) in these glasses, with Mg# ranging from ~0.65–0.94. Following Wentworth and McKay (1991), we refer to this group as having 'feldspathic' compositions.

The most populous group of glasses (n = 81) is characterised by intermediate Al_2O_3 (~12–17 wt%) and FeO_t contents (~8–13 wt%), and enrichments of incompatible elements such as Ba, Th, and the REE (blue circles; Fig. 4a, Table 1). This group is referred to here as 'KREEP-rich' glasses, reflecting their high levels of this lunar component. The population of investigated beads in sample 14163 is dominated by KREEP-rich compositions, comprising three quarters (76%) of the studied glasses.

A smaller set (n = 30) of Al-rich glasses has unusually low SiO_2 contents (<43 wt%). Similar compositions have been referred to previously as HASP (high alumina, silica poor) glasses (Naney et al., 1976). HASP glasses are characterised by systematically lower SiO_2 contents (43 to 35 wt%) as Al_2O_3 increases from ~17–25 wt% (orange dots, Fig. 3d). HASP glasses are depleted in Na_2O and K_2O relative to other spherules and they have exceptionally high Th/U, which ranges between 6 and 13, but is mostly > 10 (Fig. 4). Increasing Th/U correlates strongly with decreasing contents of volatile elements such as Na, K, and Rb (Fig. 4c) rather than with more refractory lithophile elements such as Ba and Sr (Fig. 4d and e). Refractory trace element concentrations in many of the HASP glasses are similar to those of the KREEP-rich glasses, and these two groups seem to form a continuum on some plots (e.g., SiO_2-FeO_t, SiO_2-Al_2O_3, Fig. 3a and b). The mare glasses also seem to trend toward the KREEP-rich glasses showing linear trends where increasing content of elements and oxides such as Al_2O_3 and La accompanies decreasing FeO_t (Fig. 3a and 4a).

3.3. U-Th-Pb systematics: SIMS

The U-Th-Pb SIMS data are presented in Table 2 and Fig. 5. The inverted $^{238}U/^{207}Pb$-$^{206}Pb/^{207}Pb$ concordia representation applied to discuss these data here enables presentation of data with apparent ages ranging from ~4350 Ma to a few Ma without obscuring possible linear

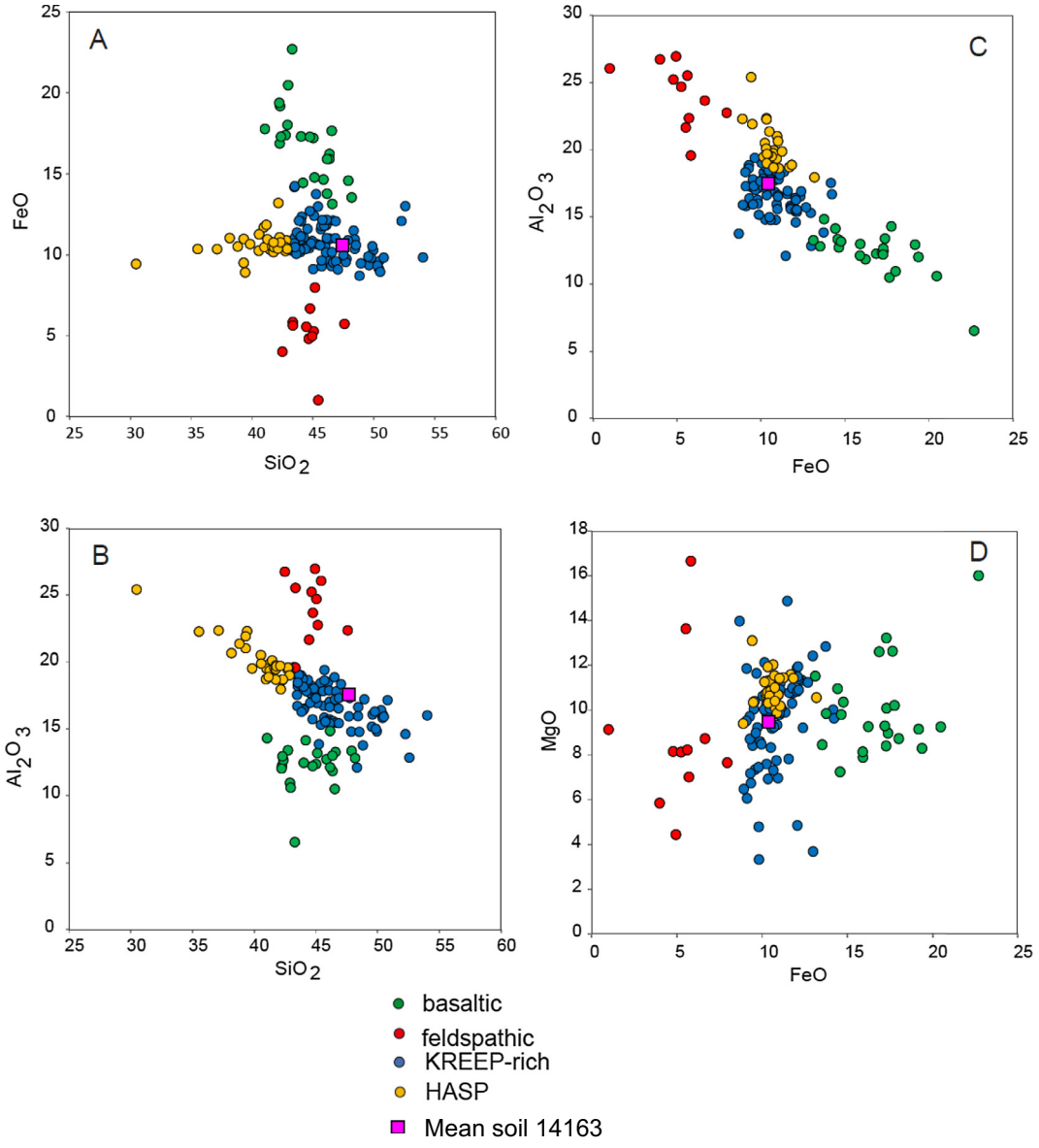

Fig. 3. Major elements variations (wt%) in the impact glasses from 14163 soil sample. Colours indicate major chemical groups of glass beads (mean composition of the soil 14163 represented by the pink square). (For interpretation of the references to colour in this figure legend, the reader is referred to the web version of this article.)

trends and was proposed initially by Tera and Wasserburg (1973). In addition, isotopic compositions of different Pb components unrelated to the in-situ accumulation of Pb from U decay after formation of the glasses, which can be incorporated by the glass beads throughout their history from their formation to laboratory handling, plot closely in the lower left corner of this diagram. The data are also plotted in $^{206}Pb/^{207}Pb$-$^{204}Pb/^{207}Pb$ coordinates to highlight contributions of Pb that was not accumulated in-situ.

Roughly 60% of the measured data fall within uncertainty or close to the $^{238}U/^{207}Pb$-$^{206}Pb/^{207}Pb$ concordia (Fig. 5), illustrating the highly radiogenic nature of the Pb isotopes in the 14163 impact glasses. A further illustration of this is provided by their very high $^{206}Pb/^{204}Pb$ of several thousand, but often reaching ten thousand (Table 2), which results in the analytical points plotting near the vertical axis on the $^{206}Pb/^{207}Pb$-$^{204}Pb/^{207}Pb$ diagram (Fig. 5). The remaining 40% of analyses are discordant. The most discordant analyses appear to form several linear trends between relatively young intercepts on the concordia curve (i.e., possible young in-situ accumulated Pb) and either lunar Pb unsupported by in-situ decay or terrestrial Pb composition, as both are nearly identical on the concordia diagram (Fig. 6b). Linear trends are also visible on $^{206}Pb/^{207}Pb$-$^{204}Pb/^{207}Pb$ diagram (Fig. 6a). One analysis appears to be off any trends on the concordia plot and two on $^{206}Pb/^{207}Pb$-$^{204}Pb/^{207}Pb$ diagram.

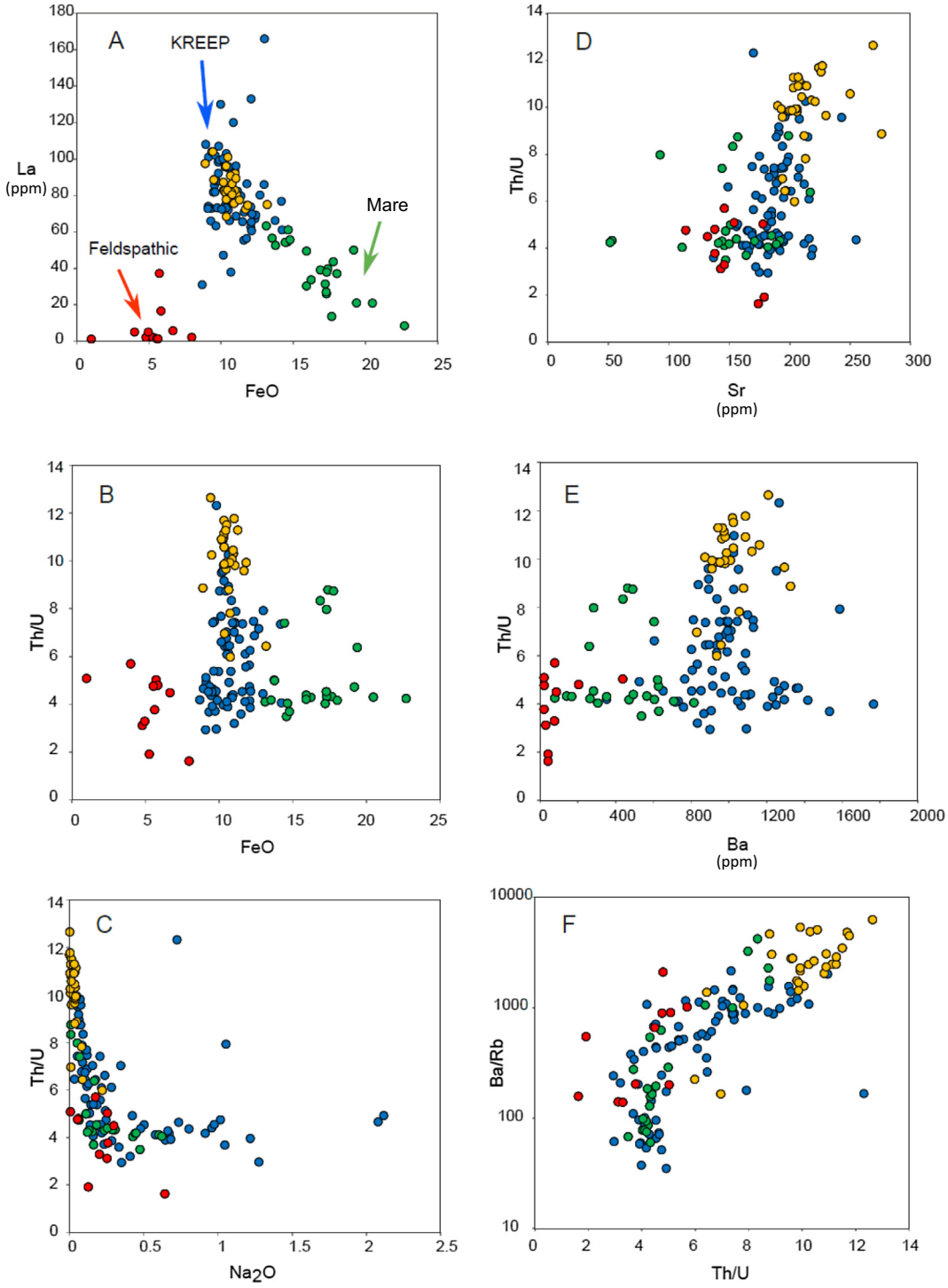

Fig. 4. Trace elements variations in the impact glasses from 14163 soil. Colours are similar to those in Fig. 2.

For the majority of the analyses, the calculated $^{208}Pb/^{232}Th$ ages uncorrected for ^{204}Pb are similar to $^{206}Pb/^{238}U$ ages within the uncertainties (Fig. 7). However, a number of glasses, in particular many HASP and high-Al (feldspathic) beads, show apparent $^{208}Pb/^{232}Th$ ages that are distinctly younger than their corresponding $^{206}Pb/^{238}U$ ages. Nevertheless, lower $^{208}Pb/^{232}Th$ ages are not correlated with any other features characterising these glasses, such as $^{204}Pb/^{206}Pb$ or discordance.

3.4. U-Th-Pb chemical ages: LA-ICP-MS

U-Th-Pb chemical ages based on elemental concentrations and isotope ratios obtained by the ICPMS analyses

Table 2
Major and trace element concentrations in the impact glasses from Apollo 14 soil 14163. FeO* is total Fe calculated as FeO. nd = not detected.

	Assigned	Major oxides (wt%)												Trace elements (ppm)																																		
OXIDE	age group	SiO2	TiO2	Al2O3	FeO*	MgO	CaO	MnO	Na2O	K2O	P2O5	Cr2O3	NiO	TOTAL	Sc	Ti	V	Cr	Mn	Co	Ni	Rb	Sr	Y	Zr	Nb	Ba	La	Ce	Pr	Nd	Sm	Eu	Gd	Tb	Dy	Ho	Er	Yb	Lu	Hf	Ta	Pb	Th	U
Basaltic																																															
ID = w4 a	2.5 Ga	46.55	0.68	10.49	17.65	12.63	10.78	0.25	0.31	0.13	0.23	0.49	0.03	100.23	41.7	4412	165	4348	2124	66.1	118	2.35	53	48.2	209	13.7	141	13.6	35.2	4.65	21.7	6.12	0.66	7.61	1.24	8.75	1.91	5.55	5.09	0.75	4.74	0.62	0.88	2.36	0.55
ID = bl9 a	500 Ma	42.75	3.82	13.39	17.39	8.97	11.51	0.28	0.04	0.02	0.14	0.25	nd	98.55	45.3	23973	84	1794	1856	32.2	41	0.27	199	142	634	39.2	464	39.7	101	13.9	66.1	19.1	2.41	22.8	3.88	26.1	5.52	15.8	13.9	2.02	14.5	1.83	0.33	6.39	0.73
ID = bl10 a	n.d.	42.27	3.17	12.25	16.87	12.61	10.91	0.25	0.01	0.02	0.09	0.21	0.05	98.71	44.0	19399	83	1852	1868	35.8	53	0.11	153	137	615	40.7	439	39.1	98.3	13.4	63.1	18.0	1.85	21.4	3.62	25.3	5.30	15.3	14.1	2.01	14.0	1.84	0.27	7.35	0.88
ID = b19 a	2.5 Ga	44.02	2.76	12.46	17.31	10.08	10.37	0.28	0.29	0.21	0.15	0.35	0.05	98.32	39.2	14765	75	2027	1625	35.5	103	3.62	192	127	754	39.0	566	37.9	95.7	12.9	59.3	17.2	2.10	20.1	3.36	23.8	4.86	14.0	13.0	1.87	16.7	1.78	2.06	6.31	1.46
ID = b20 a	3.8 Ga	45.03	2.26	12.36	17.21	9.29	10.54	0.29	0.43	0.21	0.38	0.39	0.01	98.38	52.1	13981	74	2456	1859	30.8	81	3.95	111	112	478	33.7	306	31.4	82.9	11.0	51.1	14.9	1.44	17.9	2.92	20.5	4.31	12.7	11.7	1.68	10.8	1.57	2.25	5.44	1.35
ID = b32 a	n.d.	41.06	3.47	14.29	17.77	10.20	12.05	0.27	0.01	0.00	0.04	0.24	0.01	99.41	46.3	20833	76	1539	1767	37.8	92	0.22	157	149	709	43.9	491	43.6	109	15.1	70.7	20.2	1.86	23.8	4.04	27.7	5.66	16.5	15.2	2.18	15.9	2.05	0.25	8.11	0.93
ID = g13a	2.5 Ga	43.30	1.01	6.53	22.70	16.01	8.16	0.27	0.15	0.09	0.15	0.59	0.07	99.03	38.1	5775	151	3800	2164	81.8	132	0.92	51.4	31.6	135	7.39	78.8	8.50	21.9	3.00	14.3	4.27	0.56	5.01	0.85	5.82	1.24	3.51	3.10	0.46	3.10	0.37	0.40	1.17	0.28
ID = g39a	100 Ma	42.38	1.34	12.65	17.29	13.22	11.11	0.30	0.05	0.03	nd	0.44	0.10	98.91	40.3	8018	107	2419	1818	55.6	107	0.09	92.8	88.1	403	26.8	284	26.0	65.5	9.04	41.8	11.9	1.11	13.7	2.31	16.2	3.40	10.0	9.30	1.29	9.05	1.21	0.05	4.84	0.61
ID = r9a	100 Ma	42.30	2.54	12.94	19.18	9.14	10.30	0.23	0.06	0.09	0.05	0.36	0.10	97.29	36.9	15902	83	2366	1484	125	736	1.01	147	168	771	54.3	628	50.0	127	16.9	77.4	22.2	1.93	25.8	4.34	30.7	6.51	18.6	17.3	2.42	17.1	2.39	0.13	9.92	2.10
ID = r2a	300 Ma	44.75	3.54	12.20	17.28	8.40	10.56	0.33	0.18	0.12	0.28	0.33	0.04	98.00	45.7	21543	84	2150	1768	33.9	63	1.46	185	106	417	25.7	283	27.0	70.8	9.78	46.8	13.7	1.96	17.4	2.90	19.9	4.10	11.9	10.7	1.58	10.1	1.26	0.13	4.33	0.96
ID = r4a	500 Ma	42.91	5.68	10.95	18.02	8.72	10.00	0.25	0.44	0.26	0.13	0.41	nd	97.76	44.0	35236	76	2383	1721	45.6	183	5.04	189	135	606	41.8	472	37.1	95.3	13.1	61.4	17.9	2.35	21.9	3.65	24.9	5.21	15.0	13.7	1.93	14.2	2.19	0.44	6.54	1.57
ID = r5a	500 Ma	42.24	4.67	12.02	19.38	8.29	11.01	0.28	0.17	0.05	0.12	0.22	0.01	98.45	49.8	29776	83	1991	1921	24.8	14	0.25	217	87.0	343	23.4	261	21.0	54.7	7.71	37.2	11.1	2.28	13.9	2.36	15.9	3.35	9.36	8.80	1.25	8.48	1.21	0.16	3.52	0.55
ID = r6a	1.1 Ga	42.97	3.77	10.59	20.48	9.25	10.09	0.28	0.13	0.05	0.19	0.37	0.01	98.17	47.0	23208	119	2922	1909	50.3	147	0.31	171	82.3	319	16.1	168	20.9	55.8	7.86	38.3	11.5	1.89	14.7	2.32	15.6	3.18	8.66	7.42	1.08	7.64	0.82	0.28	2.22	0.52
ID = w3 a	100 Ma	46.16	1.66	14.83	13.77	9.85	11.49	0.23	0.11	0.10	0.24	0.28	0.05	98.75	32.7	10371	72	1981	1472	37.3	128	2.17	151	163	776	54.4	623	52.6	136	18.2	82.0	22.5	2.16	25.7	4.53	30.0	6.50	18.4	17.1	2.53	17.3	2.59	0.74	9.78	1.96
ID = b8 a	700 Ma	46.59	2.07	13.25	13.13	11.52	9.92	0.21	0.60	0.44	0.59	0.29	0.05	98.64	31.0	12682	65	1920	1383	29.0	24	9.13	146	204	853	70.3	708	63.3	164	21.5	97.9	27.7	2.05	31.8	5.44	37.5	7.84	23.1	21.1	3.02	19.1	3.02	0.98	12.4	3.02
ID = bl8 a	1.1 Ga	46.36	3.27	11.84	16.23	9.26	10.50	0.29	0.24	0.16	0.18	0.45	0.08	98.85	42.0	19189	100	2605	1845	33.9	147	2.76	144	121	528	32.8	353	33.7	88.9	12.2	57.8	17.0	1.74	20.1	3.35	22.9	4.75	13.6	12.1	1.71	12.5	1.53	0.68	5.54	1.29
ID = b56a	500 Ma	45.87	3.63	12.72	14.64	9.80	9.81	0.30	0.62	0.46	0.16	0.20	0.06	98.27	34.3	22947	56	1704	1452	37.6	163	8.32	182	205	931	65.0	815	61.1	160	21.2	97.3	27.5	2.67	32.6	5.48	37.1	7.84	22.7	20.6	2.88	21.0	2.88	0.52	11.2	2.77
ID = b69a	500 Ma	44.19	2.24	14.13	14.44	10.95	11.26	0.27	0.07	0.07	0.07	0.34	0.06	98.06	36.9	12917	79	2071	1627	31.7	40	0.61	144	173	790	54.8	604	54.3	139	18.8	85.3	23.7	2.04	27.7	4.70	32.0	6.75	19.3	18.0	2.52	17.1	2.38	0.45	10.5	1.42
ID = b73a	700 Ma	48.19	2.75	12.80	13.53	8.45	10.58	0.23	0.45	0.39	0.21	0.29	0.07	97.92	35.8	16296	72	1996	1483	34.2	212	8.10	150	182	754	56.5	606	56.6	148	19.4	88.1	25.2	2.06	28.7	4.92	33.1	7.13	20.5	18.7	2.62	16.8	2.57	2.04	10.7	2.56
ID = r7a	500 Ma	46.35	3.23	12.98	15.92	7.88	10.65	0.26	0.26	0.14	0.06	0.28	0.04	98.05	41.6	18699	72	1946	1572	37.1	120	3.02	156	169	759	46.5	494	49.5	127	17.0	78.7	22.6	1.93	26.9	4.55	31.3	6.53	19.1	17.2	2.40	17.1	2.09	0.41	8.38	1.91
ID = r10a	300 Ma	45.13	3.11	13.17	14.77	10.35	10.09	0.23	0.16	0.10	0.07	0.39	0.12	97.69	37.4	19335	64	2328	1568	43.4	158	2.29	164	187	1784	57.9	629	55.7	142	18.8	86.5	24.6	2.25	29.0	4.90	34.3	7.17	21.1	20.5	2.99	43.1	2.62	0.24	11.0	2.98
ID = b7a	700 Ma	46.16	2.96	12.12	15.91	8.13	10.49	0.24	0.12	0.09	0.17	0.37	0.05	96.80	39.9	17813	110	2375	1706	31.0	85	1.44	141	102	409	25.1	265	30.3	79.5	10.7	51.2	14.6	1.68	17.2	2.87	19.0	3.93	11.1	9.69	1.39	9.26	1.15	0.06	4.02	0.95
Feldspathic																																															
ID = wl a	n.d.	44.66	0.28	25.22	4.80	8.15	15.39	0.06	0.25	0.03	nd	0.21	nd	99.04	11.0	1756	25	1022	647	9.9	12	0.22	143	8.3	30.6	2.3	30.2	2.11	5.63	0.75	3.58	1.03	0.77	1.22	0.23	1.51	0.34	0.93	0.91	0.14	0.74	0.12	0.01	0.35	0.11
ID = c10a	500 Ma	45.06	0.36	24.69	5.26	8.12	14.32	0.17	0.13	0.01	0.04	0.32	0.07	98.52	6.6	2000	41	1784	590	13.5	37	0.08	179	7.4	31.9	2.88	42.5	2.14	6.07	0.81	3.62	1.02	1.13	1.23	0.20	1.40	0.29	0.83	0.74	0.11	0.70	0.16	0.04	0.29	0.15
ID = c12a	300 Ma	47.59	0.80	22.35	5.72	7.01	13.99	0.13	0.26	0.12	0.02	0.20	0.09	98.27	16.4	5170	29	1388	776	7.9	3	2.20	178	118	551	40.9	438	37.2	94.7	12.6	57.0	15.6	1.64	18.4	3.17	21.4	4.46	13.2	12.4	1.80	12.1	1.70	0.40	7.94	1.58
ID = c1a	n.d.	42.49	0.25	26.73	4.00	5.84	15.70	0.18	0.18	0.01	nd	0.15	0.06	95.58	10.1	1721	22	878	527	8.3	20	0.08	146	17.3	70.8	6.52	77.8	5.01	12.7	1.71	7.66	2.16	0.91	2.46	0.42	3.21	0.66	1.92	2.00	0.30	1.68	0.29	0.37	1.31	0.23
ID = c2a	500 Ma	43.35	0.61	19.56	5.83	16.66	11.75	0.15	0.06	0.03	0.07	0.16	0.06	98.29	8.0	3987	28	1098	624	18.2	41	0.10	138	46.9	214	13.9	205	16.6	42.8	5.59	25.6	6.83	1.26	7.71	1.30	8.77	1.88	5.26	4.75	0.67	4.70	0.58	0.29	2.49	0.52
ID = c3a	500 Ma	44.46	0.21	21.65	5.54	13.63	12.78	0.12	0.06	0.00	0.00	0.29	0.06	98.79	9.6	1289	44	2271	648	16.3	4	0.03	114	5.9	21.6	1.62	22.2	1.50	4.91	0.53	2.48	0.74	0.59	0.98	0.16	1.03	0.23	0.70	0.64	0.09	0.48	0.08	0.03	0.26	0.05
ID = c5a	2.5 Ga	44.94	0.24	26.94	4.95	4.44	16.20	0.08	0.20	0.04	0.05	0.20	0.01	98.29	10.6	1663	23	807	614	7.2	10	0.55	146	17.5	71.2	6.42	76.7	5.06	13.1	1.69	7.79	2.27	0.84	2.57	0.46	3.09	0.70	2.11	2.07	0.31	1.62	0.31	0.37	1.28	0.39
ID = c6a	2.5 Ga	44.77	0.28	23.66	6.66	8.72	14.08	0.14	0.30	0.02	0.08	0.23	nd	98.92	9.1	1459	33	1557	761	11.5	18	0.13	132	19.3	78.8	7.07	86.2	5.74	14.9	1.91	8.70	2.51	0.78	2.61	0.47	3.59	0.71	2.25	2.21	0.32	1.91	0.32	0.40	1.49	0.33
ID = c7a	n.d.	45.44	0.28	26.05	1.01	9.13	16.43	0.06	0.01	0.02	0.07	0.14	0.05	98.68	10.3	1762	16	640	148	0.2	0	0.02	154	5.4	16.5	1.23	21.6	1.15	4.85	0.45	2.06	0.53	0.79	0.78	0.14	0.94	0.19	0.60	0.59	0.08	0.39	0.05	0.01	0.13	0.03
ID = c8a	500 Ma	45.17	0.35	22.75	7.97	7.65	13.22	0.18	0.64	0.02	nd	0.26	0.01	98.22	5.7	1949	32	1704	1035	9.5	2	0.27	174	7.3	31.4	2.8	42.7	2.13	6.03	0.75	3.55	0.96	1.12	1.26	0.19	1.32	0.27	0.85	0.68	0.11	0.74	0.15	0.04	0.28	0.18
ID = c9a	n.d.	43.36	0.24	25.52	5.63	8.22	15.24	0.11	0.26	0.02	nd	0.15	0.01	98.75	9.9	1350	27	1213	649	22.9	41	0.11	138	5.7	19	1.38	21.4	1.35	3.45	0.49	2.19	0.61	0.73	0.78	0.16	0.97	0.22	0.66	0.66	0.09	0.46	0.07	0.05	0.20	0.05
HASP																																															
ID = b11 a	n.d.	39.44	2.49	22.29	8.90	9.40	14.20	0.20	0.05	0.07	0.01	0.25	nd	97.28	30.7	14962	30	913	1060	9.0	10	0.44	276	300	1395	102	1326	97.5	237	32.7	148	41.0	4.14	47.4	8.15	54.9	11.7	33.9	31.1	4.33	30.5	4.51	0.22	18.8	2.12
ID = b14 a	n.d.	41.34	2.31	19.95	10.77	10.09	13.16	0.18	0.05	0.03	0.02	0.16	0.12	98.17																																		
ID = b22 a	2.5 Ga	39.32	2.67	21.01	10.97	10.69	13.26	0.24	0.04	0.03	0.02	0.17	0.04	98.45	29.6	15955	30	834	1196	22.3	38	0.23	218	275	1294	94.3	1122	92.0	233	31.7	143	39.6	3.14	44.8	7.46	51.2	10.8	30.4	28.5	3.91	28.0	4.12	6.63	16.8	1.63
ID = b25 a	100 Ma	42.82	1.83	19.52	10.88	9.86	12.57	0.16	0.01	0.04	0.01	0.14	nd	97.84	26.3	11067	29	809	1212	30.6	73	0.56	190	231	1044	76	873	75.6	190	25.5	116	32.2	2.53	37.1	6.26	42.0	8.80	25.5	23.5	3.37	22.9	3.29	0.21	14.4	1.43
ID = b26b a	37.13	2.21	22.34	10.34	11.30	14.25	0.15	0.00	0.00	nd	0.11	nd	97.84	30.5	13762	32	755	1235	21.1	36	0.21	224	251	1210	84.2	1019	82.9	204	28.1	128	35.1	3.06	39.8	6.88	46.5	9.80	28.3	25.9	3.65	26.3	3.73	0.23	15.9	1.36	
ID = b33 a	1.9 Ga	40.97	2.06	18.69	11.69	11.58	12.29	0.18	0.01	0.03	0.08	0.17	0.05	97.80	28.4	12642	38	992	1269	43.2	119	0.33	194	222	1058	76.8	910	72.5	186	25.0	112	30.5	2.52	35.4	5.97	41.1	8.59	24.6	23.1	3.21	23.2	3.33	2.81	14.0	1.46
ID = b30 a	700 Ma	42.17	2.22	17.94	13.19	10.55	11.97	0.21	0.09	0.06	0.02	0.15	0.08	98.64	27.6	13413	41	1275	1214	94.6	364	0.70	196	230	1092	79.5	958	75.0	194	25.7	117	32.0	2.85	36.9	6.24	43.0	9.03	25.5	24.1	3.37	24.0	3.37	1.01	14.6	2.27
ID = b39 a	100 Ma	42.74	2.13	19.41	10.23	10.64	12.56	0.19	0.01	0.03	0.01	0.16	0.08	98.20	26.6	12618	29	779	1132	24.5	54	0.47	203	250	1208	82.7	963	82.3	206	27.9	127	34.9	2.85	40.5	6.83	46.2	9.66	27.7	25.7	3.64	26.3	3.66	0.23	15.6	1.44
ID = b40 a	8 Ma	40.56	2.20	20.50	10.24	10.74	13.61	0.18	0.00	0.03	0.01	0.12	0.02	98.20	29.2	13444	32	808	1181	23.9	47	0.32	214	253	1196	84.2	980	82.6	204	28.0	128	35.3	3.01	40.5	6.93	47.0	9.95	28.2	26.1	3.70	26.0	3.66	0.01	15.6	1.43
ID = b59a	40 Ma	38.83	2.27	21.35	10.51	11.17	14.12	0.22	0.01	0.02	nd	0.12	0.01	98.63	29.4	13677	32	769	1235	22.8	45	0.30	226	258	1198	85.1	1024	84.9	208	28.5	132	36.7	3.08	41.1	7.09	48.2	10.0	28.9	26.6	3.75	25.8	3.79	0.09	16.0	1.39
ID = b64a	100 Ma	41.47	2.01	20.09	10.32	10.79	13.32	0.16	0.04	0.04	0.02	0.15	0.07	98.48	27.8	12283	30	751	1159	24.0	50	0.40	208	250	1184	82.8	974	81.5	201	27.7	127	35.4	2.87	39.7	6.83	45.7	9.68	28.1	25.7	3.64	25.9	3.57	0.22	15.7	1.41
ID = b67a	3.62 Ga	41.01	3.05	19.49	10.46	11.28	12.68	0.17	0.04	0.03	0.01	0.16	nd	98.38	28.6	18198	31	949	1184	21.8	39	0.46	230	306	1435	104	1294	101	254	34.2	156	43.4	3.49	49.3	8.39	56.5	11.9	34.2	31.6	4.47	31.6	4.74	7.49	19.3	2.00
ID = b70a	100 Ma	42.75	2.02	19.56	10.47	10.50	12.80	0.20	0.04	0.05	nd	0.11	0.01	98.51	26.6	12031	30	778	1139	30.0	87	0.66	200	240	1157	80	941	78.3	194	26.4	121	34.4	2.85	38.0	6.48	44.0	9.30	27.0	24.8	3.51	25.1	3.57	0.17	14.8	1.50
ID = b76a	500 Ma	42.27	2.20	18.61	11.07	10.18	12.37	0.19	0.04	0.04	0.10	0.16	0.05	97.27	28.7	13267	33	842	1181	26.2	62	0.56	206	251	1167	82.8	980	80.6	200	27.0	125	34.3	2.97	39.5	6.76	46.1	9.63	28.0	25.6	3.62	25.7	3.62	0.91	15.3	1.56
ID = b82a	n.d.	30.48	2.62	25.40	9.42	13.10	16.75	0.23	0.00	0.01	0.12	0.11	nd	98.24	35.4	15509	32	706	1105	14.3	26	0.19	269	324	1462	98.9	1209	104	238	34.6	160	45.3	3.65	50.7	8.68	59.6	12.4	35.4	33.2	4.61	31.1	4.47	0.33	19.6	1.55
ID = b101a	3.8 Ga	39.32	2.08	21.91	9.49	10.34	14.42	0.19	0.01	0.02	nd	0.16	nd	97.93	29.1	13028	28	702	1144	20.5	46	0.40	221	267	1228	85.1	988	88.6	224	30.3	139	38.5	2.95	42.8	7.33	49.2	10.2	29.5	27.2	3.76	26.3	3.61	7.07	16.5	1.61
ID = b95a	500 Ma	41.27	2.30	19.34	10.95	10.69	12.55	0.20	0.04	0.03	0.04	0.10	0.03	97.53	29.8	13925	33	838	1201	25.2	57	0.39	210	255	1216	85.6	1024	82.8	210	28.0	128	35.9	3.03	40.6	6.93	47.1	10.0	28.7	26.5	3.77	26.9	3.76	0.67	16.4	1.57
ID = g1a	40 Ma	41.65	2.17	19.53	10.50	10.85	12.69	0.16	0.04	0.03	0.01	0.19	nd	97.82	28.6	13087	32	899	1147	25.9	66	0.47	206	259	1240	85.7	1008	83.9	207	28.6	130	35.8	3.01	41.1	7.04	48.0	10.1	29.0	27.1	3.79	27.3	3.88	0.07	16.3	1.64
ID = g4a	3.62 Ga	41.76	2.26	19.45	10.16	11.26	12.48	0.18	0.03	0.01	0.06	0.15	0.08	97.88	26.9	13234	27	779	1126	26.1	65	0.47	207	266	1272	88.9	1088	87.2	219	29.6	134	38.4	3.04	42.3	7.23	49.6	10.3	29.6	27.4	3.85	28.0	3.90	6.43	16.9	1.55
ID = g5a	500 Ma	41.77	2.19	19.75	10.73	11.54	13.13	0.19	0.05	0.03	nd	0.20	0.11	99.68	29.2	12790	35	918	1208	24.7	46	0.18	205	250	1190	82.4	978	81.7	207	27.9	129	35.2	2.91	40.8	6.85	46.0	9.70	28.0	25.6	3.65	25.9	3.64	1.26	15.6	1.57
ID = g10a	500 Ma	39.85	2.43	19.50	10.65	12.03	12.80	0.19	0.04	0.05	nd	0.33	0.10	97.97	30.4	14403	34	987	1199	19.9	35	0.23	212	279	1338	91.4	1078	90.8	230	31.1	142	39.4	3.17	44.5	7.58	51.1	10.8	31.2	28.5	4.07	28.8	4.02	0.88	17.4	1.98
ID = g9a	8 Ma	42.88	2.02	18.99	10.35	10.38	12.45	0.23	0.04	0.05	nd	0.16	nd	97.54	26.7	12503	32	853	1172	28.3	67	0.57	202	238	1125	80.5	953	77.8	197	26.6	120	33.6	2.85	38.2	6.41	43.9	9.12	26.6	24.5	3.48	24.9	3.42	0.02	14.8	1.50
ID = g49a	n.d.	41.81	2.04	19.66	10.44	10.64	12.84	0.17	0.01	0.03	0.01	0.16	0.12	97.93	27.5	12249	30	783	1170	27.1	61	0.39	203	252	1207	83.5	966	82.9	206	28.2	129	35.3	2.94	41.2	6.85	46.3	9.72	27.8	25.9	3.66	26.6	3.58	0.22	15.9	1.41
ID = g50a	n.d.	42.13	1.96	19.69	10.37	10.31	12.85	0.23	0.01	0.05	0.02	0.10	0.04	97.74	27.9	11051	38	1085	1188	30.6	186	5.04	194	217	853	68	830	68.4	168	23.0	106	29.8	2.62	33.8	5.78	39.5	8.33	24.2	22.0	3.08	18.9	3.20	3.04	13.5	1.94

| | | |

| | | |

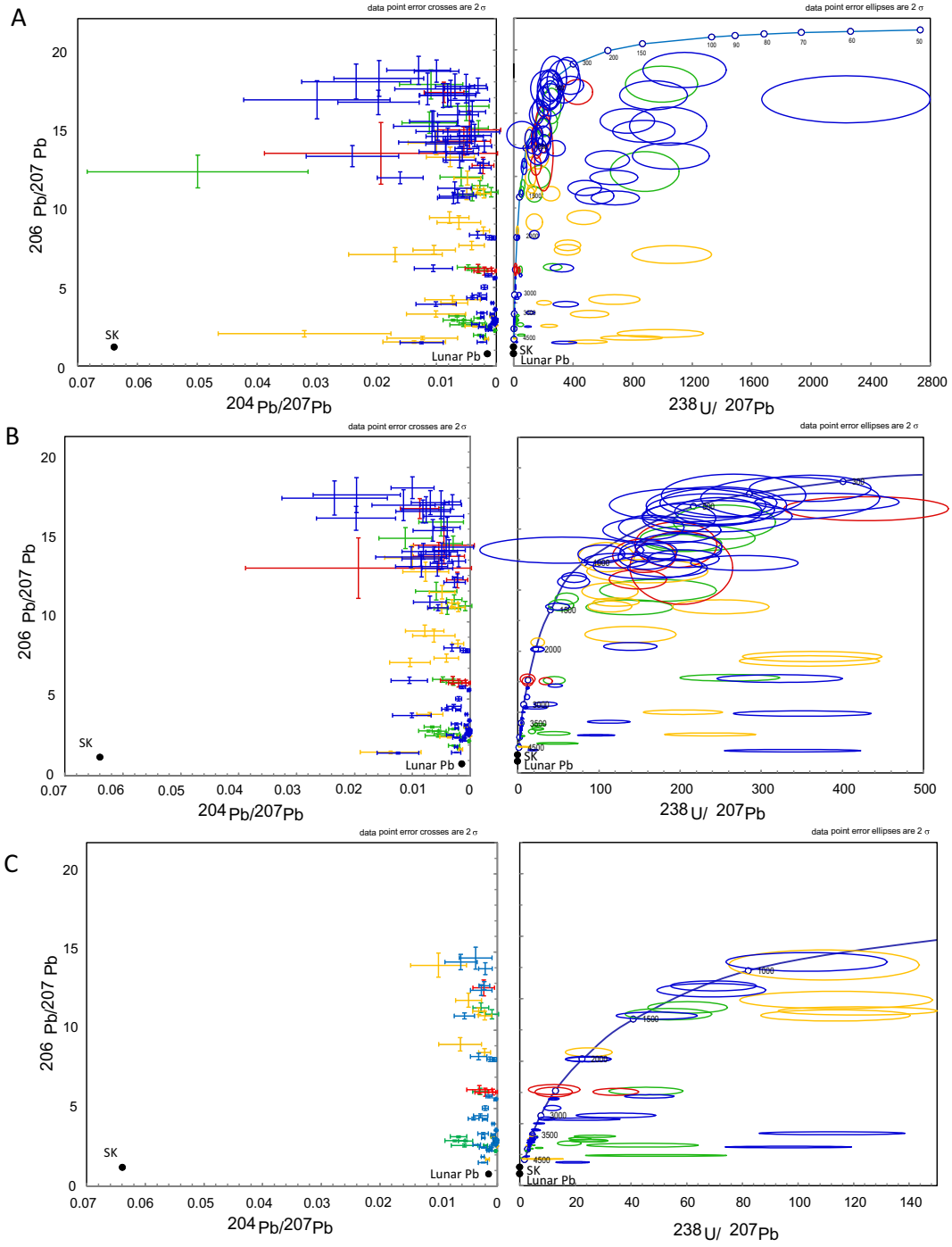

Fig. 5. U-Pb SIMS data obtained for the impact glasses from soil 14163 represented in modified Tera-Wasserburg representation. A- full set of data shown using $^{206}Pb/^{207}Pb$-$^{238}U/^{207}Pb$ concordia and corresponding $^{206}Pb/^{207}Pb$-$^{204}Pb/^{207}Pb$ plot; B and C – same diagrams successively zoomed closer to the older part of the concordia. Colours indicate major chemical groups of glass beads. Terrestrial Pb composition defined by Stacey and Kramers (1975) model and lunar unsupported Pb taken from 14163 soil analysis of Silver (1972) are shown as black circles.

about 50% of the particles studied here. The KREEP-rich glasses show relatively little variation in major element composition except for a range of MgO contents that are broadly correlated with V, Cr, and Co concentrations. REE patterns of these glasses range from La = 132-707x CI, similar to the range observed in igneous KREEP and KREEP-rich impact-melt rocks (Fig. 9). The KREEP-rich glasses continue the trend of decreasing Sr/Ba with increasing ITE observed in the feldspathic glasses (Fig. 10a) to very low values of Sr/Ba (0.11–0.60).

The HASP glasses have REE patterns similar to those of the KREEP-glasses (Fig. 9) but with a smaller range of con-

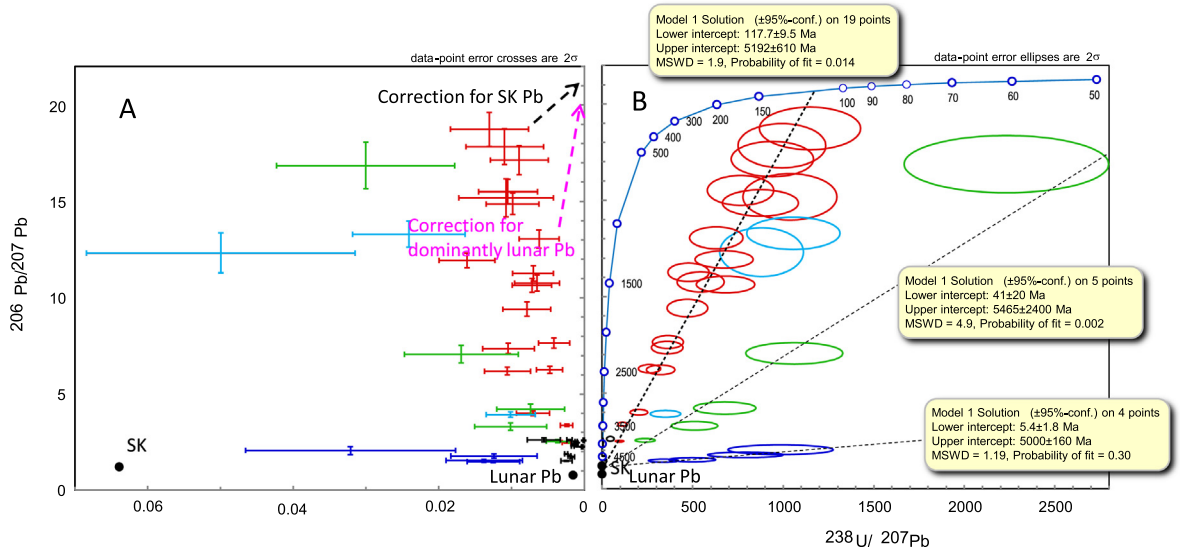

Fig. 6. Strongly discordant SIMS analyses forming linear trends on modifed Terra-Wasserburg diagrams interpreted to represent three youngest groups of glass spherules. (A) $^{206}Pb/^{207}Pb$-$^{204}Pb/^{207}Pb$ plot showing that more concordant analyses appear to have higher $^{204}Pb/^{207}Pb$, suggesting larger contribution of terrestrial Pb as compare to the unsupported lunar Pb (both shown as black circles), dashed arrows indicate projections for correction when terrestrial or lunar Pb are used; (B) $^{206}Pb/^{207}Pb$-$^{238}U/^{207}Pb$ concordia showing best fit lines drawn through the analytical points and corresponding ages determined fom these lines; these lines also intersect vertical axis between terrestrial and lunar unsupported Pb, suggesting that apparent discordance is caused by the presence of these two components in different proportion. Coulours on both diagrams represent proposed age groups. Three analyses shown in light blue appear to fall of the trends in either $^{206}Pb/^{207}Pb$-$^{238}U/^{207}Pb$ or $^{206}Pb/^{207}Pb$-$^{204}Pb/^{207}Pb$ plot.

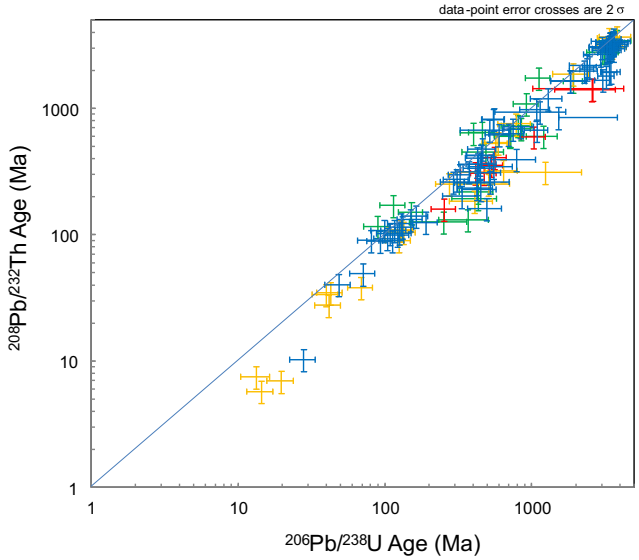

Fig. 7. Comparison of $^{208}Pb/^{232}Th$ and $^{206}Pb/^{238}U$ SIMS ages showing a general agreement between two systems over the entire range of ages, with possible hint that some of $^{208}Pb/^{232}Th$ ages are underestimated. Colours indicate major chemical groups of glass beads.

centrations (La 317-409x CI). Strontium to barium (Sr/Ba) ratios in the HASP glasses also show a clear KREEP signature (Fig. 10a) but with a more modest range (0.18–0.22). Their high contents of refractory incompatible elements, similar to those of KREEP-rich glasses, and the continuity of compositions with the KREEP-rich glasses, imply similar target lithologies but different conditions of the impacts to produce higher temperatures and volatile-loss of major and trace elements (e.g., Naney et al., 1976; Papike et al., 1977; Yakovlev et al., 2011). In contrast to the refractory incompatible elements, the HASP glasses show large ranges in moderately volatile elements such as Na, K, Rb and no correlations of these with more refractory elements of similar incompatibility such as Ba, La, or Th, which are well

Table 3
SIMS U-Pb analyses of investigated glass beads from the sample 14163.

Bead	204Pb (cps bkg corr)	1s % err	204Pb/ 206Pb	1s % err	207Pb/ 206Pb	1s % err	208Pb/ 206Pb	1s % err	238U/ 206Pb*	1s % err	232Th/ 238U*	1s % err	207/206 Age	+/- (2s)	238U/ 206Pb age	+/- (1s)	208Pb/ 232Th Age	+/- (1s)	238U/ 207Pb	1s % err	206Pb/ 207Pb	1s % err	204Pb/ 207Pb	1s % err		Model Age (Ma)	+/- (2s)	
Basaltic																									**Basaltic**			
W4	0.284	8	0.00063	8	0.4184	0.4	0.9940	0.3	1.65	9	4.11	4	3976	6	3059	290	2772	277	3.94	9	2.390	0.4	0.00150	8	W4	2419	266	**
BL9	0.022	27	0.00020	27	0.0663	1.5	2.3876	0.5	13.51	9	5.44	4	816	32	460	44	646	65	203.76	10	15.082	1.5	0.00300	27	BL9	456	190	*
B19	0.362	9	0.00076	9	0.3838	0.5	1.0203	0.4	1.60	12	4.32	12	3847	7	3123	377	2775	277	4.18	12	2.605	0.5	0.00199	9	B19	567	260	*
B20a	0.078	16	0.00013	16	0.4458	0.3	0.9272	0.3	1.24	12	4.03	12	4071	5	3801	460	3428	343	2.79	12	2.243	0.3	0.00029	16	B20a	3856	82	***
B20b	0.072	16	0.00012	15	0.4425	0.3	0.9306	0.3	1.25	12	4.03	12	4060	5	3796	459	3434	343	2.82	12	2.260	0.3	0.00026	15	B20b	3869	72	***
G13	0.071	13	0.00026	13	0.3156	0.5	1.0251	0.3	1.65	10	2.13	4	3548	7	3052	293	5158	516	5.23	10	3.169	0.5	0.00083	13	G13	2620	378	**
G39	0.037	18	0.00406	18	0.0812	4.2	2.3208	1.4	71.52	10	5.62	4	1226	83	90	9	116	12	880.74	11	12.314	4.2	0.04996	18	G39	85	35	*
R9	0.025	24	0.00061	24	0.0561	2.6	1.3309	0.8	55.70	10	2.82	4	455	58	115	11	171	17	993.60	10	17.837	2.6	0.01091	24	R9	114	48	*
R2x	0.018	35	0.00213	20	0.3841	1.8	0.4995	3.3	16.94	18	4.53	19	3848	27	370	68	131	13	44.10	19	2.604	1.8	0.00555	20	R2x	269	150	*
R4a	0.226	10	0.00208	10	0.3149	1.0	1.0848	0.8	8.50	11	4.17	11	3545	15	717	80	610	61	26.99	11	3.176	1.0	0.00659	11	R4a	567	260	*
R4b	0.188	12	0.00249	12	0.3437	1.1	1.0700	0.8	8.52	11	4.17	11	3679	17	715	80	600	60	24.79	11	2.909	1.1	0.00723	12	R4b	548	260	*
R4c	0.201	11	0.00185	11	0.3446	1.0	1.0881	0.7	8.52	11	4.17	11	3683	15	715	79	610	61	24.73	11	2.902	1.0	0.00538	11	R4c	551	260	*
R5	0.009	38	0.00031	38	0.0608	2.8	1.9476	0.8	15.48	10	3.92	4	630	60	404	39	638	64	254.76	10	16.461	2.8	0.00504	38	R5	401	170	*
R6	0.025	24	0.00024	24	0.0874	1.3	1.1509	0.5	5.28	10	2.43	4	1370	26	1119	108	1740	174	60.33	10	11.436	1.3	0.00276	24	R6	1108	204	**
W3	0.045	19	0.00075	19	0.1600	1.4	1.5715	0.7	41.83	9	5.04	4	2455	24	152	14	150	15	261.49	10	6.251	1.4	0.00472	19	W3	138	60	*
B8	0.030	23	0.00048	22	0.1646	1.6	1.1271	0.6	7.45	12	4.11	12	2504	27	812	97	731	73	45.27	12	6.074	1.6	0.00289	22	B8	748	350	*
BL8x	0.011	64	0.00008	64	0.0908	1.4	0.6300	1.3	4.85	12	4.29	12	1442	26	1208	143	602	60	53.45	12	11.014	1.4	0.00085	64	BL8x	1203	520	*
B56x	0.061	20	0.00073	20	0.0649	2.2	0.6312	1.6	14.40	13	4.04	13	771	46	433	55	218	22	221.96	13	15.412	2.2	0.01122	20	B56x	427	190	*
B69x	0.066	19	0.00049	30	0.0835	2.4	1.0231	2.8	14.44	17	7.39	17	1280	47	432	73	193	19	172.99	17	11.980	2.4	0.00587	30	B69x	421	210	*
B73b	0.113	15	0.00095	15	0.3297	0.9	1.0301	0.6	7.10	8	4.18	8	3616	14	849	64	690	69	21.53	8	3.033	0.9	0.00289	15	B73b	672	300	*
R7	0.030	28	0.00037	28	0.0921	1.8	1.2534	0.7	12.68	16	4.39	16	1468	35	489	77	450	45	137.76	16	10.863	1.8	0.00399	28	R7	475	230	*
R10x	0.013	43	0.00144	18	0.5103	1.2	0.5766	3.2	24.98	21	3.69	21	4271	17	253	53	126	13	48.95	21	1.959	1.2	0.00282	18	R10x	160	100	*
B7	0.020	27	0.00150	27	0.3665	2.0	1.0846	1.4	6.49	10	3.03	4	3777	31	924	88	1084	108	17.71	10	2.729	2.0	0.00409	27	B7	703	350	*
Feldspathic																									**Feldspathic**			
																									Feldspathic			
C10	0.004	58	0.00030	58	0.0668	4.0	0.5621	1.7	13.04	10	2.81	4	833	84	476	47	307	31	195.07	11	14.959	4.0	0.00455	58	C10	472	210	*
C12	0.045	19	0.00051	19	0.0577	1.8	1.3839	0.6	24.78	9	7.04	4	518	40	255	24	160	16	429.61	10	17.334	1.8	0.00877	19	C12	253	11	*
C2	0.009	41	0.00018	41	0.0787	2.0	1.5077	0.7	11.65	10	7.30	4	1165	40	531	51	355	36	148.01	10	12.706	2.0	0.00225	41	C2	522	230	*
C3	0.005	50	0.00143	50	0.0742	7.2	1.1549	2.6	14.96	11	4.98	4	1048	146	417	44	311	31	201.56	13	13.469	7.2	0.01931	51	C3	407	170	*
C5x	0.031	28	0.00049	35	0.1619	2.2	0.4804	2.6	2.00	31	3.29	31	2475	36	2617	800	1426	143	12.34	31	6.178	2.2	0.00305	35	C5x	2643	1080	**
C6x	0.059	20	0.00033	45	0.1662	2.1	0.6580	3.9	2.03	22	4.49	23	2520	36	2578	574	1407	141	12.23	22	6.016	2.1	0.00199	45	C6x	2600	956	**
C8	0.009	41	0.00038	41	0.0702	3.1	0.4590	1.4	10.96	10	2.06	4	934	64	563	54	407	41	156.16	10	14.249	3.1	0.00545	41	C8	557	230	*
HASP																									**HASP**			
B22	0.085	19	0.00024	19	0.3117	0.5	2.8987	0.3	1.45	9	10.31	9	3529	8	3382	295	3585	358	4.65	9	3.208	0.5	0.00076	20	B22	2894	346	**
B25	0.037	21	0.00084	21	0.1063	2.0	2.7535	0.7	50.06	10	10.19	4	1738	36	128	12	109	11	470.77	10	9.404	2.0	0.00788	21	B25	121	52	*
B33	0.043	24	0.00025	24	0.1167	1.4	2.6765	0.5	2.89	14	9.59	14	1907	24	1918	264	1866	187	24.73	14	8.567	1.4	0.00217	24	B33	1950	474	**
B30x	0.018	38	0.00041	23	0.0839	1.9	0.9858	1.3	9.55	12	6.43	12	1291	37	642	79	322	32	113.80	12	11.913	1.9	0.00485	23	B30x	629	280	*
B39	0.024	26	0.00054	26	0.1309	1.8	2.7460	0.7	47.52	10	11.15	4	2111	31	134	13	105	10	362.94	10	7.638	1.8	0.00413	26	B39	125	54	*
B40	0.029	24	0.00701	24	0.5652	3.3	1.4480	2.6	447.28	10	11.38	4	4421	48	14	1	6	1	791.30	11	1.769	3.3	0.01239	24	B40	7.8	4.1	*
B59	0.034	22	0.00143	22	0.3932	1.6	1.8996	1.0	93.15	10	10.80	4	3883	24	69	7	38	4	236.87	10	2.543	1.6	0.00364	22	B59	49	24	*
B64	0.042	17	0.00142	17	0.1360	1.9	2.9012	0.7	48.91	10	10.93	4	2177	32	130	13	109	11	359.59	10	7.352	1.9	0.01041	17	B64	120	52	*
B67	0.012	28	0.00005	28	0.3395	0.4	2.3601	0.2	1.39	10	9.65	10	3661	6	3489	344	3270	327	4.10	10	2.945	0.4	0.00015	28	B67	3626	19	****
B70	0.047	16	0.00176	16	0.2510	1.5	2.4016	0.8	51.09	10	10.58	4	3191	24	125	12	90	9	203.53	10	3.984	1.5	0.00701	16	B70	104	47	*
B76	0.049	16	0.00028	16	0.0892	0.9	2.6285	0.3	10.83	10	9.20	4	1407	18	569	54	527	53	121.45	10	11.217	0.9	0.00315	16	B76	555	230	*
B101	-0.002	41	0.00003	41	0.3869	0.4	2.5195	0.2	1.24	12	10.25	12	3859	6	3814	464	3658	366	3.20	12	2.585	0.4	0.00007	41	B101	3809	27	***
B95x	0.018	35	0.00069	29	0.1100	2.4	1.4615	2.1	15.29	16	10.45	16	1799	43	409	67	184	18	139.01	17	9.094	2.4	0.00630	29	B95x	389	260	*
G1	0.022	23	0.00239	23	0.1417	3.2	2.6413	1.3	150.20	10	10.24	4	2248	55	43	4	35	3	1059.78	10	7.056	3.2	0.01690	23	G1	39	17	*
G4	0.009	32	0.00005	34	0.3311	0.4	2.4046	0.4	1.36	12	10.90	12	3622	6	3560	412	3045	304	4.10	12	3.020	0.4	0.00015	34	G4	3585	22	****
G5x	0.044	24	0.00071	24	0.0707	2.8	2.9168	1.3	7.73	12	9.94	13	948	56	784	98	753	75	109.42	13	14.151	2.8	0.01003	24	G5x	777	340	*
G10x	0.079	18	0.00058	26	0.0755	2.3	1.3312	1.6	12.09	19	8.79	19	1082	47	512	97	252	25	160.05	19	13.243	2.3	0.00770	26	G10x	503	230	*
G9	0.034	19	0.00900	19	0.6550	2.9	1.1682	2.5	325.44	10	10.45	4	4635	41	20	2	7	1	496.86	11	1.527	2.9	0.01374	19	G9	9.1	5.1	*
G55x	0.039	27	0.00095	9	0.5803	0.5	0.4391	0.9	4.71	38	5.98	38	4459	7	1241	469	313	31	8.12	38	1.723	0.5	0.00164	9	G55x	751	650	*
R8	0.019	28	0.00019	28	0.0915	1.3	2.9377	0.5	10.39	10	10.52	4	1458	25	592	57	536	54	113.50	10	10.926	1.3	0.00208	28	R8	577	240	*
B6	0.031	22	0.01566	22	0.4877	4.8	1.6518	3.5	480.90	11	9.23	4	4205	71	13	1	8	1	985.95	12	2.050	4.8	0.03211	23	B6	7.3	3.5	*
B3	0.025	24	0.00307	24	0.3035	2.8	2.1758	1.6	154.46	10	10.28	4	3488	43	42	4	28	3	508.96	10	3.295	2.8	0.01011	24	B3	32	15	*
B2	0.014	32	0.00175	32	0.2379	3.0	2.4671	1.6	161.00	10	9.20	4	3106	48	40	4	34	3	676.78	10	4.204	3.0	0.00735	32	B2	33	15	*
B1	0.028	23	0.00046	23	0.0917	1.7	2.7957	0.6	22.90	10	9.73	4	1460	32	275	26	252	25	249.89	10	10.910	1.7	0.00497	23	B1	266	160	*
KREEP-rich																									**KREEP-rich**			
B88	0.004	39	0.00008	41	0.3419	0.6	0.9700	0.4	1.41	14	4.19	14	3671	9	3451	481	3068	307	4.13	14	2.925	0.6	0.00024	41	B88	3614	37	****

Bead	204Pb (cps bkg corr)	1s % err	204Pb/ 206Pb	1s % err	207Pb/ 206Pb	1s % err	208Pb/ 206Pb	1s % err	238U/ 206Pb*****	1s % err	232Th/ 238U*****	1s % err	207/206 Age	+/- (2s)	238U/ 206Pb age	+/- (1s)	208Pb/ 232Th Age	+/- (1s)	238U/ 207Pb	1s % err	206Pb/ 207Pb	1s % err	204Pb/ 207Pb	1s % err		Model Age (Ma)	+/- (2s)	
G26a	0.033	21	0.00006	22	0.1796	0.4	0.8470	0.2	2.12	5	3.59	5	2650	6	2488	133	2130	213	11.82	5	5.567	0.4	0.00032	22	G26a	2365	212	**
G26b	0.001	40	0.00003	40	0.1791	0.5	0.8500	0.2	2.22	5	3.59	5	2644	8	2394	128	2046	205	12.42	5	5.584	0.5	0.00015	40	G26b	2287	202	**
W2a	0.054	17	0.00006	17	0.3412	0.3	1.0677	0.2	1.45	6	4.92	6	3668	4	3388	213	2827	283	4.24	6	2.931	0.3	0.00018	17	W2a	3625	21	****
W2b	0.068	16	0.00008	16	0.3429	0.3	1.1115	0.5	1.55	6	4.92	6	3676	5	3215	202	2757	276	4.51	6	2.916	0.3	0.00023	16	W2b	3620	27	****
B31	0.054	17	0.00008	17	0.3800	0.3	1.0403	0.2	1.32	7	4.36	7	3832	5	3629	264	3355	335	3.48	7	2.632	0.3	0.00022	17	B31	3661	63	***
B27a	0.341	8	0.00028	8	0.3747	0.2	1.1097	0.2	1.38	6	4.64	6	3810	4	3511	199	3228	323	3.69	6	2.669	0.2	0.00075	8	B27a	3623	92	****
B50	0.065	19	0.00024	19	0.1739	0.8	1.1076	0.4	8.10	8	3.96	8	2595	13	750	58	687	69	46.60	8	5.751	0.8	0.00135	19	B50	686	290	*
B51	0.267	8	0.00023	9	0.3625	0.3	1.1766	0.3	1.40	6	4.74	6	3760	5	3467	225	3288	329	3.87	6	2.759	0.3	0.00064	9	B51	3599	78	****
B55	0.197	10	0.00013	10	0.3524	0.2	0.9781	0.2	1.39	6	3.98	6	3717	3	3504	222	3298	330	3.93	6	2.838	0.2	0.00037	10	B55	3628	42	****
B83	0.173	10	0.00049	10	0.2335	0.7	1.0774	0.3	5.18	25	4.40	25	3076	11	1138	288	934	93	22.18	25	4.283	0.7	0.00208	10	B83	998	620	*
B87	0.060	19	0.00004	20	0.3440	0.3	0.8482	0.2	1.41	5	3.68	5	3681	4	3454	161	3058	306	4.10	5	2.907	0.3	0.00011	20	B87	3594	32	***
G62	0.018	19	0.00003	23	0.3447	0.3	1.0626	0.2	1.39	6	4.55	6	3684	4	3498	204	3146	315	4.03	6	2.901	0.3	0.00008	23	G62	3625	23	***
G63a	0.039	20	0.00005	20	0.3428	0.2	1.0579	0.2	1.33	5	4.65	5	3675	4	3619	183	3194	319	3.87	5	2.917	0.2	0.00013	20	G63a	3572	38	***
G63b	0.019	23	0.00003	23	0.3435	0.3	1.0472	0.2	1.43	5	4.65	5	3678	4	3422	173	2958	296	4.16	5	2.911	0.3	0.00008	23	G63b	3617	24	***
G63c	0.029	20	0.00004	21	0.3410	0.3	1.0862	0.2	1.36	5	4.65	5	3667	4	3557	180	3206	321	3.98	5	2.933	0.3	0.00012	21	G63c	3575	34	***
B52x	0.046	23	0.00025	38	0.0684	2.4	0.7855	1.9	3.74	76	4.92	76	882	49	1527	1154	845	85	54.66	76	14.611	2.4	0.00367	38	B52x	1556	1200	**
G2	0.004	28	0.00014	30	0.0718	1.4	1.2483	0.5	8.74	13	4.53	13	979	28	698	93	627	63	121.81	13	13.935	1.4	0.00199	30	G2	693	310	*
B24	0.070	19	0.00053	19	0.0535	1.9	0.8531	0.6	19.31	8	2.96	8	352	43	325	27	299	30	360.71	8	18.679	1.9	0.00998	19	B24	324	130	*
B26	0.111	22	0.00007	22	0.3352	0.3	1.9149	0.2	1.44	5	4.04	5	3641	5	3398	173	5748	575	4.30	5	2.983	0.3	0.00021	22	B26	3589	26	****
B44a	0.050	18	0.00003	18	0.3342	0.2	0.9995	0.1	1.44	6	6.97	6	3636	4	3394	211	1915	191	4.32	6	2.993	0.2	0.00008	18	B44a	3616	10	****
B44b	0.020	30	0.00002	32	0.3348	0.3	0.9986	0.2	1.54	6	6.97	6	3639	4	3220	200	1794	179	4.61	6	2.987	0.3	0.00006	32	B44b	3625	9	****
B44c	0.020	25	0.00007	26	0.3349	0.4	0.9864	0.3	1.64	6	6.97	6	3640	6	3064	191	1670	167	4.91	6	2.986	0.4	0.00020	26	B44c	3590	26	****
B99x	0.051	22	0.00130	19	0.0555	3.1	2.3024	2.1	18.65	13	12.32	13	433	69	337	44	202	20	335.88	13	18.013	3.1	0.02343	19	B99x	333	150	*
W7	0.008	32	0.00005	34	0.2775	0.6	1.7244	0.3	1.51	10	7.47	10	3349	9	3275	337	2874	287	5.44	10	3.604	0.6	0.00017	34	W7	2879	432	**
W7	0.075	15	0.00004	15	0.2802	0.3	1.7312	0.2	1.67	9	6.41	4	3364	4	3028	285	3034	303	5.95	9	3.569	0.3	0.00015	15	W7	2665	382	**
BL11	0.004	33	0.00003	33	0.3341	0.3	1.0717	0.2	1.46	6	4.44	6	3636	5	3357	201	3085	309	4.38	6	2.993	0.3	0.00008	33	BL11	3618	11	**
BL11_27	0.036	28	0.00005	30	0.3317	0.3	1.0621	0.2	1.39	5			3625	4	3498	183			4.18	5	3.015	0.3	0.00015	30	BL11_27	3590	19	****
BL4	1.012	5	0.00131	5	0.5307	0.5	0.9975	0.4	1.33	15	4.11	15	4329	7	3615	539	3390	339	2.51	15	1.884	0.5	0.00247	5	BL4	2558	590	**
B9	0.030	23	0.00017	23	0.0563	1.3	1.7911	0.4	21.45	9	6.42	4	463	29	294	28	261	26	381.13	10	17.768	1.3	0.00307	23	B9	292	120	*
B10	0.035	33	0.00022	34	0.0797	1.4	1.5397	0.5	5.49	12	5.64	12	1189	27	1079	124	981	98	68.90	12	12.551	1.4	0.00272	34	B10	1084	250	*
B13	0.064	27	0.00016	28	0.3271	0.4	1.3879	0.3	1.41	8	5.57	8	3604	7	3452	267	3285	329	4.32	8	3.057	0.4	0.00048	28	B13	2915	304	**
B18x	0.086	17	0.00044	28	0.0580	2.5	1.0761	2.3	13.76	13	6.87	14	528	54	452	60	229	23	237.47	14	17.254	2.5	0.00763	28	B18x	450	210	*
B21x	0.034	27	0.00063	22	0.2218	1.3	0.9658	1.8	7.65	17	6.43	17	2994	21	792	134	393	39	34.51	17	4.508	1.3	0.00282	22	B21x	693	350	*
B23	0.034	22	0.00047	22	0.0766	1.8	1.8489	0.6	48.26	9	6.69	4	1111	36	132	13	115	12	629.84	10	13.050	1.8	0.00618	22	B23	129	55	*
B29x	60.317	1	0.00040	27	0.0628	2.2	0.9838	1.5	11.18	17	5.12	17	703	47	552	91	344	34	177.98	17	15.913	2.2	0.00644	27	B29x	549	270	*
B28x	0.101	16	0.00160	16	0.6617	1.0	0.6074	2.1	12.52	13	6.08	13	4650	14	495	64	161	16	18.92	13	1.511	1.0	0.00242	16	B28x	256	160	*
B43	0.078	15	0.00017	15	0.2499	0.5	1.7880	0.4	1.72	12	7.36	12	3184	7	2954	344	2670	267	6.88	12	4.002	0.5	0.00069	15	B43	2690	460	**
B48	0.030	28	0.00025	28	0.0621	2.0	1.1772	0.6	10.22	10	3.71	10	677	43	602	59	618	62	164.58	10	16.109	2.0	0.00401	28	B48	660	270	*
B47	0.064	19	0.00013	18	0.3463	0.4	2.3286	0.3	1.37	11	9.50	11	3691	6	3524	391	3316	332	3.97	11	2.887	0.4	0.00039	18	B47	3597	48	****
B46	0.050	18	0.00071	18	0.2966	1.0	2.0037	0.6	33.28	9	9.69	4	3452	16	191	18	125	13	112.21	10	3.372	1.0	0.00240	18	B46	153	71	*
B45	0.048	20	0.00005	22	0.3504	0.3	1.0142	0.2	1.43	6	4.28	6	3709	4	3424	210	3109	311	4.07	6	2.854	0.3	0.00015	22	B45	3589	45	***
B62a	0.608	8	0.00044	7	0.3945	0.2	0.7929	0.2	1.32	6	3.89	6	3888	4	3625	214	2892	289	3.36	6	2.535	0.2	0.00111	7	B62a	3600	150	****
B62b	0.727	6	0.00068	6	0.4333	0.2	0.9819	0.2	1.31	6	3.89	6	4029	4	3646	215	3549	355	3.03	6	2.308	0.2	0.00156	6	B62b	3608	240	****
B62c	0.907	6	0.00068	6	0.4336	0.3	0.9805	0.2	1.42	6	3.89	6	4030	4	3427	202	3292	329	3.29	6	2.306	0.3	0.00157	6	B62c	3606	240	****
B63	0.032	19	0.00068	19	0.0645	2.0	1.9845	0.6	49.28	10	6.62	4	757	43	130	12	123	12	764.43	10	15.513	2.0	0.01048	19	B63	127	54	*
B65	0.030	20	0.00062	20	0.0888	1.8	2.1834	0.6	42.40	10	7.88	4	1400	34	150	14	132	13	477.34	10	11.258	1.8	0.00699	20	B65	145	62	*
B68a	0.038	25	0.00014	25	0.1229	0.9	1.9023	0.4	3.02	14	7.39	14	1999	16	1843	249	1652	165	24.58	14	8.134	0.9	0.00118	25	B68a	1839	462	**
B68b	0.020	38	0.00006	38	0.1233	0.8	1.8916	0.3	3.02	14	7.39	14	2004	13	1843	249	1643	164	24.51	14	8.111	0.8	0.00047	38	B68b	1839	456	**
B71	0.049	16	0.00181	16	0.0752	2.6	2.3045	0.8	79.38	10	6.49	4	1075	51	81	8	90	9	1055.11	10	13.293	2.6	0.02409	16	B71	78	33	*
B74	0.104	13	0.00040	13	0.2003	1.4	1.5397	0.3	2.33	11	6.43	11	2828	22	2301	245	1977	198	11.64	11	4.993	1.4	0.00201	13	B74	2163	366	**
B75	0.029	20	0.00069	20	0.0534	2.4	1.7093	0.7	61.31	10	6.03	4	345	54	104	10	93	9	1148.50	10	18.734	2.4	0.01300	21	B75	103	44	*
B77	0.055	15	0.00170	15	0.1616	1.7	2.4515	0.7	52.20	10	9.55	4	2473	28	122	12	99	10	322.97	10	6.187	1.7	0.01054	15	B77	110	48	*
B78	0.089	12	0.00135	12	0.0839	1.6	1.1358	0.6	56.49	10	4.53	4	1289	31	113	11	90	9	673.71	10	11.925	1.6	0.01609	12	B78	109	46	*
B79	0.024	22	0.00052	22	0.0583	2.2	1.8497	0.6	54.82	10	6.29	4	543	48	117	11	108	11	939.67	10	17.140	2.2	0.00891	22	B79	115	49	*
B84	0.086	14	0.00006	14	0.3682	0.3	0.9351	0.2	1.33	5	3.92	5	3784	4	3623	182	3345	334	3.60	5	2.716	0.3	0.00017	14	B84	3654	45	***
B81	0.156	15	0.00051	16	0.0917	0.8	1.1104	0.4	4.51	12	4.06	12	1461	16	1291	156	1189	119	49.19	12	10.907	0.8	0.00559	16	B81	1304	308	**
B86x	0.315	10	0.00062	27	0.0736	2.5	1.4716	1.6	11.78	17	9.57	17	1031	51	525	89	262	26	160.01	17	13.581	2.5	0.00843	27	B86x	517	260	*
B89	0.045	16	0.00258	16	0.2557	1.9	2.3936	1.0	89.64	10	10.99	4	3220	29	72	7	49	5	350.56	10	3.911	1.9	0.01009	17	B89	59	26	*
B90	0.034	19	0.00067	19	0.0941	1.7	1.3525	0.7	64.13	10	3.94	4	1510	32	100	10	108	11	681.72	10	10.630	1.7	0.00717	19	B90	96	41	*
B91	0.053	22	0.00043	22	0.0696	1.7	1.9353	0.6	7.18	11	7.46	11	918	35	840	95	717	72	103.13	11	14.359	1.7	0.00618	22	B91	836	360	*
B92	0.060	14	0.00845	14	0.6770	2.1	1.2352	1.8	229.34	10	10.56	4	4683	30	28	3	10	1	338.74	10	1.477	2.1	0.01248	14	B92	12	7.4	*
B93	0.030	20	0.00036	20	0.0726	1.5	3.0162	0.4	20.29	10	10.94	4	1003	30	310	30	273	27	279.41	10	13.774	1.5	0.00491	20	B93	305	120	*
B94	0.152	11	0.00093	11	0.2314	1.0	1.6363	0.4	2.22	12	6.45	12	3062	16	2394	294	2184	218	9.61	12	4.322	1.0	0.00404	11	B94	2222	452	**
B98x	0.069	19	0.00108	19	0.0549	3.1	1.0361	1.5	14.63	13	6.10	13	409	70	426	57	233	23	266.31	14	18.208	3.1	0.01963	19	B98x	423	190	*

B97	0.538	6	0.00076	6	0.3225	0.6	1.0344	0.3	1.85	5			3582	9	2781	144	0	0	5.75	5	3.101	0.6	0.00235	6	B97	2372	204	**
G3	0.021	24	0.00060	24	0.0929	2.0	2.2338	0.7	50.51	10	8.64	4	1486	38	126	12	103	10	543.72	10	10.764	2.0	0.00647	24	G3	121	52	*
G7	0.009	22	0.00021	27	0.3032	0.8	1.0077	0.5	1.40	8	7.16	8	3486	12	3481	262	1940	194	4.61	8	3.299	0.8	0.00068	27	G7	2980	318	**
G8x	0.099	17	0.00118	17	0.0599	2.3	0.5860	1.5	11.92	9	3.20	9	599	50	519	47	308	31	199.07	9	16.706	2.3	0.01974	17	G8x	514	210	*
G11	1.047	16	0.00132	9	0.3782	0.4	0.9794	0.3	1.32	6	4.17	6	3825	6	3627	220	3301	330	3.50	6	2.644	0.4	0.00349	9	G11	2942	262	**
G21x	0.036	26	0.00027	38	0.0594	2.5	1.1959	1.6	14.59	15	6.43	15	582	54	427	65	256	26	245.61	15	16.833	2.5	0.00457	38	G21x	425	190	*
G30	0.018	35	0.00029	35	0.0569	2.5	1.8248	0.8	11.94	19	4.52	19	488	56	519	96	672	67	209.78	19	17.575	2.5	0.00507	35	G30	518	240	*
G29	0.023	21	0.00017	21	0.0779	1.0	1.2917	0.4	5.44	9	7.02	9	1145	20	1089	98	673	67	69.73	9	12.830	1.0	0.00219	21	G29	1096	190	**
G28a	0.041	15	0.00004	17	0.3429	0.2	0.9411	0.2	1.41	6	4.11	6	3676	3	3456	214	3042	304	4.11	6	2.916	0.2	0.00011	17	G28a	3595	28	***
G28b	0.014	23	0.00002	24	0.3430	0.2	0.9451	0.2	1.51	6	4.11	6	3676	3	3276	203	2865	286	4.40	6	2.915	0.2	0.00007	24	G28b	3623	21	***
G36	0.015	56	0.00028	56	0.0674	2.4	1.4496	0.8	13.37	11	4.53	11	849	50	465	50	478	48	198.42	11	14.843	2.4	0.00420	56	G36	460	210	*
G43	0.080	12	0.00097	12	0.4020	0.7	1.0571	0.5	38.80	10	3.91	4	3917	11	164	16	140	14	96.53	10	2.488	0.7	0.00242	12	G43	115	58	*
G46a	-0.003	34	0.00003	38	0.3608	0.4	1.4955	0.3	1.32	12	6.61	12	3753	7	3644	452	3207	321	3.65	12	2.772	0.4	0.00008	38	G46a	3694	30	***
G46b	-0.009	56	0.00001	58	0.3566	0.4	1.4829	0.3	1.42	12	6.61	12	3735	6	3445	427	2973	297	3.97	12	2.804	0.4	0.00003	58	G46b	3711	18	***
G46c	0.001	36	0.00004	36	0.3599	0.5	1.5792	0.3	1.33	12	6.61	12	3749	7	3623	449	3349	335	3.68	12	2.779	0.5	0.00011	36	G46c	3665	42	***
G47a	0.043	24	0.00042	24	0.0744	1.8	1.3870	0.6	13.72	11	4.74	11	1052	36	454	49	427	43	184.41	11	13.445	1.8	0.00569	24	G47a	446	190	*
G47b	0.063	22	0.00056	23	0.0687	1.8	1.3658	0.6	13.62	11	4.74	11	890	37	457	49	423	42	198.19	11	14.556	1.8	0.00809	23	G47b	451	190	*
G51	0.030	20	0.00178	20	0.0593	3.6	2.2411	1.0	132.32	10	8.48	4	577	78	49	5	40	4	2232.35	10	16.871	3.6	0.03003	20	G51	47	20	*
G53a	0.030	28	0.00034	28	0.0688	2.0	1.3516	0.6	11.10	9	2.94	9	893	41	556	48	821	82	161.36	9	14.531	2.0	0.00491	28	G53a	550	230	*
G53b	0.045	29	0.00072	30	0.0705	2.4	1.3536	0.8	11.20	9	2.94	9	944	49	551	48	815	81	158.87	9	14.179	2.4	0.01023	30	G53b	543	220	*
G59a	0.044	19	0.00060	20	0.0711	1.7	1.5757	0.6	14.54	9	5.37	9	961	35	429	37	404	40	204.43	9	14.063	1.7	0.00846	20	G59a	422	170	*
G59b	0.018	27	0.00048	28	0.0583	2.2	1.3986	0.7	14.44	9	5.37	9	541	47	432	37	361	36	247.58	9	17.149	2.2	0.00817	29	G59b	429	170	*
G58	0.036	18	0.00066	18	0.0673	1.9	1.2452	0.6	58.82	10	4.19	4	846	39	109	10	102	10	874.36	10	14.864	1.9	0.00982	18	G58	107	45	*
G61x	0.044	24	0.00039	24	0.0565	2.2	1.6430	1.2	13.97	12	7.02	12	470	49	446	52	336	34	247.51	12	17.714	2.2	0.00693	24	G61x	444	190	*
G64x	0.044	24	0.00066	24	0.0570	2.9	1.3570	1.7	13.96	14	5.39	14	491	63	446	63	361	36	244.92	14	17.547	2.9	0.01151	24	G64x	444	210	*
B5	0.016	30	0.00071	30	0.0659	3.2	1.7909	1.0	68.26	10	5.96	4	802	68	94	9	89	9	1036.46	10	15.183	3.2	0.01072	30	B5	92	39	*
B4	0.031	22	0.00038	22	0.1204	1.3	2.4874	0.5	16.75	10	9.47	4	1963	23	374	36	314	31	139.05	10	8.304	1.3	0.00315	22	B4	354	170	*

* Constrained using 3 point planes fit through analysis, unsupported lunar Pb (Silver, 1972) and terrestrial Pb (Stacey and Kramers, 1975).

** Estimated by projecting individual analyses to concordia parallel to the planes defined for separate groups of glasses in 238U/206Pb-207Pb/206Pb-204Pb/206Pb coordinates.

*** Corrcted using unsupported Pb composition of Silver (1972).

**** Corrected for mixed lunar-contamination Pb composition, determined from intercept of best fit line drawn through the data in 207Pb/206Pb-204Pb/206Pb coordinates and mixing line between Stacey and Kramers (1975) Pb and lunar Pb from Silver (1972).

***** Ratios estimated using BCR-2G concentrations from: Gao et al., 2002 (Pb = 10.9 ppm; U = 1.7 ppm; Th = 5.5 ppm). Norman et al., 1998 (Pb = 11.5 ppm; U = 1.73 ppm; Th = 6.1 ppm). Dulski, 2001 (Pb = 10 ppm; U = 1.664 ppm; Th = 5.99 ppm). Jochum and Nohl, 2008 (Pb = 11 ppm; U = 1.69 ppm; Th = 5.9 ppm).

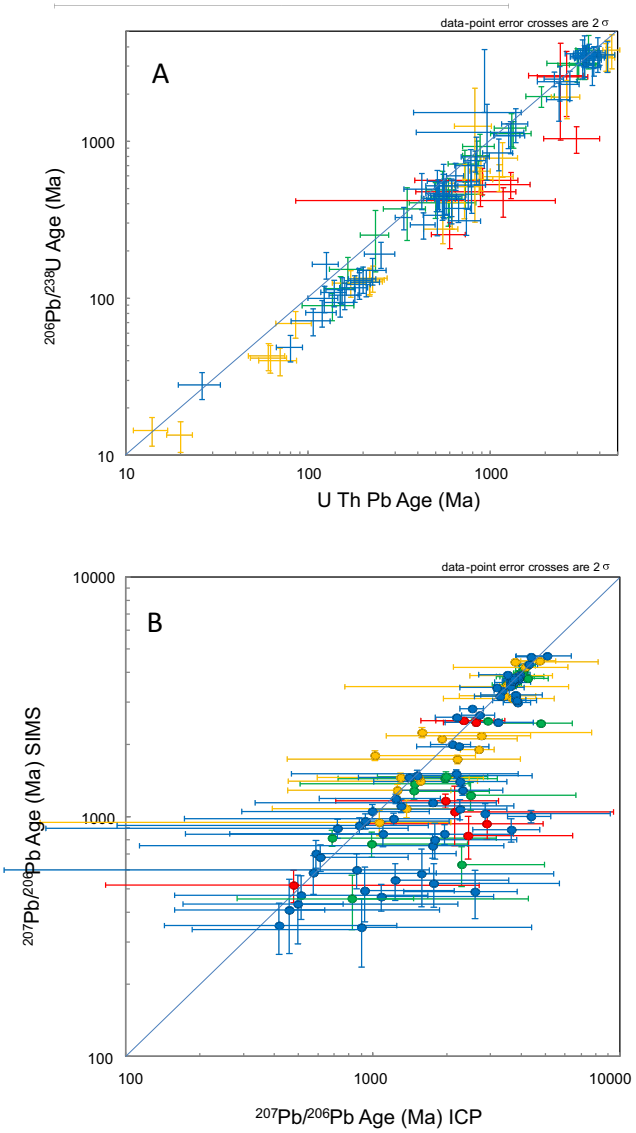

Fig. 8. Comparison of SIMS and ICP MS ages showing remarkable similarity of A –Total ICP MS ages and $^{206}Pb/^{238}U$ SIMS ages and B - $^{207}Pb/^{206}Pb$ ages obtained by both methods. Colours indicate major chemical groups of glass beads.

correlated with each other. Somewhat surprisingly, U concentrations in the HASP and KREEP-rich glasses are correlated more strongly with the moderately volatile elements than with refractory elements (Fig. 11a and b). The anomalously low U concentrations in these glasses may reflect volatile loss of U as increasing Th/U is correlated with low concentrations of other volatile elements such as Na, K, and Rb (e.g., high Ba/Rb) but not with more refractory elements such as Sr and Ba (Fig. 4c, d, e and f). Uranium, therefore, appears to behave as a moderately volatile element during formation of the HASP glasses, possibly due to the volatility of U-oxide species (e.g., Ackermann et al., 1956; Chapman and Meadows 1963).

The impact-generated mare glasses analysed for this study have TiO_2 contents ranging from 0.68 wt% (VLT) to 5.68 wt% (low-Ti), presumably reflecting the diversity of mare basalt flow compositions contributing to these glasses. In comparison, volcanic glasses from the same sample of regolith have lower TiO_2 concentrations with only one out of 26 investiaged beads having TiO_2 contents slightly higher than 2 wt% and another two around 1.2% (Nemchin et al., 2011). The rest of the volcanic glasses have TiO_2 concentration near to or lower than 1 wt%. The mare impact glasses also have systematically higher Sc, V, Mn, and Cr contents than the other chemical groups (Fig. 12), consistent with a greater fraction of mare basalt in these glasses. Rare earth element patterns of the mare glasses range from slightly to strongly LREE-enriched (Fig. 9), consistent with incorporation of a KREEP component into these glasses either during impact melting or during magmatic evolution of the target basalts.

The REE patterns of the feldspathic glasses are highly variable and range from La ~ 6x CI with positive Eu anomalies to more enriched compositions with La ~ 160x

Table 4
ICP MS U-Pb analyses of investigated glass beads from the sample 14163.

	Measured								BCR corrected														
	207Pb/206Pb	1s (abs)	208Pb/206Pb	1s (abs)	206Pb/238U	1s (abs)	232Th/238U	1s (abs)	207Pb/206Pb	1s (abs)	208Pb/206Pb	1s (abs)	206Pb/238U	1s (abs)	232Th/238U	1s (abs)	Pb (ppm)	Th (ppm)	U (ppm)	Th U Pb age	+/- (1s)	7/6 age	+/- (1s)
Basaltic																							
W4	0.43	0.05	0.99	0.09	0.803	0.108	3.2	0.5	0.43	0.05	1.00	0.09	0.751	0.108	4.1	0.5	0.876	2.36	0.546	3294	286	3998	130
BL9	0.07	0.05	2.32	0.49	0.097	0.018	6.5	0.8	0.07	0.05	2.35	0.49	0.091	0.018	8.2	0.8	0.327	6.39	0.727	730	89	686	1240
BL10	0.12	0.41	2.47	0.63	0.064	0.014	6.2	0.7	0.12	0.41	2.50	0.63	0.060	0.014	7.8	0.7	0.271	7.35	0.882	523	66	2414	2656
B19	0.37	0.05	1.48	2.94	0.666	0.075	3.3	0.4	0.38	0.05	1.50	2.94	0.623	0.075	4.1	0.4	2.06	6.31	1.46	3000	476	3842	339
B20	0.44	0.04	0.93	0.05	0.859	0.097	3.0	0.3	0.44	0.04	0.94	0.05	0.803	0.097	3.8	0.3	2.25	5.44	1.35	3458	257	4038	125
B32	0.54	0.20	2.10	0.43	0.065	0.014	6.5	0.9	0.55	0.20	2.12	0.43	0.061	0.014	8.2	0.9	0.253	8.11	0.928	450	60	4342	346
G13	0.30	0.06	1.02	0.13	0.703	0.154	3.2	0.7	0.30	0.06	1.03	0.13	0.658	0.154	4.0	0.7	0.396	1.17	0.276	3059	351	3483	218
G39	0.09	0.32	2.87	3.01	0.018	0.009	5.9	0.8	0.10	0.32	2.91	3.01	0.017	0.009	7.5	0.8	0.046	4.84	0.607	136	21	2496	2079
R9	0.06	0.07	1.33	0.35	0.023	0.005	3.5	0.3	0.06	0.07	1.35	0.35	0.021	0.005	4.4	0.3	0.126	9.92	2.1	151	14	826	1722
R2	0.44	0.17	1.10	0.30	0.063	0.011	3.4	0.4	0.45	0.17	1.12	0.30	0.059	0.011	4.3	0.4	0.131	4.33	0.956	349	45	4111	415
R4	0.35	0.07	1.06	0.13	0.126	0.013	3.1	0.2	0.35	0.07	1.07	0.13	0.118	0.013	3.9	0.2	0.436	6.54	1.57	725	70	3695	156
R5	0.18	0.18	1.76	0.43	0.087	0.026	4.7	0.6	0.18	0.18	1.79	0.43	0.081	0.026	5.9	0.6	0.162	3.52	0.552	597	119	2292	1335
R6	0.09	0.04	1.15	0.19	0.235	0.044	3.2	0.6	0.09	0.04	1.17	0.19	0.220	0.044	4.0	0.6	0.28	2.22	0.516	1337	168	1479	486
W3	0.57	0.18	1.60	0.32	0.090	0.037	3.7	0.4	0.57	0.18	1.62	0.32	0.084	0.037	4.7	0.4	0.738	9.78	1.96	166	86	4800	808
B8	0.21	0.04	1.09	0.12	0.143	0.016	3.1	0.2	0.21	0.04	1.10	0.12	0.134	0.016	3.9	0.2	0.979	12.4	3.02	846	71	2924	209
BL8	0.10	0.03	1.16	0.18	0.220	0.024	3.2	0.2	0.11	0.03	1.18	0.18	0.206	0.024	4.0	0.2	0.684	5.54	1.29	1310	130	1965	620
B56	0.06	0.03	1.21	0.17	0.074	0.009	3.0	0.2	0.06	0.03	1.22	0.17	0.069	0.009	3.8	0.2	0.515	11.2	2.77	500	41	992	715
B69	0.09	0.05	2.11	0.34	0.074	0.012	5.6	0.5	0.09	0.05	2.14	0.34	0.069	0.012	7.0	0.5	0.453	10.5	1.42	589	56	1472	751
B73	0.41	0.03	1.03	0.12	0.373	0.026	3.1	0.3	0.41	0.03	1.05	0.12	0.349	0.026	4.0	0.3	2.04	10.7	2.56	1910	170	3931	106
R7	0.11	0.03	1.23	0.16	0.084	0.012	3.3	0.2	0.11	0.03	1.25	0.16	0.079	0.012	4.2	0.2	0.406	8.38	1.91	545	49	1982	468
R10	0.50	0.11	0.94	0.19	0.043	0.008	2.7	0.2	0.50	0.11	0.96	0.19	0.040	0.008	3.5	0.2	0.244	11	2.98	235	21	4221	171
B7	0.51	0.22	1.17	0.51	0.029	0.009	3.1	0.4	0.51	0.22	1.18	0.51	0.027	0.009	4.0	0.4	0.059	4.02	0.954	879	17	4244	444
Feldspathic																							
W1	0.54	2.27	1.24	3.55	0.054	0.050	2.6	1.0	0.54	2.27	1.26	3.55	0.050	0.050	3.3	1.0	0.0069	0.352	0.113	191	91	3132	3408
C10	0.09	0.18	0.73	0.47	0.185	0.078	1.5	0.5	0.09	0.18	0.74	0.47	0.173	0.078	1.8	0.5	0.036	0.285	0.149	885	248	2437	2008
C12	0.06	0.05	1.49	0.25	0.085	0.016	3.7	0.4	0.06	0.05	1.51	0.25	0.080	0.016	4.7	0.4	0.402	7.94	1.58	601	63	479	1113
C1	0.17	0.08	1.39	0.23	0.608	0.177	4.4	1.2	0.18	0.08	1.40	0.23	0.569	0.177	5.6	1.2	0.371	1.31	0.23	2975	502	2617	407
C2	0.12	0.09	1.38	0.37	0.208	0.043	3.6	0.6	0.12	0.09	1.39	0.37	0.195	0.043	4.5	0.6	0.29	2.49	0.519	1299	178	1971	632
C5	0.17	0.06	0.91	0.15	0.535	0.153	2.6	0.8	0.17	0.06	0.92	0.15	0.501	0.153	3.3	0.8	0.368	1.28	0.389	2429	404	2614	341
C6	0.14	0.06	1.16	0.21	0.526	0.109	3.5	0.9	0.14	0.06	1.18	0.21	0.492	0.109	4.5	0.9	0.401	1.49	0.332	2622	403	2338	386
C7	0.20	2.19	0.59	2.40	0.086	0.672	1.7	8.5	0.20	2.19	0.60	2.40	0.080	0.672	2.1	8.5	0.0091	0.127	0.025	842	844	5941	1577
C8	0.22	0.24	0.69	0.39	0.201	0.174	1.3	0.7	0.23	0.24	0.70	0.39	0.188	0.174	1.7	0.7	0.041	0.284	0.175	905	259	2902	988
C9	0.55	0.90	1.44	0.94	0.692	1.185	4.4	5.0	0.56	0.90	1.46	0.94	0.647	1.185	5.6	5.0	0.045	0.196	0.052	2143	955	4508	753

HASP																							
B11	0.23	0.16	2.57	0.87	0.021	0.005	6.5	0.5	0.23	0.16	2.61	0.87	0.020	0.005	8.3	0.5	0.222	18.8	2.12	173	20	2830	576
B22	0.31	0.03	2.62	0.17	0.738	0.060	7.7	0.7	0.31	0.03	2.65	0.17	0.690	0.060	9.7	0.7	6.63	16.8	1.63	4432	202	3518	126
B25	0.14	0.12	2.54	0.94	0.030	0.009	7.3	0.7	0.14	0.12	2.58	0.94	0.028	0.009	9.3	0.7	0.207	14.4	1.43	218	19	2206	878
B26b	0.16	0.20	3.41	1.08	0.026	0.008	8.6	1.1	0.17	0.20	3.45	1.08	0.024	0.008	10.9	1.1	0.228	15.9	1.36	225	27	2484	995
B33	0.18	0.04	2.52	0.19	0.370	0.048	7.3	0.9	0.18	0.04	2.55	0.19	0.346	0.048	9.2	0.9	2.81	14	1.46	2634	236	2685	209
B30	0.08	0.03	1.91	0.24	0.112	0.013	4.8	0.3	0.08	0.03	1.93	0.24	0.105	0.013	6.1	0.3	1.01	14.6	2.27	887	56	1261	405
B39	0.12	0.11	2.78	0.76	0.029	0.008	8.0	0.7	0.12	0.11	2.82	0.76	0.027	0.008	10.1	0.7	0.23	15.6	1.44	227	22	1899	972
B40	3.17	9.33	7.97	20.32	0.004	0.003	8.1	0.8	3.22	9.33	8.07	20.32	0.003	0.003	10.2	0.8	0.014	15.6	1.43	14	1	3775	2201
B59	0.50	0.55	2.77	2.20	0.014	0.006	8.3	0.8	0.50	0.55	2.81	2.20	0.013	0.006	10.5	0.8	0.087	16	1.39	85	9	3911	714
B64	0.19	0.16	2.92	0.92	0.028	0.006	8.1	0.7	0.19	0.16	2.95	0.92	0.026	0.006	10.2	0.7	0.222	15.7	1.41	219	21	2749	808
B67	0.33	0.02	2.34	0.12	0.768	0.071	7.3	0.6	0.33	0.02	2.37	0.12	0.718	0.071	9.2	0.6	7.49	19.3	2	4319	183	3636	122
B70	0.31	0.21	2.58	0.99	0.024	0.007	7.3	0.8	0.31	0.21	2.62	0.99	0.022	0.007	9.2	0.8	0.168	14.8	1.5	171	18	3406	582
B76	0.09	0.03	2.71	0.45	0.108	0.015	7.2	0.6	0.09	0.03	2.75	0.45	0.101	0.015	9.1	0.6	0.913	15.3	1.56	871	81	1556	550
B82	0.54	0.23	2.00	0.56	0.054	0.012	9.3	1.2	0.55	0.23	2.03	0.56	0.050	0.012	11.8	1.2	0.33	19.6	1.55	268	38	4331	477
B101	0.39	0.04	2.47	0.10	0.863	0.098	7.8	0.9	0.39	0.04	2.50	0.10	0.807	0.098	9.8	0.9	7.07	16.5	1.61	4648	252	3863	107
B95	0.08	0.05	2.99	0.40	0.070	0.011	7.9	0.8	0.08	0.05	3.03	0.40	0.065	0.011	10.0	0.8	0.674	16.4	1.57	617	55	1020	795
G1	0.13	0.44	4.27	9.30	0.009	0.004	7.3	0.7	0.13	0.44	4.32	9.30	0.008	0.004	9.2	0.7	0.065	16.3	1.64	61	7	1585	3063
G4	0.32	0.03	2.53	0.13	0.788	0.085	8.2	0.8	0.32	0.03	2.56	0.13	0.737	0.085	10.3	0.8	6.43	16.9	1.55	4389	223	3584	101
G5	0.08	0.04	2.82	0.31	0.138	0.016	7.5	0.9	0.08	0.04	2.85	0.31	0.129	0.016	9.5	0.9	1.26	15.6	1.57	1166	124	1060	508
G10	0.09	0.04	2.52	0.54	0.088	0.016	6.7	0.7	0.09	0.04	2.55	0.54	0.083	0.016	8.4	0.7	0.881	17.4	1.98	722	77	1370	489
G49	0.21	0.18	3.07	0.96	0.027	0.007	8.3	0.8	0.21	0.18	3.11	0.96	0.025	0.007	10.5	0.8	0.22	15.9	1.41	215	23	2869	799
G50	0.82	0.15	1.00	0.19	0.745	0.159	5.5	1.4	0.84	0.15	1.01	0.19	0.697	0.159	7.0	1.4	3.04	13.5	1.94	2645	668	4894	462
G55	0.70	0.10	0.90	0.10	0.227	0.080	4.4	0.4	0.71	0.10	0.91	0.10	0.212	0.080	5.5	0.4	1	15.2	2.54	825	95	4737	379
R8	0.09	0.04	3.07	0.54	0.137	0.022	8.3	0.7	0.10	0.04	3.11	0.54	0.128	0.022	10.5	0.7	1.12	14.9	1.32	1123	104	1525	465
B6	0.98	1.85	3.88	11.61	0.005	0.002	5.8	0.4	0.99	1.85	3.93	11.61	0.004	0.002	7.3	0.4	0.023	16.4	2.1	20	2	4143	1011
B3	0.29	0.42	2.98	1.71	0.010	0.005	8.7	0.9	0.29	0.42	3.02	1.71	0.009	0.005	11.0	0.9	0.068	17.3	1.47	62	7	3486	1356
B2	0.46	0.51	3.07	2.55	0.009	0.004	7.3	0.8	0.47	0.51	3.11	2.55	0.009	0.004	9.3	0.8	0.067	14.5	1.46	70	8	3684	877
B1	0.08	0.06	3.11	0.62	0.063	0.012	7.9	0.8	0.08	0.06	3.15	0.62	0.059	0.012	9.9	0.8	0.668	18.4	1.74	548	58	1295	757
KREEP-rich																							
B88	0.32	0.04	0.98	0.07	0.757	0.099	3.2	0.5	0.33	0.04	0.99	0.07	0.708	0.099	4.0	0.5	1.36	3.72	0.888	3221	237	3608	129
G26	0.18	0.01	0.86	0.04	0.503	0.025	2.6	0.1	0.18	0.01	0.87	0.04	0.471	0.025	3.3	0.1	3.61	14.5	4.04	2245	136	2707	208
W2	0.34	0.02	1.12	0.05	0.739	0.043	3.7	0.3	0.34	0.02	1.14	0.05	0.691	0.043	4.6	0.3	7.39	21	4.27	3322	198	3664	121
B31	0.38	0.02	1.03	0.05	0.808	0.055	3.2	0.2	0.38	0.02	1.05	0.05	0.756	0.055	4.1	0.2	4.62	11.5	2.64	3489	142	3822	96
B27	0.38	0.02	1.11	0.04	0.774	0.041	3.5	0.2	0.39	0.02	1.12	0.04	0.724	0.041	4.4	0.2	8.03	20.6	4.44	3496	157	3834	94
B50	0.13	0.02	1.14	0.08	0.132	0.010	2.9	0.1	0.14	0.02	1.16	0.08	0.123	0.010	3.7	0.1	1.67	21.2	5.36	831	59	2194	198
B51	0.37	0.02	1.17	0.04	0.761	0.046	3.6	0.2	0.38	0.02	1.18	0.04	0.712	0.046	4.5	0.2	8.23	21.2	4.47	3513	188	3797	74
B55	0.40	0.02	0.98	0.03	0.772	0.046	3.0	0.2	0.40	0.02	1.00	0.03	0.722	0.046	3.8	0.2	8.03	20.4	5.12	3329	238	3882	116
B83	0.40	0.11	1.06	0.11	0.206	0.049	3.3	0.3	0.40	0.11	1.07	0.11	0.193	0.049	4.2	0.3	1.67	19.1	4.34	960	284	3796	188
B87	0.34	0.02	0.84	0.03	0.758	0.033	2.8	0.1	0.34	0.02	0.85	0.03	0.709	0.033	3.5	0.1	7.16	19.8	5.38	3038	134	3675	152
G62	0.34	0.02	1.06	0.04	0.770	0.042	3.3	0.2	0.35	0.02	1.07	0.04	0.721	0.042	4.2	0.2	7.43	20	4.4	3357	176	3668	135
G63	0.34	0.01	1.08	0.04	0.749	0.035	3.4	0.2	0.35	0.01	1.09	0.04	0.700	0.035	4.3	0.2	7.99	22.2	4.77	3310	141	3664	105
B52	0.51	0.41	1.24	0.24	0.286	0.202	3.8	1.0	0.52	0.41	1.26	0.24	0.267	0.202	4.8	1.0	0.566	7.03	1.43	929	275	3642	552
G2	0.07	0.02	1.25	0.18	0.122	0.015	3.4	0.3	0.07	0.02	1.27	0.18	0.114	0.015	4.3	0.3	0.709	10.2	2.25	782	71	1215	521

B24	0.05	0.02	0.88	0.10	0.055	0.004	2.2	0.1	0.05	0.02	0.90	0.10	0.052	0.004	2.7	0.1	0.696	19.5	6.58	336	18	417	418
B26	0.33	0.01	1.84	0.23	0.742	0.035	5.8	0.7	0.33	0.01	1.86	0.23	0.694	0.035	7.3	0.7	11.9	32	4.04	3996	116	3613	74
B44	0.33	0.01	1.00	0.03	0.741	0.043	3.1	0.2	0.34	0.01	1.01	0.03	0.693	0.043	3.9	0.2	10.8	28.9	6.97	3259	156	3639	88
B99	0.06	0.04	3.40	0.59	0.057	0.007	9.2	0.9	0.06	0.04	3.44	0.59	0.054	0.007	11.6	0.9	0.937	28.7	2.33	511	41	498	856
W7	0.27	0.03	1.73	0.10	0.708	0.068	5.6	0.6	0.28	0.03	1.76	0.10	0.662	0.068	7.1	0.6	4.43	13	1.74	3707	179	3340	114
BL11	0.33	0.02	1.07	0.05	0.731	0.041	3.3	0.2	0.33	0.02	1.08	0.05	0.683	0.041	4.2	0.2	6.02	16.3	3.67	3315	206	3732	308
BL4	0.52	0.08	1.01	0.06	0.804	0.112	3.1	0.3	0.53	0.08	1.02	0.06	0.752	0.112	3.9	0.3	3.77	9.86	2.4	3300	360	4293	181
B9	0.07	0.04	1.72	0.28	0.059	0.010	4.5	0.3	0.07	0.04	1.74	0.28	0.055	0.010	5.6	0.3	0.499	15	2.44	430	33	1085	999
b10	0.08	0.02	1.51	0.17	0.195	0.021	4.2	0.4	0.08	0.02	1.53	0.17	0.182	0.021	5.3	0.4	1.29	11.9	2.11	1293	125	1243	318
B13	0.33	0.02	1.35	0.07	0.757	0.055	4.2	0.3	0.34	0.02	1.37	0.07	0.708	0.055	5.3	0.3	5.3	13.7	2.46	3698	179	3630	111
B18	0.06	0.03	1.98	0.26	0.078	0.010	5.2	0.6	0.06	0.03	2.00	0.26	0.073	0.010	6.6	0.6	0.667	14.5	2.11	612	62	1767	1970
B21	0.38	0.08	1.45	0.15	0.140	0.022	4.8	0.4	0.39	0.08	1.47	0.15	0.131	0.022	6.1	0.4	0.928	14.2	2.21	840	74	3870	246
B23	0.08	0.10	1.99	0.37	0.025	0.005	5.0	0.4	0.08	0.10	2.02	0.37	0.023	0.005	6.3	0.4	0.214	14.4	2.13	201	17	1301	1219
B29	0.05	0.03	2.01	0.26	0.096	0.015	5.2	0.4	0.06	0.03	2.04	0.26	0.089	0.015	6.6	0.4	0.899	15.8	2.25	757	56	589	794
B28	0.54	0.10	1.12	0.15	0.085	0.010	4.5	0.4	0.55	0.10	1.14	0.15	0.080	0.010	5.7	0.4	0.578	17.7	2.91	421	43	4378	297
B43	0.25	0.03	1.87	0.11	0.622	0.068	5.5	0.5	0.25	0.03	1.90	0.11	0.581	0.068	6.9	0.5	4.45	13.4	1.82	3626	201	3274	347
B35	0.17	0.04	2.20	0.20	0.185	0.024	6.5	0.6	0.17	0.04	2.23	0.20	0.173	0.024	8.3	0.6	1.32	14.2	1.59	1295	125	2543	245
B48	0.06	0.02	1.05	0.14	0.105	0.010	2.8	0.2	0.06	0.02	1.07	0.14	0.098	0.010	3.5	0.2	0.878	14.1	3.8	645	35	614	387
B47	0.34	0.03	2.37	0.12	0.778	0.081	7.2	0.7	0.35	0.03	2.40	0.12	0.728	0.081	9.1	0.7	6.95	17.2	1.81	4411	209	3657	105
B46	0.28	0.21	2.59	1.34	0.034	0.009	7.0	0.6	0.29	0.21	2.63	1.34	0.032	0.009	8.9	0.6	0.239	14.2	1.48	251	24	3182	461
B45	0.35	0.02	1.04	0.03	0.749	0.043	3.2	0.2	0.35	0.02	1.06	0.03	0.701	0.043	4.0	0.2	6.89	18	4.21	3352	147	3701	80
B62	0.40	0.02	0.91	0.04	0.807	0.045	2.9	0.2	0.41	0.02	0.92	0.04	0.755	0.045	3.7	0.2	6.13	15.6	4.01	3295	176	3946	155
B63	0.11	0.09	2.09	0.50	0.025	0.006	5.4	0.4	0.11	0.09	2.12	0.50	0.023	0.006	6.9	0.4	0.208	15.2	2.05	190	16	1752	819
B65	0.12	0.07	2.29	0.58	0.029	0.006	6.1	0.5	0.13	0.07	2.32	0.58	0.027	0.006	7.8	0.5	0.238	15.1	1.81	227	20	2257	625
B68	0.13	0.02	1.96	0.14	0.354	0.045	5.5	0.5	0.13	0.02	1.98	0.14	0.331	0.045	7.0	0.5	2.97	15.3	2.07	2380	174	2103	195
B71	0.11	0.15	2.24	1.02	0.015	0.004	5.4	0.5	0.11	0.15	2.26	1.02	0.014	0.004	6.9	0.5	0.133	15.5	2.11	119	11	2257	625
B74	0.17	0.02	1.64	0.10	0.459	0.046	4.8	0.4	0.17	0.02	1.66	0.10	0.429	0.046	6.1	0.4	3.05	12.6	1.96	2736	168	2532	137
B75	0.06	0.09	2.30	0.92	0.020	0.005	5.4	0.5	0.06	0.09	2.33	0.92	0.019	0.005	6.9	0.5	0.176	15.4	2.08	159	15	900	1755
B77	0.24	0.16	2.51	0.72	0.024	0.005	6.7	0.5	0.25	0.16	2.55	0.72	0.023	0.005	8.5	0.5	0.185	14.3	1.56	191	14	3211	626
B78	0.15	0.10	1.26	0.31	0.023	0.005	3.2	0.2	0.15	0.10	1.27	0.31	0.022	0.005	4.0	0.2	0.19	14.2	3.25	154	14	2313	522
B79	0.08	0.08	2.11	0.56	0.022	0.005	4.9	0.4	0.08	0.08	2.13	0.56	0.020	0.005	6.2	0.4	0.203	15.2	2.26	180	16	1234	1159
B84	0.39	0.02	0.90	0.06	0.806	0.038	2.9	0.2	0.40	0.02	0.91	0.06	0.754	0.038	3.6	0.2	7.22	18.3	4.67	3313	216	3887	155
B81	0.09	0.02	1.11	0.10	0.237	0.027	3.0	0.2	0.09	0.02	1.12	0.10	0.222	0.027	3.8	0.2	1.54	11.5	2.83	1378	112	1403	265
B86	0.08	0.05	2.77	0.40	0.091	0.014	7.2	0.7	0.08	0.05	2.80	0.40	0.085	0.014	9.1	0.7	0.846	15.6	1.63	789	75	2854	3162
B89	0.41	0.22	1.96	0.63	0.018	0.005	7.3	0.6	0.41	0.22	1.98	0.63	0.017	0.005	9.2	0.6	0.112	15.9	1.62	106	13	3796	527
B90	0.12	0.12	1.39	0.41	0.018	0.004	3.7	0.3	0.13	0.12	1.41	0.41	0.017	0.004	4.6	0.3	0.125	12.4	2.47	123	11	2178	854
B91	0.07	0.02	2.00	0.20	0.149	0.016	5.6	0.4	0.07	0.02	2.02	0.20	0.139	0.016	7.0	0.4	1.5	17.9	2.4	1115	104	885	396
B92	1.19	1.52	2.35	6.10	0.009	0.004	8.0	0.9	1.21	1.52	2.38	6.10	0.008	0.004	10.1	0.9	0.027	16	1.46	26	3	5084	641
B93	0.54	0.15	1.78	0.36	0.155	0.060	7.5	0.8	0.55	0.15	1.80	0.36	0.145	0.060	9.5	0.8	0.795	16	1.56	738	74	4388	439
B94	0.35	0.05	1.36	0.08	0.481	0.055	4.8	0.5	0.36	0.05	1.38	0.08	0.450	0.055	6.1	0.5	3.09	14.9	2.31	2411	299	3825	385
B98	0.06	0.04	1.73	0.20	0.073	0.009	4.6	0.3	0.06	0.04	1.76	0.20	0.068	0.009	5.8	0.3	0.706	16.6	2.72	545	48	461	701
B96	0.16	0.13	2.07	0.56	0.022	0.005	5.8	0.5	0.16	0.13	2.10	0.56	0.021	0.005	7.3	0.5	0.182	16	2.03	161	12	2356	659
G3	0.08	0.13	2.46	0.62	0.026	0.005	6.4	0.6	0.09	0.13	2.49	0.62	0.024	0.005	8.1	0.6	0.199	13.9	1.59	209	19	1512	1457
G7	0.32	0.02	1.72	0.08	0.765	0.054	5.4	0.5	0.33	0.02	1.74	0.08	0.716	0.054	6.8	0.5	5.87	15.4	2.15	3950	180	3600	103
G8	0.07	0.02	0.97	0.10	0.090	0.008	2.4	0.2	0.07	0.02	0.99	0.10	0.084	0.008	3.0	0.2	0.727	12.7	3.97	554	29	863	416

G11	0.38	0.02	0.96	0.04	0.807	0.046	3.1	0.2	0.39	0.02	0.97	0.04	0.755	0.046	3.9	0.2	7.93	20.1	4.82	3392	227	3839	138
G21	0.06	0.03	2.33	0.35	0.073	0.010	5.7	0.5	0.06	0.03	2.36	0.35	0.069	0.010	7.2	0.5	0.854	19.2	2.5	613	59	575	617
G30	0.19	0.12	1.27	0.16	0.090	0.016	3.3	0.3	0.19	0.12	1.29	0.16	0.084	0.016	4.2	0.3	0.784	16.1	3.56	555	56	2595	629
G29	0.08	0.02	1.39	0.11	0.197	0.017	3.7	0.2	0.08	0.02	1.41	0.11	0.184	0.017	4.7	0.2	1.64	15	2.93	1257	100	1748	707
G28	0.34	0.01	0.94	0.03	0.758	0.044	3.0	0.1	0.34	0.01	0.95	0.03	0.709	0.044	3.8	0.1	6.89	19.4	4.72	3131	141	3668	98
G36	0.07	0.03	1.25	0.14	0.080	0.008	3.3	0.3	0.07	0.03	1.26	0.14	0.075	0.008	4.2	0.3	0.591	13	2.87	519	39	1100	418
G43	0.31	0.13	1.17	0.31	0.019	0.004	2.8	0.2	0.32	0.13	1.18	0.31	0.018	0.004	3.6	0.2	0.139	12	3.11	126	10	3516	412
G46	0.36	0.02	1.53	0.10	0.812	0.094	4.9	0.5	0.36	0.02	1.55	0.10	0.760	0.094	6.1	0.5	3.73	9.65	1.46	3895	191	3735	103
G47	0.07	0.02	1.33	0.13	0.078	0.008	3.5	0.2	0.07	0.02	1.35	0.13	0.073	0.008	4.4	0.2	0.662	14.6	3.08	528	35	997	351
G51	0.08	0.14	2.54	1.49	0.009	0.003	5.4	0.4	0.08	0.14	2.57	1.49	0.009	0.003	6.9	0.4	0.095	16.6	2.24	80	7	1579	1908
G53	0.06	0.02	0.81	0.10	0.096	0.008	2.1	0.2	0.06	0.02	0.82	0.10	0.090	0.008	2.7	0.2	0.778	14.1	4.8	512	30	720	336
G59	0.06	0.03	1.47	0.13	0.074	0.006	3.9	0.2	0.06	0.03	1.49	0.13	0.069	0.006	5.0	0.2	0.922	22.3	4.15	507	38	931	555
G58	0.12	0.10	1.40	0.46	0.020	0.004	3.3	0.2	0.12	0.10	1.41	0.46	0.019	0.004	4.2	0.2	0.155	13	2.86	139	11	1948	886
G61	0.06	0.03	1.89	0.24	0.077	0.008	5.1	0.3	0.06	0.03	1.92	0.24	0.072	0.008	6.4	0.3	0.792	18.6	2.65	572	41	513	582
G64	0.07	0.04	1.56	0.24	0.077	0.010	3.9	0.3	0.07	0.04	1.58	0.24	0.072	0.010	4.9	0.3	0.567	12.4	2.3	559	44	928	602
B5	0.11	0.10	1.77	0.62	0.021	0.006	4.6	0.4	0.11	0.10	1.80	0.62	0.019	0.006	5.8	0.4	0.142	12.5	2	150	14	1783	1024
B4	0.14	0.05	2.26	0.29	0.088	0.010	6.5	0.6	0.14	0.05	2.29	0.29	0.082	0.010	8.2	0.6	0.743	15.9	1.82	667	54	2233	364

BCR-2G analyses

	207Pb/206Pb	1s (abs)	208Pb/206Pb	1s (abs)	238U/206Pb	1s (abs)	232Th/238U	1s (abs)
BCR-2G-01	0.816	0.033	2.053	0.073	1.688	0.168	2.95	0.35
BCR-2G-02	0.833	0.037	2.073	0.078	1.705	0.146	2.99	0.30
BCR-2G-03	0.820	0.042	2.028	0.075	1.705	0.185	3.15	0.36
BCR-2G-04	0.825	0.030	2.038	0.063	1.767	0.174	3.03	0.28
BCR-2G-05	0.816	0.026	2.051	0.075	1.738	0.178	2.94	0.31
BCR-2G-06	0.832	0.031	2.053	0.072	1.821	0.157	3.02	0.26
BCR-2G-07	0.817	0.030	2.036	0.073	1.714	0.150	2.90	0.25
BCR-2G-08	0.815	0.034	2.021	0.077	1.752	0.142	2.96	0.27
BCR-2G-09	0.820	0.032	2.030	0.068	1.776	0.144	2.98	0.25
BCR-2G-10	0.817	0.033	2.029	0.084	1.722	0.130	2.93	0.23
BCR-2G-11	0.813	0.030	2.026	0.070	1.811	0.158	2.93	0.30
BCR-2G-12	0.815	0.042	2.018	0.069	1.777	0.149	2.93	0.25
Average	**0.820**		**2.038**		**1.748**		**2.97**	
SD	**0.007**		**0.016**		**0.043**		**0.07**	
True values Woodhead & Hergt, 2000	0.8330		2.0644		1.64	0.08	3.76	0.13

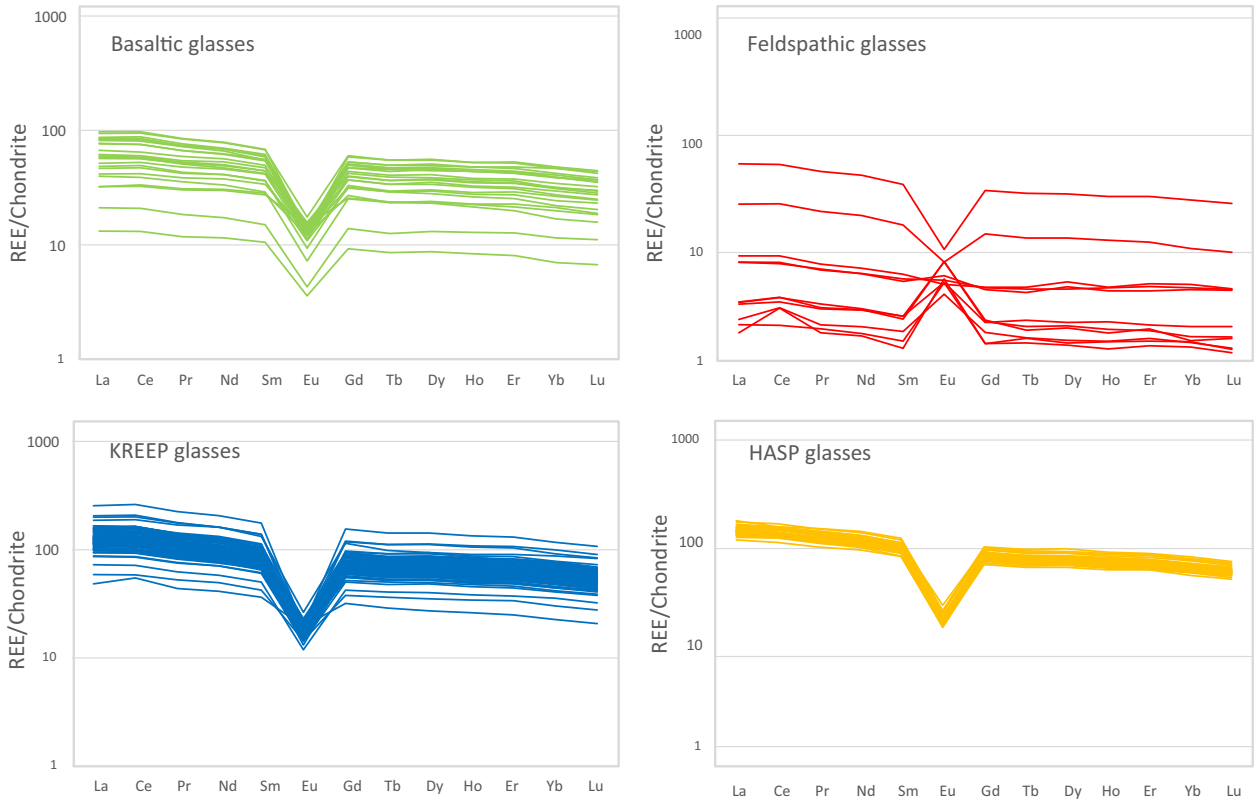

Fig. 9. REE patterns displayed by four identified chemical groups of impact spherules from soil 14163.

CI and negative Eu anomalies (Fig. 9). These compositions are more enriched than is typical for ferroan anorthositic suite rocks and are more similar to the REE compositions of Mg-suite troctolites and norites. Sr/Ba ratios, which can help distinguish ferroan anorthositic from Mg-suite rocks (Norman et al., 2019), are anti-correlated with incompatible trace elements (ITE) in the feldspathic glasses, and range from values of 0.4–7.1 (Fig. 10a). These Sr/Ba ratios are consistent with a predominance of Mg-suite and/or KREEP-bearing target lithologies contributing to the feldspathic glasses studied here. Other trace element ratios that can help discriminate Mg-suite from FAS sources include Ti/Sm, Sc/Sm, and Al/Eu (Norman et al., 2003). These ratios are consistent with mixing of a modest amount of KREEP and/or Mg-suite rocks with ferroan anorthosites (Fig. 10b and c).

As a general observation, the major- and trace-element compositions of the suite of glasses investigated here indicate that their source terrains contained various proportions of KREEPy or KREEP-related material. Most importantly, the population of analysed spherules is dominated by compositions that are enriched in incompatible elements to the levels comparable to those observed in KREEP basalts. The basaltic glasses also appear to show some signs of KREEP addition, such as increased concentrations of LREE, resulting in negative slopes of their REE patterns. Even the feldspathic glasses with relatively low concentrations of incompatible elements have Al_2O_3 contents of 19.6–26.9 wt%, more mafic than the Ferroan Anorthosite Suite (FAS) rocks, which have 25–35 wt% Al_2O_3. In addition, the Mg#'s (molar 100*MgO/(MgO + FeO)) of the feldspathic glasses are among the highest of any glass measured in this study (61.5–94.2) and their Sr/Ba ratios are lower than those observed in the FAS and more similar to those of Mg-suite cumulates, which are often linked with KREEP in their petrogenesis (e.g., Shearer et al., 2015). We conclude that the major- and trace-element compositions of the feldspathic beads are more consistent with source terrains consisting of relatively anorthositic members of the Mg-suite than with mixing of FAS rocks with KREEPy materials in the impact targets. Although magnesian anorthositic rocks are rare in the sample collection, Pieters et al. (2014) identified several locations of anorthositic rocks with magnesian spinels and Prissel et al. (2014) provided experimental evidence that such lithologies are likely related to the Mg-suite. It is also important to note that the refractory element characteristics in the KREEP-rich and HASP glasses suggests that both of these groups of spherules have very similar compositions of their source rocks.

The strong KREEPy flavor to the glasses studied here and the clustering of their compositions around that of the bulk soil in which they were found implies a local or regional provenance for the large majority of these spherules. This is consistent with the study by Zellner et al (2002) that linked compositional variations of 778 individual glasses in Apollo 14 soil to the regional geology based on Clementine data. Compositions of the glasses investi-

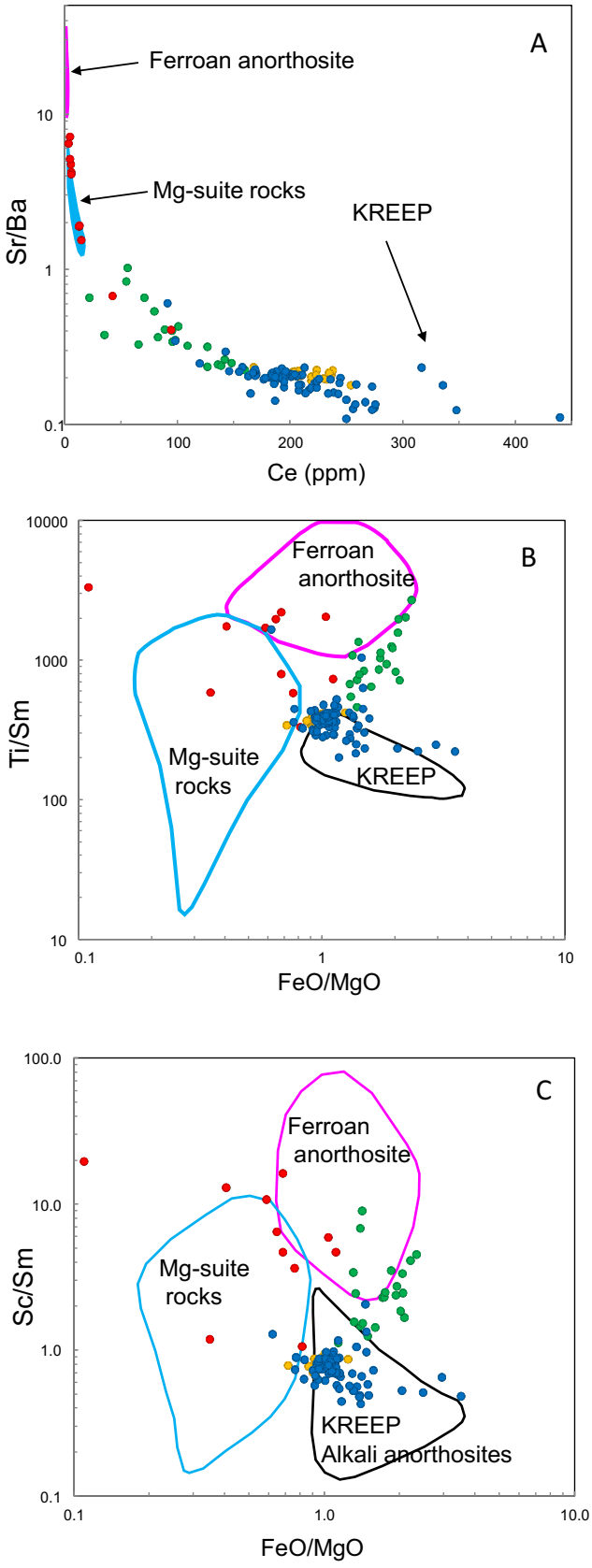

Fig. 10. (a) Sr/Ba, (b) Ti/Sm, and (c) Sc/Sm versus FeO/MgO discrimination diagrams showing compositional fields of the main highland rock types. Colours of the dots (representing analysd glasses) indicates four chemical groups as in previous figures.

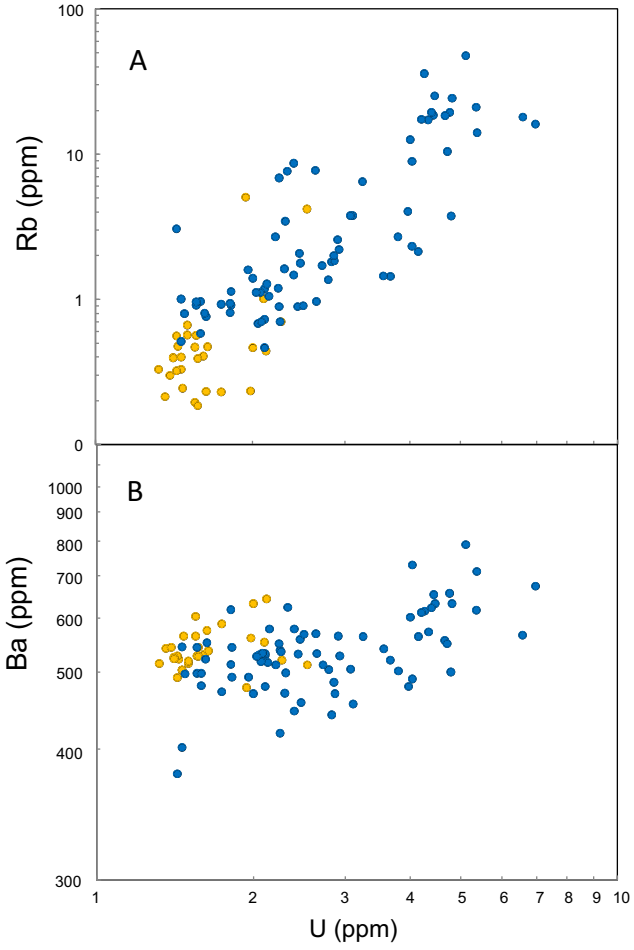

Fig. 11. Rb and Ba versus U concentrations in KREEP-rich (blue circles) and HASP (yellow circles) glasses, showing correlation of U and volatile elements suggesting volatile behaviour of U in some impact glasses. (For interpretation of the references to colour in this figure legend, the reader is referred to the web version of this article.)

gated here are indistinguishable from those presented by Zellner et al. (2002) when plotted on a Ti-(Fe-Ti)-Al ternary diagram (Fig. 13). It is worth noting that data from Zellner et al. (2002) include analyses of both spherules (black squares in Fig. 13) and shards (light blue squares in Fig. 13) and there does not appear to be any chemical difference between these two morphological glass types, contrary to recent discussions of potential differences suggested to be linked to the distance between a sample collection site and target regions of beads and shards (e.g., Delano et al., 2007; Zellner, 2019). Consequently, the existing question of how far glass beads can be transported from the target to deposition sites remains unresolved. Contributions from far-distant impacts to the glass population of 14163 cannot be fully excluded, but there is no compelling compositional evidence for a substantial contribution from distal terrains such as the Feldspathic Highlands or high-Ti mare sources such as those at Apollo 11 and 17. Therefore, the compositional range of glass spherules studied here can be explained mostly by a local (10′s-100′s of km?) sources of the beads.

4.2. Age groups and Pb unsupported by in-situ U decay (SIMS data)

4.2.1. Correction for unsupported Pb

The U-Th-Pb SIMS data presented here have not been corrected for possible contributions of Pb by sources other than in-situ decay, which may compromise determination of the true formation age of the spherules and can originate from a number of different sources:

(1) In-situ isotopic dating of lunar impact glasses using the U-Th-Pb system is most straightforward if all of the Pb that had accumulated in the target rocks or regolith prior to the glass-forming impact is lost from the melt due to the high volatility of Pb. However, this may not always be the case as it is possible that some of this ‘initial’ lunar Pb can be retained in the glasses. This would make the inferred ages artificially old as most lunar Pb is highly radiogenic as a result of the general depletion of Pb in the Moon, resulting in high U/Pb ratios in all lunar rocks.

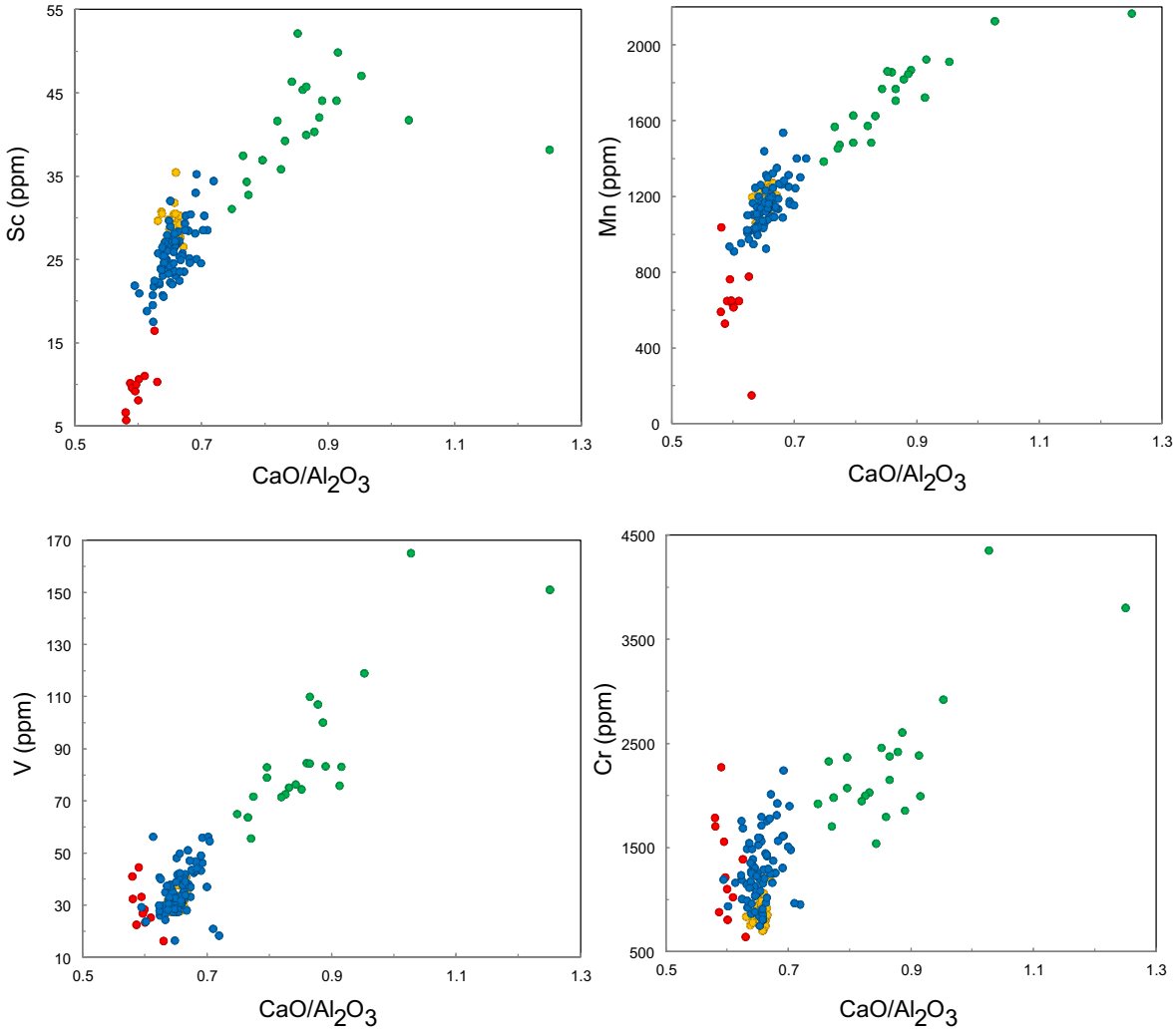

Fig. 12. Sc, Mn, V and Cr distribution in the glasses of four identified chemical groups (colours similar to those in Figs. 3 and 4).

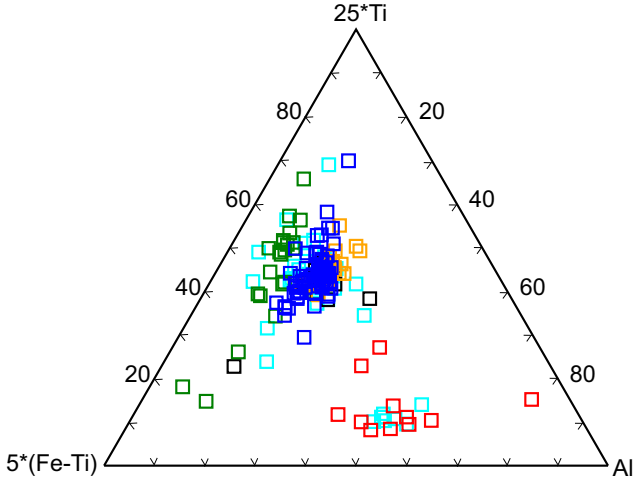

Fig. 13. Ternary diagram showing variation of refractory major elements in the Apollo 14 glass beads and shards. Colours represent chemical types for glass spherules analysed here and are similar to those in the previous plots. Light blue and black squares represent data from Zellner et al. (2002), Zellner and Delano (2015) and Nguyen and Zellner (2019) with light blue indicating shards and black representing spherules. (For interpretation of the references to colour in this figure legend, the reader is referred to the web version of this article.)

(2) Significant mobility of Pb in lunar soils has been noticed since the earliest studies of Apollo samples (e.g., Silver, 1972, 1974). This unsupported regolith Pb might be introduced into the glasses either by diffusion or transport along pathways such microfractures and again artificially increase the inferred ages.
(3) If the glasses experienced even localized reheating associated with impacts, Pb might be partially lost from the spherules. Although subsolidus diffusion of divalent Pb in silicate glass is expected to be slow (Fanara et al., 2017), any Pb loss would result in the analysed Pb composition representing a mixture of Pb accumulated after this secondary event and some residual Pb that is related to the preceding U-Th decay. In general, such mixed compositions should fall on discordia lines with the intercepts of concordia dating both primary and secondary events, although more than one bead with an independently verified origin and affected by the same secondary event would need to be analysed to constrain the discordia and both ages.
(4) Even though glass beads are analysed in polished mounts, which expose their inner parts and are thoroughly cleaned prior to the analyses, the presence of small quantities of terrestrial Pb from laboratory contamination cannot be fully excluded as a possible contribution to the measured isotopic composition.

Compared to terrestrial Pb, the other potential sources of Pb in lunar impact glasses that might confound interpretation of their ages (i.e., (1) Pb inherited from the target, (2) unsupported Pb added to glasses during their residence in the soil and (3) Pb left in the glasses during secondary reheating) will produce somewhat similar isotope characteristics that will be highly radiogenic and difficult to distinguish from each other. Isotope compositions of terrestrial contamination approximated as the model Pb composition of average modern continental crust (Stacey and Kramers, 1975) are shown in Figs. 5 and 6. These figures also show an approximation of lunar Pb isotopic composition taken from the study of unsupported Pb in regolith sample 14163 made by Silver (1972). The composition of lunar regolith Pb proposed by Silver (1972) is similar to that determined by Nemchin et al. (2017) for Apollo 14 breccias at about 3.9 Ga. Both can be taken as reasonable approximations of volatile unsupported Pb that can be present in the soil and possibly contaminate the glasses. To combat uncertainties associated with the choice of terrestrial and/or lunar Pb, all calculations made here assume 50% errors in the $^{204}Pb/^{206}Pb$ and 20% errors in the $^{207}Pb/^{206}Pb$ that were selected for these two Pb isotopic compositions. These uncertainties are arbitrary, but they follow the approach of Ludwig (1980) for U-Pb geochronology of terrestrial samples. Because uncertainties for non-insitu Pb isotope composition are not independently determined, the assigned uncertainties include all possible variations of these Pb compositions. The applied uncertainties of 50 and 20% for the $^{204}Pb/^{206}Pb$ and $^{207}Pb/^{206}Pb$ ratios cover a range of terrestrial Pb compositions produced over last 3 Ga as defined by the Stacey and Kramers (1975) model. For lunar Pb it covers all compositions ranging from the most radiogenic Pb observed at the Apollo 14 landing site at 3.9 Ga to the initial compositions of lunar mare basalts at 3.2–3.1 Ga.

If any individual particle experienced incomplete resetting, the $^{207}Pb/^{206}Pb$ of lunar initial Pb and any residual Pb in the glasses will both be age dependent but generally located between compositions provided by Silver (1972) and Nemchin et al. (2017) and terrestrial Pb. The $^{204}Pb/^{206}Pb$ of lunar initial Pb is expected to be lower than that of Silver (1972) due to continuous ingrowth of radiogenic ^{206}Pb from U decay, while this ratio for the remnants of incompletely lost Pb has to be zero. Consequently, $^{207}Pb/^{206}Pb$ of all non in-situ Pb components will vary within a relatively narrow range, while $^{204}Pb/^{206}Pb$ can have several orders of magnitude variability. Such substantial differences make the calculated ages very sensitive to the choice of isotopic compositions used for the correction of any non-in situ Pb component, especially if the correction is based on $^{204}Pb/^{206}Pb$, such as, for example, the correction for common Pb in terrestrial zircon analyses. As a result, U-Pb isotopic ages cannot be calculated with confidence for the majority of individual glass spherules by simply taking out excess Pb proportionate to the measured ^{204}Pb and some assumptions have to be made to determine these ages. In addition, different approaches have to be used for younger and older glasses.

For the younger glasses an assumption is made that the analyses falling along linear trends on the concordia diagram can represent glasses with similar ages and post-formation histories. In other words, we assume that these linear trends represent binary mixtures of in situ and non-in situ Pb, and the true age of the glasses falling along individual trends can be estimated from the best fit lines drawn through the data. Younger glasses would contain smaller quantities of in-situ produced ^{207}Pb such that $^{207}Pb/^{206}Pb$ is determined with an increasingly larger analytical uncertainty, thereby making their $^{207}Pb/^{206}Pb$ ages less precise. However, the concordia curve becomes sub-horizontal after about 300 Ma, which improves precision of the inferred $^{238}U/^{206}Pb$ ages (Figs. 5 and 6). Consequently, a concordia diagram (e.g., $^{238}U/^{207}Pb$-$^{206}Pb/^{207}Pb$) can be used to constrain the best fit lines by combining different glasses, and ages can be calculated from these lines. In these coordinates, terrestrial and lunar Pb plot close to each other and as a result the choice of isotope composition used for correction is less critical. In addition, the best-fit lines do not rely on a precise knowledge of the composition of the excess Pb, which can be estimated as an independent parameter from the fits. The data set presented here provides a novel test of the $^{238}U/^{207}Pb$-$^{206}Pb/^{207}Pb$ approach and further work is needed to determine if it can be applied to other populations of lunar glasses. However, the interpreted ages from these coordinates do not require knowledge of error correlations for ratios (unlike the standard concordia plots, $^{207}Pb/^{235}U$-$^{206}Pb/^{238}U$) and this projection is better suited for visualisation of populations with the large range of ages than the commonly used Tera-Wasserburg diagram ($^{238}U/^{206}Pb$-$^{207}Pb/^{206}Pb$).

Consequently, it is probably better suited for general analysis of lunar glass age populations.

The line-fitting approach appears to work for all glasses with apparent ages less than 1000 Ma, although uncertainties determined for the best fit line age estimates increase from younger to older (closer to 1000 Ma) glasses. For older than 1000 Ma glasses, compositions plot close to concordia on $^{238}U/^{207}Pb$-$^{206}Pb/^{207}Pb$ diagram and even visual distinction of individual linear trends within analytical uncertainties becomes impossible (Fig. 5). As a result, further assumptions and use of 3D representations are made to calculate the ages for these glasses. For these calculations, it is assumed that two end members of unsupported Pb are represented by (i) modern Pb composition for terrestrial contamination (Stacey and Kramers, 1975) , and (ii) an unsupported lunar regolith Pb composition identified by Silver (1972). In this case, analyses that fall on different planes in $^{238}U/^{206}Pb$-$^{207}Pb/^{206}Pb$-$^{204}Pb/^{206}Pb$ space and constrained by these two end member compositions can be assumed to represent glasses with the same age that experienced variable addition of these two unsupported Pb components.

The oldest group of glasses (>3.6 Ga) allows the use of several additional combinations of coordinates (ratios) to obtain age estimates, which increases the confidence in the estimated ages of the glasses when different combinations give ages similar within uncertainties. In addition to plane fitting using fixed Pb compositions for unsupported Pb components, planes or lines can be fitted through the data points in $^{238}U/^{206}Pb$-$^{207}Pb/^{206}Pb$-$^{204}Pb/^{206}Pb$ space, eliminating the need to guess the composition of unsupported Pb (Fig. 15). It is also possible to use linear trends observed in $^{207}Pb/^{206}Pb$-$^{204}Pb/^{206}Pb$ where intercepts of the best fit lines and vertical axis represent estimates of the ages of the glass populations falling on these linear trends (Fig. 15b).

A practical approach to identifying groups of glasses with similar ages (i.e., those that might belong to the same age groups) involves interrogating data from the apparently youngest beads (Fig. 6). For example, a line can be fitted through analyses of four glasses (blue ellipses in Fig. 6b). Adding any other analysis from the population would destroy the statistical significance of the fit. Following a similar approach, five further analyses (green ellipses in Fig. 6b) and 19 analyses (red ellipses in Fig. 6b) can produce statistically significant fits. Three analyses (light blue ellipses in Fig. 6b) fall outside of any of these fits and could be treated as a separate group although a best fit line drawn using these three analyses has a negative intercept on the vertical axis, which would require an unrealistic unsupported Pb composition. Consequently, relationships between these three glasses fail to follow a simple assumption that the glasses represent a single group related by binary mixing of in situ accumulated Pb and a single composition somewhere between terrestrial Pb and unsupported lunar Pb. As mentioned above, this approach of systematic fitting of best fit lines through the analyses from youngest to oldest can be applied to the glasses younger than 1000 Ma. Further assignment of the groups (older than 1000 Ma) is done in a similar manner, but using 3D planes rather than linear fits to find glasses that might belong to common age groups.

As mentioned earlier, a simple correction using $^{204}Pb/^{206}Pb$, as commonly applied in terrestrial geochronology, is not possible for the analyses of lunar impact glasses due to the highly radiogenic composition of lunar Pb, complex mixing of Pb accumulated in the beads from U decay after their formation, and at least two unsupported components represented by lunar Pb (probably present in the soil samples) and terrestrial (laboratory) contamination. However, if the non-in situ components of the mixtures are assumed to be represented by i) modern Pb of Stacey and Kramers (1975) and (ii) regolith Pb as determined by Silver (1972), planes can be constructed through those two compositions and individual analyses of the glass beads in $^{238}U/^{206}Pb$-$^{207}Pb/^{206}Pb$-$^{204}Pb/^{206}Pb$ space, rather than the approach discussed earlier of fitting planes through analyses of multiple beads with an assumption of their common history. Concordia intercepts of these planes define a model age for individual glasses, providing yet another way for age estimation of these spherules. This approach does not rely on a precise knowledge of proportions of lunar unsupported Pb and terrestrial contamination for each analytical point and is applicable for the younger glasses (<1000 Ma).

A poorly resolved component that contributes to uncertainties in the ages presented here is the variable inheritance of older Pb from the target sources. Older glasses accumulate in-situ Pb for longer periods of time and therefore generate more of the in-situ radiogenenic component, making their $^{207}Pb/^{206}Pb$ age estimates less sensitive to corrections. On the other hand, the youngest glasses have $^{206}Pb/^{238}U$ ages that are less sensitive to corrections as the concordia curve becomes subparallel to the horizontal axes on the concordia diagrams (Figs. 5 and 6). Glasses with intermediate ages are most sensitive to the choice of initial Pb compositions used for the correction. Consequently, the following sections are organised in order of the reliability of estimated ages. First we address the oldest and youngest ages, both of which are relatively insensitve to corrections, then we address the intermediate ages, which have larger uncertainties.

4.2.2. Concordant analyses with ages older than 3.6 Ga

Thirty-two analyses of 18 KREEP-rich and 2 HASP glasses are concordant within their uncertainties (Fig. 14a) and show a spread of ages uncorrected for non-in situ Pb that range between about 4.05 and 3.60 Ga. These analyses demonstrate linear relationships in the $^{207}Pb/^{206}Pb$-$^{204}Pb/^{206}Pb$ coordinates (Fig. 14b), with 18 analyses of 12 spherules defining an approximately linear array with a relatively shallow slope. This array defines an intercept age of 3615 ± 6 Ma on the vertical axis. An identical age of 3614 ± 8 Ma is defined by constraining a line through the sample data set in the 3D $^{238}U/^{206}Pb$-$^{207}Pb/^{206}Pb$-$^{204}Pb/^{206}Pb$ system (Fig. 14c). This array intersects a mixing line between terrestrial Pb and unsupported lunar Pb, close to the latter (Fig. 14b), which indicates that non in-situ Pb is dominated by the lunar component. The remaining 12 analyses of 8 spherules form a

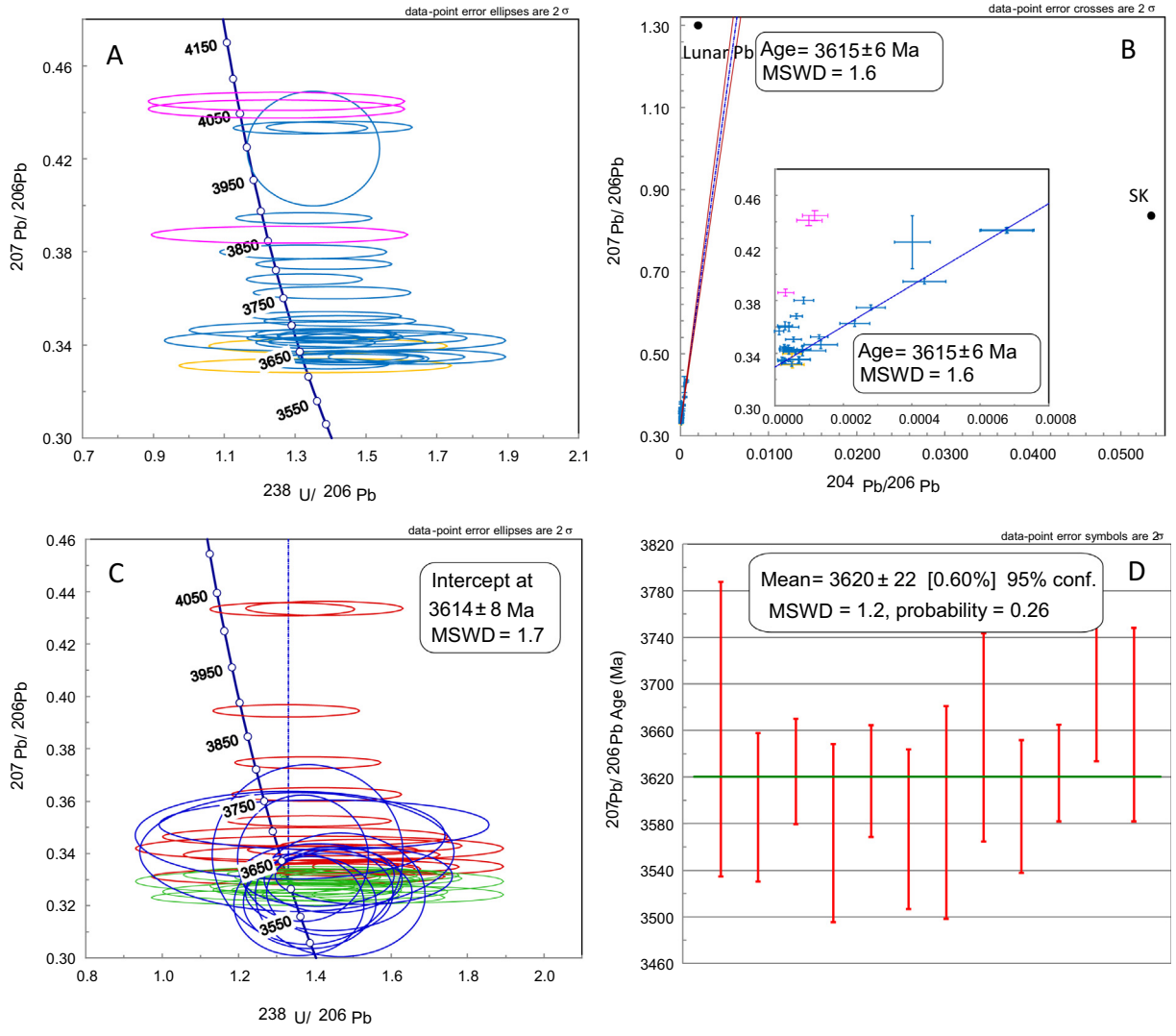

Fig. 14. U-Pb data for KREEP-rich and HASP glasses with apparent ages older than 3.6 Ga. (A) Tera – Wasserburg diagram, showing subvertical distribution of analyses; –(B) $^{207}Pb/^{206}Pb$-$^{204}Pb/^{206}Pb$ plot showing best fit line through the analyses falling along a shallower slope, in relation to terrestrial Pb and lunar unsupported Pb, red curves represent error envelope. Insert shows distribution of analyses near the vertical axis also includes analyses that are above the best fit line and probably contain mostly lunar Pb. (C) projection of best fit line through the same group of analyses (i.e. falling along the shallow slope) in 3D $^{206}Pb/^{238}U$-$^{207}Pb/^{206}Pb$-$^{204}Pb/^{206}Pb$ coordinates (red ellipces represent original data; green ellipses represent projection of the analyses along the line, also shown data that fall off the line, but corrected for pure unsupported Pb component – blue ellipses); (D) Weighted mean of $^{207}Pb/^{206}Pb$ ages for analyses that fall off the linear trend on $^{207}Pb/^{206}Pb$-$^{204}Pb/^{206}Pb$ plot, these data are corrected for unsupported Pb component, which eliminates difference in ages observed in uncorrected analyses. (For interpretation of the references to colour in this figure legend, the reader is referred to the web version of this article.)

steeper trend in $^{207}Pb/^{206}Pb$-$^{204}Pb/^{206}Pb$ coordinates (Fig. 14b), suggesting that their unsupported Pb is mostly lunar. Correcting these analyses individually for a pure unsupported lunar Pb component (from Silver, 1972) brings them close to the first group of 18 analyses on the concordia (Fig. 14c) and results in $^{207}Pb/^{206}Pb$ ages that define a weighted average age of 3620 ± 22 Ma (Fig. 14d). Consequently, considering the similarities in ages and chemical compositions observed within this KREEP-HASP compositional group of glasses, it seems plausible that all 20 of these spherules were formed by a single impact at 3.62 Ga. Alternatively, they may have been formed by a cluster of impacts into similar composition targets at about the same time.

There are two ion probe analyses of a single basaltic bead (B20 in Table 2) and one analysis of HASP bead (B101, Table 2) that cannot be combined with the rest of the 3.62 Ga spherules under the assumptions made here in relation to corrections for terrestrial and unsupported lunar Pb. These compositions are concordant within their respective uncertainties (pink ellipces in Fig. 14a) and fall along a steeper trend in $^{207}Pb/^{206}Pb$-$^{204}Pb/^{206}Pb$ coordinates (pink crosses in Fig. 14b). However, they also have extremely high $^{206}Pb/^{204}Pb$ nearing 10000, so that even

when corrected for pure lunar Pb these glasses define $^{207}Pb/^{206}Pb$ ages of 3863 ± 45 Ma (two analyses of basaltic glass B20 combined) and 3809 ± 42 Ma (single analysis of HASP glass B101, error is 2 sigma), which are indistinguishable within uncertainties and significantly older than the ages estimated for all other beads. Consequently, we infer that these glasses must have formed by a separate impact (or impacts) prior to 3.62 Ga.

4.2.3. Strongly discordant analyses of glasses younger than 150 Ma

Analyses of 31 glasses representing mostly KREEP-rich and HASP chemical groups but also including three basaltic spherules appear to be strongly discordant. Their compositions form three linear trends on the inverse concordia diagram (Fig. 6b). This linear behaviour coupled with their broadly similar chemical compositions suggests that these glasses could be genetically related, although it is likely the HASP glasses require different impact conditions (Yakovlev et al., 2011; Papike et al., 1977). The best fit lines calculated for these arrays yield upper intercept ages older than those of the Solar System, implying that the arrays do not represent suites of cogenetic spherules with variably reset U-Pb systems but rather a mixing of Pb accumulated from U decay in some relatively young glasses with unsupported Pb, either from terrestrial contamination or from volatile lunar Pb that was mobilized within the regolith. Any residual Pb remaining in the young glasses after partial resetting would have had $^{207}Pb/^{206}Pb$ ratios significantly lower than those indicated by the intercepts of the arrays with the vertical axis. Consequently, the assumption of post-formation mixing of Pb accumulated in-situ from U decay with external Pb added from the soil and/or contamination is the most plausible explanation of these compositions. The complexity of this mixing is apparent in plots of $^{206}Pb/^{207}Pb$ versus $^{204}Pb/^{207}Pb$ (Fig. 6a), where mixing of in-situ accumulated (time integrated, U-supported) Pb with a single exogenous component should result in linear trends with positive slopes that intersect the vertical axis at $^{206}Pb/^{207}Pb$ ratios that correspond to the ages of the glasses. In contrast, the data for the arrays identified in the $^{206}Pb/^{207}Pb$ versus $^{238}U/^{207}Pb$ diagram appear to form trends with negative slopes, which suggests systematic but variable mixtures of terrestrial and unsupported lunar Pb added to the in-situ accumulated Pb as indicated by the arrows in Fig. 6a. These relationships also imply that the unsupported Pb in the compositions located closer to the lower concordia intercept is dominated by terrestrial Pb (contamination), while those further away from the intercept have higher proportions of unsupported lunar Pb. While it is obvious that mixing proportions of three components would be different in the individual analyses, three point planes constrained using (i) terrestrial Pb (Stacey and Kramers 1975), (ii) unsupported lunar Pb (Silver 1972), and (iii) the Pb compositions measured in individual spherules can be used to define concordia intercept ages using separate analyses of individual glass beads. The model age estimates for all glasses are presented in Table 2. Weighted average estimates obtained from these ages for three groups are 108 ± 10, 38 ± 8 and 8 ± 2 Ma, which are indistinguishable from 114 ± 10, 41 ± 20 and 5 ± 2 Ma estimates determined from the intercepts of the lines drawn through the data points and on the $^{206}Pb/^{207}Pb$ versus $^{238}U/^{207}Pb$ concordia (Fig. 6b).

4.2.4. Concordant and discordant analyses of glasses with the apparent ages between 1000 and 300 Ma

The three point-3D approach can be also applied to glasses with apparent ages between 300 and 1000 Ma. While the resulting errors are much larger than those for the younger spherules, this approach helps to identify statistically related groups of glasses that can be considered as single populations. This does not necessarily imply that they formed by the same impact, but it defines a minimum number of events that are needed to produce these populations. Even if multiple impacts were involved in the formation of a single age population, they must be closely timed within the estimated variance of the individual ages. Using this approach, three groups of glasses that include all compositional types of beads can be identified (Fig. 15a). Ages of these groups are: 308 ± 22 Ma (three basaltic, one HASP and six KREEP-rich beads), 485 ± 20 Ma (seven basaltic, four feldspathic, four HASP and thirteen KREEP-rich beads, total of 33 analyses) and 717 ± 62 Ma (three basaltic, three HASP and five KREEP-rich beads). These ages are indistinguishable within uncertainties from 269 ± 41, 472 ± 36 and 715 ± 110 Ma determined as weighted averages of ages obtained for individual glasses (Table 2) using the three point-3D approach.

Projected into vertical cross-sections of $^{238}U/^{207}Pb$-$^{206}Pb/^{207}Pb$-$^{204}Pb/^{207}Pb$ 3D-space, constructed along the three best fit lines determined on the concordia diagram (Fig. 15b, c and d), the data suggest that the relative contribution of different Pb components for the three age groups is similar to that observed for the younger beads. Compositions that fall closer to concordia tend to have higher $^{204}Pb/^{207}Pb$, suggesting that they have higher proportions of terrestrial contamination relative to unsupported lunar Pb, whereas the latter increases in analyses that are more discordant. This highlights that $^{204}Pb/^{206}Pb$ in lunar spherules cannot be used as a measure of the total amount of unsupported Pb (either lunar or terrestrial) that has been added to the in-situ accumulated radiogenic Pb, in contrast to terrestrial U-bearing minerals. Rather, $^{204}Pb/^{206}Pb$ in lunar spherules is a measure of the relative proportions of terrestrial and unsupported lunar Pb, i.e., higher $^{204}Pb/^{206}Pb$ corresponds to larger proportions of terrestrial Pb. Importantly, the statistically identical ages across a wide range of glass compositions may require multiple contemporaneous impacts on the Moon.

4.2.5. Concordant analyses of glasses with apparent ages between 3.62 and 1.0 Ga

The U-Pb isotopic systematics in glasses that appear to have nearly concordant ages between about 3.6 and 1.0 Ga are the most difficult to correct for mixed contributions of terrestrial and unsupported lunar Pb. Their concordance is misleading as they still contain some ^{204}Pb, which indicates the presence of unsupported Pb. Linear trends in $^{207}Pb/^{206}Pb$-$^{204}Pb/^{206}Pb$ coordinates are more difficult

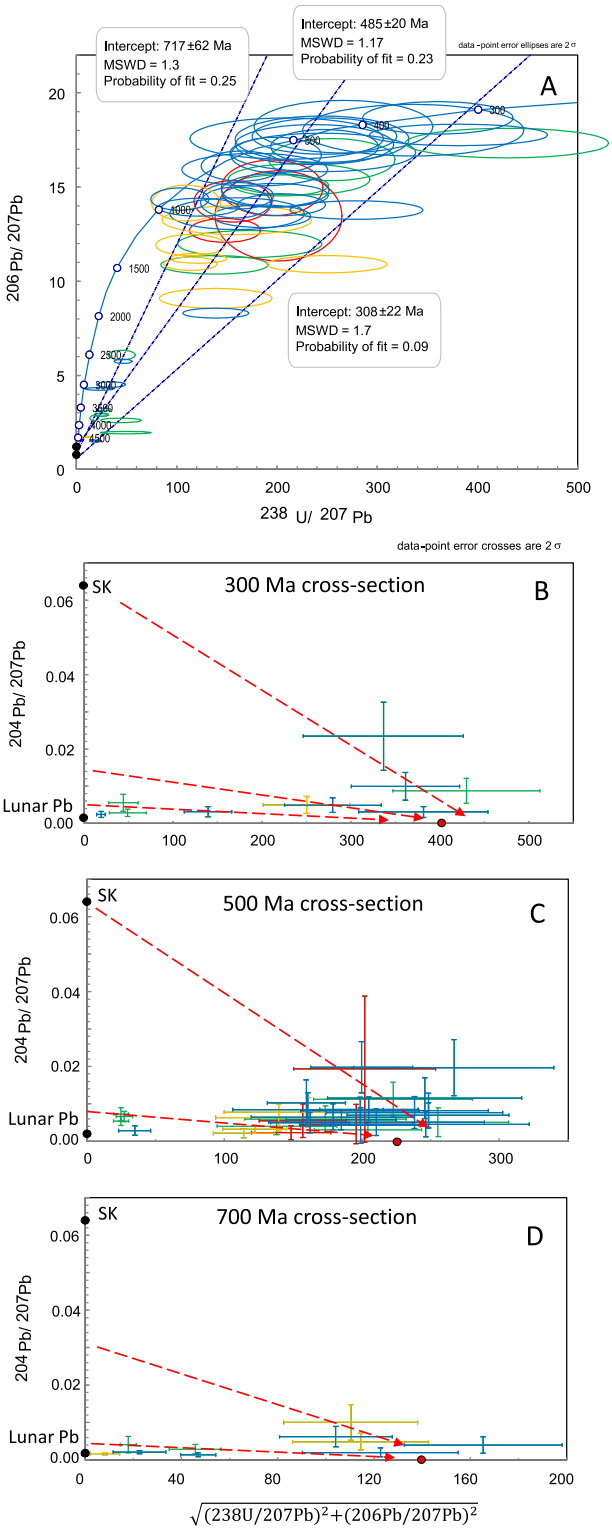

Fig. 15. U-Pb SIMS data for the glasses younger than 1000 Ma. A-modeifed Tera-Wasserburg concordia, showing best fit lines through three groups of glasses with statistically different ages. B, C and D – sections of 3D $^{238}U/^{207}Pb$-$^{206}Pb/^{207}Pb$-$^{204}Pb/^{207}Pb$ system drawn along the best fit lines from A; These sctions show that more concordant (uncorrected) data have generally higher $^{204}Pb/^{207}Pb$, suggesting higher proportion of contamination relative to the unsupported lunar Pb.

to establish as glasses of different ages can potentially fall within the same location on the diagram. At the same time, the sub-parallel orientation of concordia and the correction projections from both terrestrial and lunar Pb for this time interval results in a high sensitivity of $^{207}Pb/^{206}Pb$ to the choice of Pb isotope composition used for this correction (Fig. 16a), while also producing large uncertainties in the age estimates based on $^{206}Pb/^{238}U$ obtained for individual glasses due to the larger analytical errors commonly obtained for this ratio in this time interval (Fig. 16b).

The distribution of analyses in $^{207}Pb/^{206}Pb$-$^{204}Pb/^{206}Pb$ coordinates (Fig. 16a) shows that some of the higher $^{207}Pb/^{206}Pb$ compositions cannot be corrected using only terrestrial Pb contamination as that would result in unrealistically old ages that predate deposition of Imbrium ejecta at about 3.9 Ga. In contrast, a substantial number of analyses with $^{204}Pb/^{206}Pb$ in excess of 0.0002 cannot be corrected using only unsupported lunar Pb as that would make their ages negative. The distribution of compositions on the $^{207}Pb/^{206}Pb$-$^{204}Pb/^{206}Pb$ diagram (Fig. 16a) suggests several age groups if the data are corrected assuming a composition dominated by lunar Pb with a minor terrestrial component. However, confidently assigning individual glasses to specific groups is difficult as the proportions of lunar and terrestrial Pb seems to be variable. There are, however, four groups of glasses that fall on common planes in $^{238}U/^{206}Pb$-$^{207}Pb/^{206}Pb$-$^{204}Pb/^{206}Pb$ coordinates, and also pass through Pb compositions that represent terrestrial contamination and unsupported lunar Pb. The projections of these planes are shown in Fig. 16b and their concordia intercepts define ages of these four groups as 1142 ± 110 Ma, 1856 ± 280 Ma, 2534 ± 170 Ma and 3260 ± 340 Ma. Analyses of the spherules representing groups based on 3D constraints do not fall on the same linear trends in $^{207}Pb/^{206}Pb$-$^{204}Pb/^{206}Pb$ coordinates, highlighting variable mixing of unsupported lunar Pb and terrestrial contamination also observed in other groups of glasses. The combination of variable mixing of terrestrial contamination and unsupported Pb in the individual analyses, and mixing trends generally becoming sub-parallel to the concordia in this time interval increases their uncertainties and therefore reduces confidence in the determined ages.

4.2.6. Age – compositional relationships.

Three age groupings at around 100 Ma, 500 Ma and 3.62 Ga contain the most abundant populations of glass spherules (21, 28 and 20 particles respectively), which collectively account for nearly 50% of all beads analysed for this study. Age populations at about 300 Ma (n = 9), 700 Ma (n = 10) and 2.5 Ga (n = 12) comprise the next most populated groups. Age groups at about 8 Ma, 40 Ma, 1.1 Ga and 3.3 Ga are represented by four to six beads each, with minor populations at 1.9 Ga (n = 2) and 3.8–3.9 Ga (n = 2).

KREEP-rich materials appear to dominate the source terranes of all age groups identified in the glasses extracted from regolith sample 14163. KREEP and HASP glasses comprise almost 80% of the total population (112 out of 145 homogenous glasses where U-Th-Pb system was analysed) and these compositions are present in all of the age

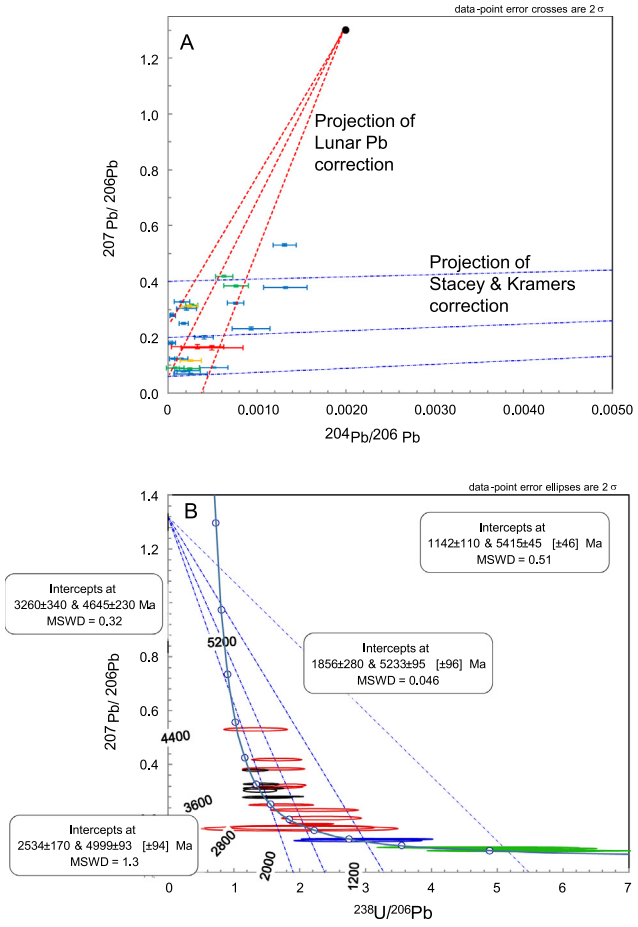

Fig. 16. U-Pb SIMS data for the glasses with apparent ages between 1000 Ma and 3620 Ma. A - $^{206}Pb/^{207}Pb$-$^{204}Pb/^{207}Pb$ diagram showing data and trends indicating terrestrial and lunar Pb correction. B - Tera-Wasserburg concordia, showing projections of planes drawn through data points and compositions defined for terrestrial contamination (e.g. Stacey and Kramers, 1975) and lunar unsupported Pb (taken from Silver, 1972). Lower intercepts define best estimates for the ages of the glasses.

groups. In addition, five of the age populations defined by multiple beads contain exclusively KREEP-rich and HASP glasses, raising the possibility of multiple impacts with a range of ages into a relatively restricted target composition. This includes the two oldest populations with ages of 3.6 Ga and 3.3 Ga. Two other groups populated only by KREEP-rich and HASP glasses are the youngest in the set at about 8 and 40 Ma. Two KREEPy beads have ages around 1.9 Ga. The small number of analyses precludes any meaningful discussion of the chemical variability of this group. In addition there is a single HASP glass with the age of 3809 ± 42 Ma. All these glasses could possibly represent impacts into deposits of the Fra Mauro formation or regolith derived from these deposits and are therefore proximal to the Apollo 14 landing site.

There are, however, subtle differences within the chemistry of the KREEP-rich and basaltic glasses, respectively, across the age groups. For example, the 100 Ma and 500 Ma glasses have a restricted range of compositions, which supports the inference that they were produced in a single event. In contrast, the 3.62 Ga glasses have a wider range of chemical variation characterised by higher abundances of volatile lithophile elements, TiO_2, and Ba (Figs. 17, 18), possibly indicating contributions from multiple sources that might be related to impact events. These compositional characteristics point to a strong regionality of source terrains, but impacts anywhere within the Procellarum-KREEP terrane cannot be excluded as potential sources for most of these glasses.

Basaltic glasses occur within six age groups plus the single spherule with an age of 3863 ± 45 Ma (bead B20 in Table 2). Six beads are assigned to the 500 Ma group, while others are distributed almost equally among the 100 Ma, 300 Ma, 700 Ma, 1.1 Ga and 2.5 Ga groups, with two to three glasses in each. Although the number of basaltic glasses studied here is relatively small (total of 20 analysed beads) and distributed between several age groups, these spherules can be tentatively classified into two compositional groups based on their TiO_2 (Fig. 18). The 300 Ma, 500 Ma and 1.1 Ga spherules appear to show higher Ti content (mostly > 3 wt% of TiO_2), whereas the 100 Ma, 700 Ma and 2.5 Ga beads, and the single spherule dated at 3863 ± 45 Ma, have TiO_2 concentrations <3 wt%.

The clustering of ages and compositions in the KREEP-rich and basaltic glasses suggests that single impacts may have delivered multiple compositionally distinct glasses to

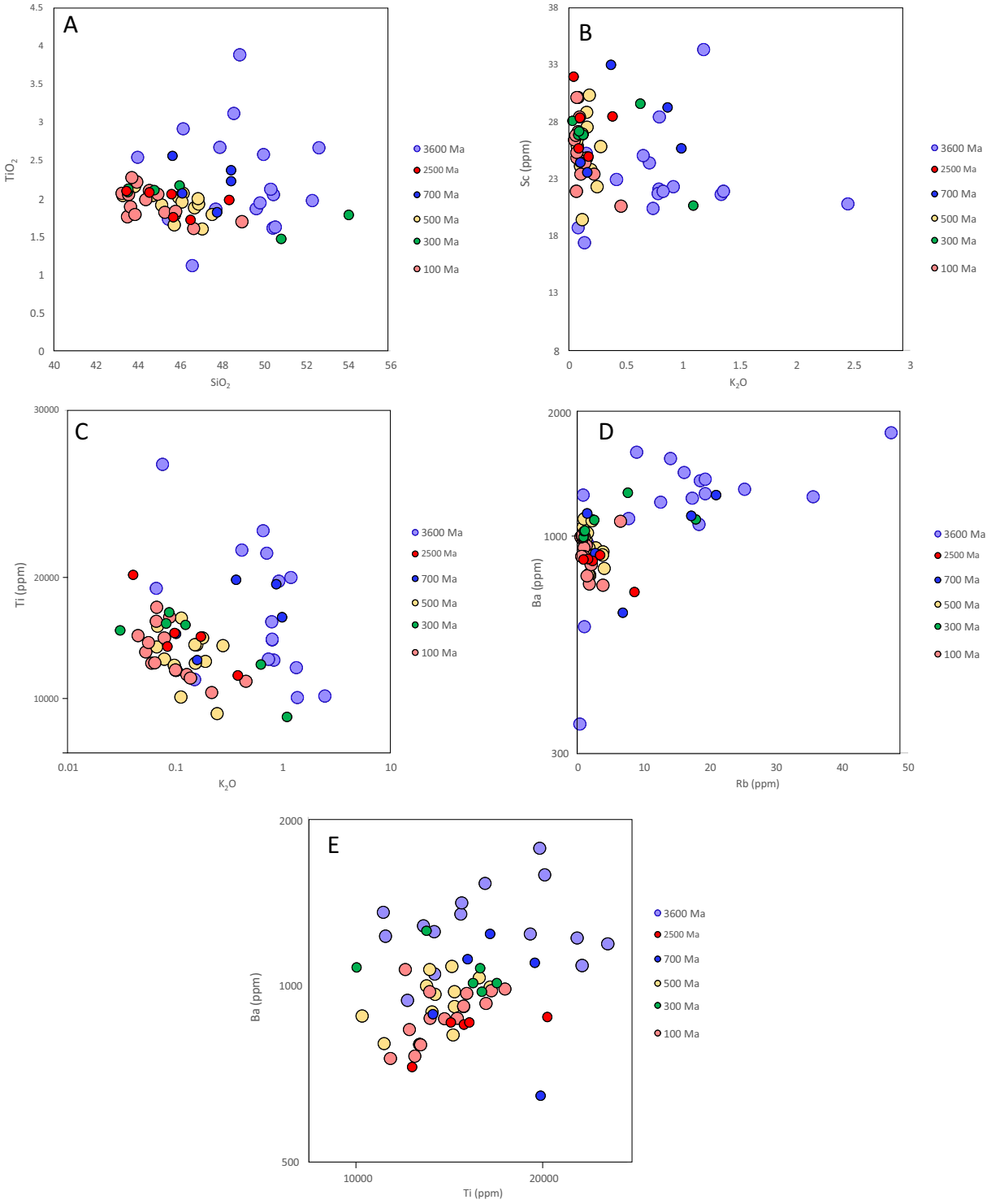

Fig. 17. Some major (wt%) and trace elements (ppm) variations in the KREEP-rich impact glasses from different age groups, indicating possibility of subtle differences in chemistry of KREEP glasses dependent on age.

the Apollo 14 landing site. This conclusion contrasts with that of Norman et al. (2019), who proposed that only a few glasses (not more than 8 out of 30 analysed) represented potential duplicates based on a statistical evaluation of corresponding ages and compositions. However, considering the limited evidence for compositional variability in cogenetic glasses produced by a single impact, their assumption that ages and compositions should be identical within the analytical uncertainties may be too strict. Further studies of compositional variability in lunar impact

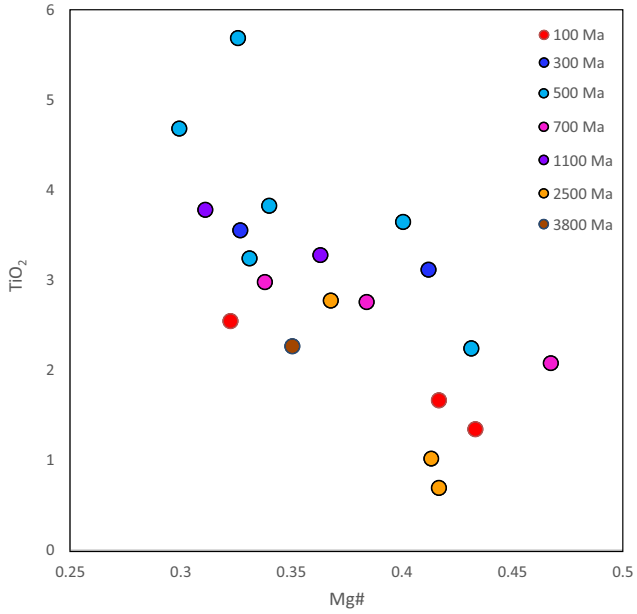

Fig. 18. Ti (wt%) versus #Mg diagram for basaltic impact glasses from different age groups, hinting possibility of age related chemical differences in basaltic beads.

glasses that can be linked to a single impact using independent criteria will be necessary to evaluate this.

Feldspathic glasses are not abundant in the sample suite studied here. Only seven have been dated, with four at ~500 Ma, two at ~2500 Ma, and one at ~300 Ma. The lack of feldspathic glasses in this sample set, and their compositional affinity with Mg-suite crustal rocks rather than the Ferroan Anorthositic Suite may imply relatively modest transport of these impact glasses over distances of ~100–1000 km.

4.3. Comparison of SIMS and LA-ICP-MS ages of glasses

One advantage of quadrupole ICP-MS compared to SIMS analysis is that the U-Pb data can be obtained simultaneously with the trace elements analysis. However, the uncertainties of individual U-Pb isotopic analyses are several times larger in the ICP-MS data, and ICP-MS does not give information indicative of the proportions of unsupported Pb as ^{204}Pb is not measured due to high instrumental backgrounds. Consequently, the range of isotopic ratios available for age calculations is more limited and internal checks, using different age estimation protocols, is less possible. Nevertheless, this study allows a comparison of U-Pb ages obtained by SIMS and ICP-MS analyses on the same beads. The latter provides ^{206}Pb/^{238}U, ^{207}Pb/^{206}Pb and total U-Th-Pb (chemical) ages. ^{207}Pb/^{206}Pb ages are imprecise as the ratio is determined with increasingly poor uncertainties in the younger glasses. U-Th-Pb chemical ages appear to overestimate ages when compared to SIMS ages of the glasses, likely due to the presence of unsupported lunar Pb or terrestrial contamination. However, the ^{206}Pb/^{238}U ages obtained from the ICP-MS data show remarkable similarities to those determined by SIMS. Plotted on a probability density diagram (Fig. 19), ICP-MS ^{206}Pb/^{238}U ages clearly highlight the three major groups of glasses that were also identified by SIMS at about 3.62 Ga, 500 Ma and 100 Ma. In addition some shoulders are present on two of the younger peaks and some small peaks are present between 1 and 3 Ga. Applying the "unmix" algorithm of Sambridge and Compston (1994) to the ICP-MS analyses presented here identifies eight age groups, similar to those identified by SIMS: 103 ± 11 Ma (114 ± 11 Ma as determined by SIMS), 341 ± 45 Ma (308 ± 22 Ma determined by SIMS), 502 ± 31 Ma (485 ± 20 Ma determined by SIMS), 787 ± 86 Ma (717 ± 62 Ma determined by SIMS), 1201 ± 160 Ma (1142 ± 110 Ma determined by SIMS), 2070 ± 250 Ma (1856 ± 280 Ma determined by SIMS), 2590 ± 250 Ma (2534 ± 170 Ma determined by SIMS) and 3644 ± 87 Ma (two groups with ages of 3620 ± 22 and 3614 ± 8 Ma determined by SIMS). Three groups of a few glasses identified by SIMS at 5 ± 2, 41 ± 20 and 3260 ± 340 Ma appear to be invisible in ICP-MS data due to the larger uncertainties of ICP-MS analyses. Nevertheless, confirmation of the majority of age groups by two independent analytical procedures increases confidence in the determined ages and separation of the glasses into different age groups.

4.4. Comparison of U-Pb and ^{40}Ar-^{39}Ar ages of Apollo 14 impact glasses

Culler et al. (2000) analysed 155 spherules from soil sample 14163 using the ^{40}Ar-^{39}Ar method. Their data were presented using probability density plots and a histogram of individual analyses; consequently, U-Pb ages of individual glasses in the data set presented here have to be estimated in order to make a direct comparison. As discussed earlier for the beads younger than 1 Ga, these U-Pb ages can be

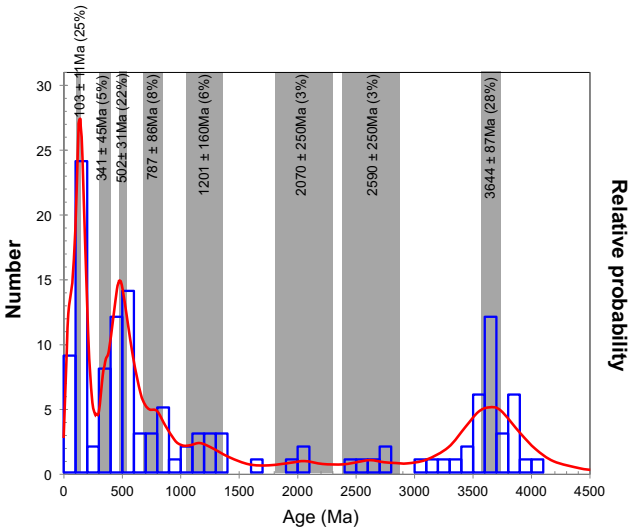

Fig. 19. Probability density and histogram plot of $^{206}Pb/^{238}U$ ICP MS ages, grey bands reflect ages and uncertainties of groups identified from ICP MS data using "unmix" algorithm of Sambridge and Compston (1994). The values for ages and uncertainties are also shown inside the bands. The values in brackets represent estimated proportion of glasses for each group in the total population.

estimated from each SIMS analysis by calculating concordia intercepts of the planes drawn in 3D $^{238}U/^{206}Pb$-$^{207}Pb/^{206}Pb$-$^{204}Pb/^{206}Pb$ coordinates (presented in Table 2 as model ages). This approach is more difficult to apply to older glasses as the planes get progressively closer to concordia with increasing age. The ages of individual glasses in the time interval between about 1 and 3.6 Ga are the most difficult to estimate. The approach advocated here involves fitting planes through the data points in $^{238}U/^{206}$-Pb-$^{207}Pb/^{206}Pb$-$^{204}Pb/^{206}Pb$ compositional space and finding ages for groups of glasses based on intercepts of these planes with concordia. Using this approach, the only way to determine ages of individual glasses in these groups would be to project points representing analyses of these individual glasses to concordia parallel to the planes defined for each group. The results of this projection are also presented in Table 2. Glasses older than 3.6 Ga fall on two separate trends in $^{207}Pb/^{206}Pb$-$^{204}Pb/^{206}Pb$ coordinates. A line drawn through the steeper trend passes directly through the unsupported Pb isotopic composition determined by Silver (1972) in the bulk soil sample. Consequently, ages of glasses falling on this line can be estimated by correcting analyses for unsupported Pb with this composition. The best fit line drawn through the compositions falling on the shallower trend passes between unsupported lunar Pb composition of Silver (1972) and terrestrial Pb defined from the Stacey and Kramers (1975) model on $^{207}Pb/^{206}Pb$-$^{204}Pb/^{206}Pb$ plot. This implies that Pb not produced by in situ decay of U in these samples is a mixture of unsupported lunar Pb and terrestrial contamination. However, this mixed composition can be estimated from the intercept of the best fit line constrained from the data and a line connecting the Pb compositions of Silver (1972) and Stacey and Kramers (1975). This estimated composition in its turn can be used to correct individual analyses and determine model ages of individual glasses (Table 2).

Probability density plots and histograms of ^{40}Ar-^{39}Ar ages of Apollo 14 glasses from Culler et al. (2000) and U-Pb ages obtained here are shown in Fig. 20. Following Culler et al. (2000) the bin width for the histograms was selected as 400 Ma. The general pattern of age distribution is similar, with bimodal distributions having peaks at 3–4 Ga and 0–0.5 Ga). However, there are also differences in the distributions, for example, U-Pb data plotted on histograms show a significant peak between 3.6 and 4.0 Ga that tails quickly for ages younger than 3.6 Ga. In contrast the ^{40}Ar-^{39}Ar analyses suggest a broader peak between 2.0 and 4.0 Ga. As discussed by Zellner (2019), the overabundance of 3.2–3.6 Ga glasses in the dataset of Culler et al. (2000) may be explained by the inclusion of some volcanic glasses in their population of analysed glasses due to the lack of chemical filtering. In addition, the ^{40}Ar-^{39}Ar data indicate a substantial proportion of glasses between 1.0 and 2.0 Ga, whereas the number of glasses with U-Pb ages in this interval is limited to a few beads. Furthermore, the number of ^{40}Ar-^{39}Ar ages around 500 Ma is relatively small, while 500 Ma is one of the most abundant groups in the U-Pb data set. In general, it appears that the overall population of ^{40}Ar-^{39}Ar data for Apollo 14 glasses in the dataset of Culler et al. (2000) is shifted towards somewhat younger ages compared to U-Pb results. This could be explained by higher diffusivity of Ar compared to Pb in the spherules, which increased the probability of resetting of ^{40}Ar-^{39}Ar system. A broadly similar pattern of ^{40}Ar-^{39}Ar ages for Apollo 14 glasses with abundance peaks at <400 Ma and at ~3.6 Ga is present in the dataset of Nguyen and Zellner (2019) based on a much smaller number of samples (n = 22).

More generally, the pattern of the U-Pb ages (Fig. 19) is strikingly similar to the compiled dataset of ^{40}Ar-^{39}Ar ages for lunar impact glasses of "sufficient size" to retain their primary ages as compiled by Zellner and Delano (2015) and Zellner (2019). We suggest that this agreement among the Ar and U-Pb systems provides strong evidence that both of these isotope systems are recording the primary ages of glass-forming impact events, although both systems

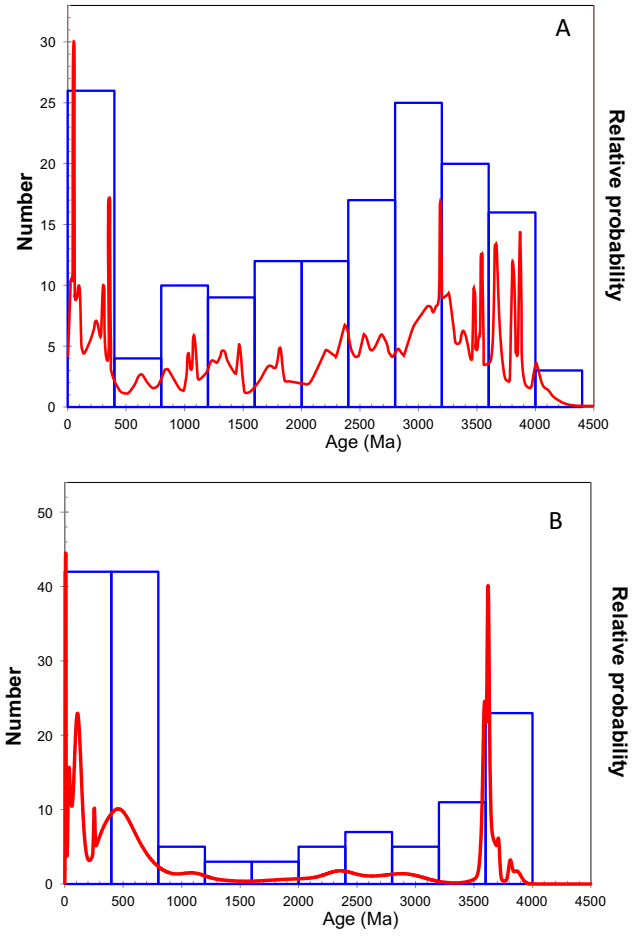

Fig. 20. Probability density and histogram plots of (A) $^{39}Ar/^{40}Ar$ ages of Apollo 14 glasses from Culler et al. (2000) and (B) SIMS model U-Pb ages of Apollo 14 glasses (this study).

clearly have complications relating to sample selection and interpretation of the data that must be taken into account.

4.5. Implications for lunar impact history

Eleven age groups of impact glasses extracted from sample 14163 represent the minimum number required to explain the U-Pb isotopic data at the level of currently achievable analytical uncertainty and our understanding of Pb systematics. Improved analytical precision and a better understanding of the composition and behavior of Pb within the lunar regolith and sources of terrestrial contamination may define further age differences within some of these groups. The range of ages determined for these groups is between about 8 Ma and 3.62 Ga, which covers nearly 80% of the history of the Solar System, with some analyses of individual glasses indicating ages of up to ~3.8 Ga. Nevertheless, three of these age groups include close to 50% of the glass population recovered from the sample (i.e., forming clusters represented by 20 to 30 individual beads each), and the chemical compositions of glasses within these groups suggests that they represent discrete impact events. Significant questions are whether these groups truly represent single separate impacts, and what are the processes that control the abundance of glasses in the different groups in a single split of lunar regolith. Limiting interpretations of the observed ages are: (i) the eleven age groups correspond to eleven impacts and (ii) each glass originated in a separate impact event. The latter interpretation would support a common practice of plotting ages of glasses as histograms or probability density plots and interpreting visible peaks as changes in the overall flux of impactors. It would also imply that the ages of impacts responsible for formation of different spherules within an age group are confined by the limit of uncertainties determined for this group. It would probably also indicate that the individual impacts are relatively small with transport distances <100 s of kilometres.

In contrast, the possibility that lunar regolith glasses were emplaced by a relatively small number of impacts suggests that specific conditions are required to produce these glasses (perhaps analogous to terrestrial tektites) and would question the validity of attempts to investigate temporal changes in the Solar System's impact flux on the basis of histograms or probability density plots based on the ages of lunar impact glasses. Observed peaks on these histograms may simply represent the most abundant groups of glasses where each group is formed by a single impact. In this case the peaks may be a reflection of the size of individual impacts and/or proximity of the crater to the sample collection site, rather than the flux of impactors.

Future studies of glasses from different samples and landing sites combining chemical information and ages obtained by a variety of methods can potentially help to clarify the significance of the age groups in the glass populations, and the processes that influence age interpretations based on different isotope systems, such as unsupported Pb, diffusivity, mobility of regolith components, and potential biases that might be introduced by mechanical preservation within the regolith, e.g., analysis of glass droplets versus fragments (e.g., Zellner 2019; Norman et al., 2019). Sample 14163 shows 5 age groups (almost half of the total number) that were sourced entirely from KREEP-rich targets. Others are represented by mixed KREEP, basaltic and feldspathic materials. The latter, however, is unlikely to be sourced from crustal terranes dominated by the Ferroan Anorthosite Suite. These observations raise another long-standing question, whether the glasses originate primarily from lunar regolith or underlying rocks (e.g., Reid et al., 1972; Zellner et al., 2002; Norman et al., 2012; Hörz et al., 2020). The uppermost layers of the lunar regolith are homogenised at least to some degree by impact processes. Most of this mixing is vertical, as shown by the regolith at lithologically diverse sites such as Apollo 17 site where the regolith is heterogeneous across the site and the stratigraphy of closely space regolith cores shows a strong vertical heterogeneity and no lateral continuity (e.g., Korotev and Morris 1993). Nevertheless, glasses formed primarily by remelting of regolith materials should probably be more homogenous than those formed by melting of rocks in the target, which might generate compositionally diverse populations of glasses, provided that different lithologies are present in the target and given the larger depth of melting that produced the glasses. Consequently, compositionally mixed populations in 14163 (and other samples) may come from larger impacts into primarily population of rocks rather than regolith, which also means that these impacts can be more distal from the sample collection site. In contrast, homogeneous, KREEP-dominated glass groups can be sourced from the regolith (or underlying breccia units) near the sample collection site. This interpretation, however, is applicable only if the age groups are interpreted as mainly resulting from single impacts. If multiple impacts are considered as a possibility for individual age groups, mixed chemical populations can be formed by multiple small impacts, each targeting a specific rock type. This would also require that different rocks are present near the sampling site and accessible for melting by small impacts, i.e., not covered by a thick layer of homogenised regolith.

There have now been a number of published studies that provide impact ages of lunar regolith glasses (see Introduction), but detailed cross-site comparisons aimed at understanding critical aspects such as the implications for impact flux and regolith evolution remain uncertain. In part this is due to the lack of detailed compositional data in some studies, large uncertainties of some dates due to either analytical limitations or uncertainties in the behavior of the isotopic systems during the impact and/or subsequent residence in the regolith, local variations in site geology, possible short-term variations in impact flux, and incomplete understanding of fundamental aspects of impact processes that produce the regolith glassses, such as size of crater, sampling depth, transport distance, extent of resetting of geochronologic systems, and the compositional dispersion of impact glasses produced by individual impact events. The abundance of relatively young ages seems to be a general feature of lunar impact glasses, especially those with droplet shapes, but understanding the genetic significance of this observation will require additional studies of diverse locations using a variety of geochemical and isotopic systems. The data presented here enable discussion of the issues and identification of possible solutions, but further study will be required to reach a more precise understanding of the processes that form lunar impact glasses and their significance for lunar impact history.

5. CONCLUSIONS

Eleven statistically distinct age groups of impact glass spherules from lunar regolith sample 14163 have been identified using U-Th-Pb ion probe and LA-ICP-MS analysis of 168 individual spherules from Apollo 14 soil sample 14163. It is not possible to say for certain that glasses with different compositions but the same age are produced by single or separate impacts, but different age groups must form in distinct impact events. Consequently, eleven groups represent a minimum number of impacts required to account for the population of spherules studied here.

The combination of ion probe and LA-ICP-MS analyses of the same spherules indicates that both methods are capable of providing similar chronological information, but also highlights advantages and disadvantages of two techniques. Unlike ion probe, LA-ICP-MS gives an opportunity to obtain ages and trace elements data in the same analytical session. However, the age information obtained by quadrupole LA-ICP-MS is less precise and more restricted in the application of different data reduction algorithms that can be used to deal with the issue of complex mixing of different Pb components with different origin, existing in the glasses.

Analyses of glass beads indicate the ubiquitous presence of at least three main types of Pb with only one of those related to the in-situ accumulation from U decay after impact melting, i.e., directly related to the age of the glasses. There appears to be a small but unavoidable proportion of terrestrial Pb that can be only linked to laboratory contamination, despite care taken to avoid this contamination. Many of the glasses show evidence of of lunar Pb that is unsupported by U decay inside the beads that is likely sourced from the host soil. Different methods of data reduction allows age estimates to be made for individual glasses or groups of glasses. The similarity of ages obtained using these different methods increases confidence in the accuracy of the chronological information.

Three main chemical groups can be distinguished: (i) basaltic impact glasses, (ii) feldspathic impact glasses and (iii) KREEP rich impact glasses. These chemical groups can be associated with the main types of rocks represented in lunar sample collections, possibly indicative of the dominant composition of the target of the impacts that form glass spherules. KREEP-rich materials dominate the glass

population in the sample. Several age groups consist entirely of glasses with a strong KREEP signature. However, other groups include other chemical types of spherules. Nevertheless, even basaltic and feldspatic glasses found in the sample 14163 show chemical features indicative of admixture of a KREEP or KREEP-related component, most likely in the area where the spherules have been formed during the impacts. The persistent presence of KREEP suggests that most glasses could have been sourced "locally" within the Procellarum KREEP terrane and do not require transport of hundreds of kilometres from the Apollo 14 landing site. Precise transport distances, source crater sizes, and whether the source terrain was dominated by rocks or regolith are open questions. The broadly similar patterns of age distributions obtained from both the U-Pb and ^{40}Ar-^{39}Ar ages of Apollo 14 glasses suggests that both datasets are recording primary impact ages although the significance of these patterns for lunar impact history and formation of lunar regolith glasses requires further study.

Declaration of Competing Interest

The authors declare that they have no known competing financial interests or personal relationships that could have appeared to influence the work reported in this paper.

ACKNOWLEDGEMENTS

We would like to thank Randy Korotev and two anonymous reviewers for their thoughtfull and extensive comments, which helped greatly to improve the manuscript. At the time of analysis, the NordSIMS facility operated as a joint Nordic infrastructure regulated by NOS-N and financed by the research funding agencies of Denmark, Norway and Sweden (Swedish Research Council infrastructure grant 2009-6245), the Geological Survey of Finland, the University of Iceland and the Swedish Museum of Natural History; this is NordSIMS publication 697.

APPENDIX A. SUPPLEMENTARY MATERIAL

Supplementary data to this article can be found online at https://doi.org/10.1016/j.gca.2021.12.013.

REFERENCES

Ackermann R. J., Gilles P. W. and Thorn R. J. (1956) High-temperature thermodynamic properties of uranium dioxide. *J. Chem. Phys.* **25**, 1089–1097.

Brown S. M. and Grove T. L. (2015) Origin of the Apollo 14, 15, and 17 yellow ultramafic glasses by mixing of deep cumulate remelts. *Geochim. Cosmochim. Acta* **171**, 201–215.

Chao E. C. T., Best J. B. and Minkin J. A. (1972b) Apollo 14 glasses of impact origin and their parent rock types. *Proc. 3rd Lunar Sci. Conf.*, 907–925.

Chapman A. T. and Meadows R. E. (1963) Volatility of $UO_{2\pm x}$ and phase relations in the system uranium—oxygen. *J. Am. Ceram. Soc* **47**, 614–621.

Culler T. S., Becker T. A., Muller R. A. and Renne P. R. (2000) Lunar impact history from ^{40}Ar/^{39}Ar dating of glass spherules. *Science* **287**, 1785–1788.

Delano J. W. (1986) Pristine lunar glasses: Criteria, data and implications. *Proc. 16th Lunar Planet Sci. Conf. in J. Geophys. Res* **91**, D201–D213.

Delano J. W. and Livi K. (1981) Lunar volcanic glasses and their constraints on mare petrogenesis. *Geochim. Cosmochim. Acta* **45**, 2137–2149.

Delano J. W., Zellner N. E. B., Barra F., Olson E., Swindle T. D., Tibbetts N. J. and Whittet D. C. B. (2007) An integrated approach to understanding Apollo 16 impact glasses: Chemistry, isotopes and shape. *Meteorit. Planet. Sci.* **42**, 993–1004.

Delano J. W., Lindsley D. H. and Rudowski R. (1981) Glasses of impact origin from Apollo 11, 12, 15 and 16: Evidence for fractional vaporization and mare/highland mixing. *Proc. 12th Lunar Planet. Sci. Conf.* 339–370.

Dulski P. (2001) Reference materials for geochemical studies: New analytical data by ICP-MS and critical discussion of reference values. *Geostandards Newslett.* **25**, 87–125.

Fanara S., Sengupta P., Becker H. W., Rogalla D. and Chakraborty S. (2017) Diffusion across the glass transition in silicate melts: Systematic correlations, new experimental data for Sr and Ba in calcium-aluminosilicate glasses and general mechanisms of ionic transport. *J. Non-Cryst. Solids* **455**, 6–16.

Fulchignoni M., Funiciello R., Taddeucci A., Trigila R. (1971) Glassy spheroids in lunar fines from Apollo 12 samples 12070,37; 12001,73; and 12057,60. *Proc of the 2d Lunar Sci. Conf.*, 937.

Gao S., Liu X., Yuan H., Hattendorf B., Günther D., Liang Chen L. and Hu S. (2002) Determination of forty two major and trace elements in USGS and NIST SRM glasses by laser ablation-inductively coupled plasma-mass spectrometry. *Geostandards Newslett.* **26**, 181–196.

Glass B. P. (1976b) Major element compositions of glasses from Apollo 11, 16 and 17 soil samples. *Proc. 7th Lunar Sci. Conf.* 679–693.

Hörz F., Basilevsky A. T., Head J. W. and Cintala M. J. (2020) Erosion of lunar surface rocks by impact processes: A synthesis. *Planet. Space Sci.* **194** 105105.

Huneke, J. C. (1978). ^{40}Ar-^{39}Ar microanalysis of single 74220 glass balls and 72435 brecciaclasts. *Proc of the 9th Lunar Sci. Conf.*, 2345–2362.

Hughes S. S., Delano J. W., and Schmitt R. A. (1990) Chemistries of individual mare volcanic glasses: Evidence for distinct regions of hybridized mantle and a KREEP component in Apollo 14 magmatic sources. *Proc. 20th Lunar Planet. Sci. Conf.* 127–138.

Jochum K. P. and Nohl U. (2008) Reference materials in geochemistry and environmental research and the GeoReM database. *Chem. Geol.* **253**, 50–53.

Korotev R. L. and Morris R. V. (1993) Composition of Apollo 16 regolith core 60013/14. *Geochim. Cosmochim. Acta* **57**, 4813–4826.

Korotev R. L., Zeigler R. A. and Floss C. (2010) On the origin of impact glass in the Apollo 16 regolith. *Geochim. Cosmochim. Acta* **74**, 7362–7388.

Levine J., Becker T. A., Muller R. A. and Renne P. R. (2005) 40Ar/39Ar dating of Apollo 12 impact spherules. *Geophys. Res. Lett.* **32**, L15201.

Ludwig K. R. (1980) Calculation of uncertainties of U-Pb isotope data. *EPSL* **46**, 212–220.

Ludwig K. R. (2008) *User's Manual for Isoplot 3.60, A geochronological toolkit for Microsoft Excel. Berkeley Geochronological Center Special Publication 4*, Berkeley, California: Berkeley Geochronological Center.

McKay D. S., Greenwood W. R. and Morrison D. A. (1970) Origin of small lunar particles and breccias from the Apollo 11 site. *Proc. Apollo 11 Lunar Sci. Conf.,* 673–693.

Naney M. T., Crowl D. M. and Papike J. J. (1976) The Apollo 16 drill core: Statistical analysis of glass chemistry and the characterization of a high alumina-silica poor HASP. *Proc. 7th Lunar Sci. Conf.,* 155–184.

Nemchin A. A., Whitehouse M. J., Grange M. L. and Muhling J. R. (2011) On the elusive isotopic composition of lunar Pb. *Geochim. Cocmochim. Acta* **75**, 2940–2964.

Nemchin A. A., Jeon H., Bellucci J. J., Timms N. E., Snape J. F., Kilburn M. R. and Whitehouse M. J. (2017) Pb-Pb ages of feldspathic clasts in two Apollo 14 breccia samples. *Geochim. Cosmochim. Acta* **217**, 441–461.

Nguyen P. and Zellner N. (2019) Using size and composition to assess the quality of lunar impact glass ages. *Geosciences* **9**, 85.

Norman M. D., Adena K. and Christy A. G. (2012) Provenance and Pb isotopic ages of lunar volcanic and impact glasses from Apollo 17 landing site. *Aust. J. Earth Sci.* **50**, 291–306.

Norman M. D., Garcia M. O. and Bennett V. C. (2004) Rhenium and chalcophile elements in basaltic glasses from Ko'olau and Moloka'i volcanoes: Magmatic outgassing and composition of the Hawaiian plume. *Geochim. Cosmochim. Acta* **68**, 3761–3777.

Norman M. D., Jourdan F. and Hui S. S. M. (2019) Impact history and regolith evolution on the moon: geochemistry and ages of glasses from the Apollo 16 site. *JGR Planets* **124**, 3167–3180.

Norman M. D., Griffin W. L., Pearson N. J., Garcia M. O. and O'Reilly S. Y. (1998) Quantitative analysis of trace element abundances in glasses and minerals: a comparison of laser ablation ICPMS, solution ICPMS, proton microprobe, and electron microprobe data. *J. Anal. At. Spectrom.* **13**, 477–482.

Norman M. D., Borg L. E., Nyquist L. E. and Bogard D. D. (2003) Chronology, geochemistry, and petrology of a ferroan noritic anorthosite from Descartes breccia 67215: Clues to the age, origin, structure and impact history of the lunar crust. *Meteor. Planet. Sci.* **38**, 645–661.

Papike J. J., Spilde M. N., Adcock C. T., Fowler G. W. and Shearer C. K. (1977) Trace-element fractionation by impact-induced volatilization; SIMS study of lunar HASP samples. *Am. Mineral.* **82**, 630–634.

Pieters C. M., Hanna K. D., Cheek L., Dhingra D., Prissel T., Jackson C., Moriarty D., Parman S. and Taylor L. A. (2014) The distribution of Mg-spinel across the Moon and constraints on crustal origin. *Am. Mineral.* **99**, 1893–1910.

Prissel T. C., Parman S. W., Jackson C. R. M., Rutherford M. J., Hess P. C., Head J. W., Cheek L., Dhingra D. and Pieters C. M. (2014) Pink Moon: the petrogenesis of pinkspinel anorthosites and implications concerning Mg-ssuite magmatism. *EPSL* **403**, 144–156.

Reid A. M., Warner J., Ridley W. I., Johnston D. A., Harman R. S., Jakes P. and Brown R. W. (1972a) The mojor element compositions of lunar rocks inferred from glass compositions in lunar soils. *Proc. 3rd Lunar Sci. Conf.* 363–379.

Ridley W. I., Reid A. M., Warner J. L. and Brown R. W. (1973) Apollo 15 green glasses. *Phys. Earth Planet. Interiors* **7**, 133–136.

Sambridge M. S. and Compston W. (1994) Mixture modeling of multi-component data sets with application to ion-probe zircon ages. *EPSL* **128**, 373–390.

Shearer C. K. and Papike J. J. (1993) Basaltic magmatism on the Moon: A perspective from volcanic picritic glass beads. *Geochim. Cosmochim. Acta* **57**, 4785–4812.

Shearer C. K., Papike J. J., Simon S. B., Shimizu N., Yurimoto Y. and Sueno S. (1990) Ion microprobe studies of trace elements in Apollo 14 volcanic glass beads: Comparisons to Apollo 14 mare basalts and petrogenesis of picritic magmas. *Geochim. Cosmochim. Acta* **54**, 851–867.

Shearer C. K., Papike J. J., Galbreath K. C. and Shimizu N. (1991) Exploring the lunar mantle with secondary ion mass spectometry: A comparison of lunar picritic glass beads from the Apollo 14 and Apollo 17 sites. *EPSL* **102**, 134–147.

Shearer C. K., Elardo S. M., Petro N. E. and Borg L. E. (2015) Origino f the lunar highlands Mg-suite: an integrated petrology, geochemistry, chronology, and remote sensing perspective. *Am. Mineral.* **100**, 294–325.

Silver L. T. (1972) U-Th-Pb abundances and isotopic characteristics in some Apollo 14 rocks and soils (abs). *Lunar Sci.* III. Lunar Planetary Institute, Houston. pp. 704–706.

Silver L. T. (1974a) Patterns for U, Th, Pb distributions and isotopic relationships in Apollo 17 soils (abs). *Lunar Sci. V.* Lunar Planetary Institute, Houston. pp. 706–708.

Simon S. B., Papike J. J., Shearer C. K., Hughes S. S., Schmitt R. A. (1989) Petrology of Apollo 14 regolith breccias and ion microprobe studies of glass beads. *Proc. 19th Lunar Planet. Sci. Conf.*, 1–17.

Spangler R. R. and Delano J. W. (1984) History of the Apollo 15 yellow impact glass and samples 15426 and 15427. *Proc. 14th Lunar Planet. Sci. Conf. in J. Geophys. Res.* **89**, B478–B486.

Stacey J. C. and Kramers J. (1975) Approximation of terrestrial lead isotope evolution by a two-stage model. *Earth Planet. Sci. Lett.* **26**, 207–221.

Tera F. and Wasserburg G. J. (1973) A response to a comment on U-Pb systematics in lunar basalts. *EPSL* **19**, 213–217.

Wentworth S. J. and McKay D. (1991) Apollo 14 glasses and the origin of lunar soils. *Proc. 21st Lunar Planet. Sci. Conf.*. Lunar Planetary Institute, Houston. pp. 185–192.

Williams I. S. (1998) U-Th-Pb geochronology by ion microprobe. In Applications of microanalytical techniques to understanding mineralising processes (eds. M. A. McKibben, W. C. Shanks and W. I Riley). *Reviews in Economic Geology* **7,** 1–35.

Woodhead J. D. and Hergt J. M. (2000) Pb-isotope analyses of USGS reference Materials. *Geostandards Geoanal. Res.* **24**, 33–38.

Yakovlev O. I., Gerasimov M. V. and Dikov Y. P. (2011) Estimation of temperature conditions for the formation of HASP and GASP glasses from the lunar regolith. *Geochem. Int.* **49**, 213–223.

Zeigler R. A., Korotev R. L., Jolliff B. L., Haskin L. A. and Floss C. (2006) The geochemistry and provenance of Apollo 16 mafic glasses. *Geochim. Cosmochim. Acta* **70**, 6050–6067.

Zellner N. E. B. (2019) Lunar impact glasses: Probing the Moon's surface and constraining its impact history. *JGR Planets* **124**, 2686–2702.

Zellner N. E. B. and Delano J. W. (2015) $^{40}Ar/^{39}Ar$ ages of lunar impact glasses: Relationships among Ar diffusivity, chemical composition, shape, and size. *Geochim. Cosmochim. Acta* **161**, 203–218.

Zellner N. E. B., Delano J. W., Swindle T. D., Barra F., Olsen E. and Whittet D. C. B. (2009) Evidence from $^{40}Ar/^{39}Ar$ ages of lunar impact glasses for an increase in the impact rate ~800 Ma ago. *Geochim. Cosmochim. Acta* **73**, 4590–4597.

Zellner N. E. B., Spudis P. D., Delano J. W. and Whittet D. C. B. (2002) Impact glasses from the Apollo 14 landing site and implications for regional geology. *JGR* **107**, 5102–5115.

Zellner N. E. (2017) Cataclysm no more: new views on the timing and delivery of lunar impactors. *Origins Life Evolut. Biospheres* **47**, 261–280.

Associate editor: James M.D. Day